Simulation based methods to determine linear equivalent models of power system devices

by

B. W. H. Akbo Rupasinghe

A thesis submitted to the Faculty of Graduate Studies of

The University of Manitoba

in partial fulfillment of the requirements of the degree of
Doctor of Philosophy

Department of Electrical and Computer Engineering

University of Manitoba

Winnipeg, Canada

To my father, mother, little brother and my love, Gayamini...

Acknowledgements

First and foremost I would like to express my sincere gratitude to my advisor Prof. Udaya Annakkage for his continuous guidance and support for my research and for helping to achieve my academic and professional goals during my time at University of Manitoba as a graduate student. My co-advisor, Dr. Chandana Karawita's valuable inputs and advice to improve my research are greatly appreciated. I am thankful to members of the examining committee, Prof. Miroslaw Pawlak and Dr. Jason Morrison for continuous review of my work. I am also grateful to Dr. Hiranya Suriyaarachchi, Dr. Janath Geeganage and Dr. Prasad Wadduwage for their support.

I would like to thank RTDS Technologies, MITACS and Natural Sciences and Engineering Research Council of Canada (NSERC) for their financial support for the research. The support I got from Ms. Amy Dario, Mr. Erwin Dirks, Ms. Tracy Gledhill and the staff of the Department of Electrical and Computer Engineering of University of Manitoba are greatly appreciated.

Nothing would have been possible if not for the support and the encouragement of my parents and brother, and I am thankful to them with all my heart. Lastly, I am grateful to my beautiful wife, Gayamini, for being a pillar of strength with love, warmth and patience throughout the five years of my research.

Akbo Rupasinghe

January, 2019

Palo Alto, California
USA.

Abstract

Small signal stability analysis (linear analysis) of power systems is a very useful component in any power system study. Greater insight into the system can be obtained by it. It also opens the power systems and its controllers to a large body of knowledge on linear systems and controls.

It has become the trend of the power system device manufacturers to make available an *as built* detailed model of their product. Such a model is usually in the electromagnetic transient (EMT) simulation domain. The model is made available as a device that can be connected to a larger power system on a simulation case running on an EMT software. Due to proprietary constraints, the model may be black-boxed and only a limited number of outputs and inputs may be available to the user. In instances it is not black boxed, it is usually a device with complex controllers, making it a tedious task to determine its mathematical model. In both cases, the complete mathematical model is not available to the user.

Since it is not possible to linearize the system without the knowledge of all the devices in the power system, small signal stability analysis is often skipped in a power system study. This research focuses on using available input and output signals of black boxed EMT simulation models of power system devices, and utilize other

available knowledge of the system to determine model data of their linear equivalent models, in such a way, complete small signal stability studies can be carried out at any operating point, and connected to any network.

Power system devices can be divided into two main subsystems. (1) The current injection device, which is operating point dependent. (2) The auxiliary controller, which is operating point independent within a given operating mode. Dynamic data of the current injection device subsystem (i.e. synchronous machine, induction machine) can be considered as *a priori* knowledge of the system. A Prony Analysis method, augmented by eigenstructure assignment has been proposed to incorporate the *a priori* knowledge of the system to the system identification process. Using a result derived from Mason's Gain Rule, the linearized model of the power system device is divided into the known subsystem of the operating-point-dependent current injection device; and the operating-point-independent unknown subsystem of the auxiliary controller. The modes identified from the proposed system identification procedure at multiple operating points are then used to solve a system of polynomial equations, for the unknown auxiliary controller transfer functions.

Table of Contents

List of Figures

List of Tables

Chapter 1

Introduction

1.1 Power System Simulation

A power system is a dynamic system where devices such as electrical generators are connected to a transmission network which transfers electric power to loads. At steady state, the mechanical power given to the generators should be equal to the sum of active power at the loads and the active power loss in the system. Any change or perturbation to the power system causes transients. A power system rarely stays at a steady state as loads and other conditions of a the system frequently change. Stability of a power system is its ability to achieve a feasible steady state, subsequent to a perturbation. In order to ensure continuous supply of power to loads, the stability of the power system is paramount.

As power systems grew into multiple synchronous machines connected to a transmission network that spanned a wider area, the operator needed to understand the behaviour of the system in detail, so that predictions about the power system's re-

sponse to perturbations could be made. Mathematical models were then developed for power system components such as generators, transmission lines and loads. The dynamic system could then be represented by a set of nonlinear first order differential equations (state space) and a complementing set of algebraic equations. The behaviour of the power system could be simulated by numerical integration of the nonlinear state-space, starting from a desired initial condition. For stability of the simulation, the desired initial condition is always a steady state operating point, at which the power flow is converged.

Complexity of the mathematical models of power system components grew over time. The more detailed the mathematical model is, the more accurate the simulation is. The accuracy is reflected by the frequency contents of the simulation. In order to represent higher frequency contents, more detailed models have to be used. Also, the integration time step of the dynamic equations has to be made smaller to simulate higher frequency dynamics. Electromagnetic Transient (EMT) simulation and transient simulation are two power system simulation regimes with different simulation details.

Parameter estimation for the mathematical model too has become more complex with the complexity of the models. Over the last fifty years, extensive research has been done in this area and there are well established dynamic equivalent models for generators, power transmission network and individual loads with equally well established parameter estimation methods.

1.2 Linear Analysis of a Power System

Due to the nonlinearities in the power system mathematical model, only time-domain responses could be obtained from numerical integration of the dynamic equations. Small signal stability analysis for a power system is performed with the assumption that a small perturbation would cause the state variables of a power system to vary only linearly. Small signal behaviour describes the dynamics of state variables of the power system when subjected to a small disturbance at a specific steady state operating point of the system. The operating point is defined by the steady state power flow in the network.

Linearization of a one-dimensional nonlinear function (one state variable) is illustrated in Fig. 1.1

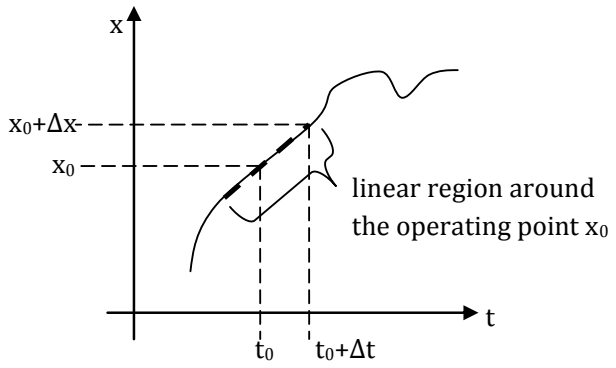

Fig. 1.1: Illustration of linearization of a 1-dimensional nonlinear function

Greater insights to the system dynamics can be obtained from a linear state space. Theoretically, there could be a steady state operating point of a power system which is small signal unstable. This means, even if there is a power balance between generation and loads, a small perturbations could cause the system to collapse. While the

detailed nonlinear simulations reveal the fast transients between two steady state operating points, small signal stability determines the stability of a steady state (mostly post-fault) for small perturbations. Such a stability can also be determined by looking at time-domain responses of a nonlinear simulation. However, small signal stability analysis gives much more information than variation of a few chosen variables as in a nonlinear simulation. Therefore, it is an essential part of a power system stability study.

There are two classes of linear analysis of power systems [2]. Namely:

1. Model based linear analysis

2. Measurement based linear analysis

In model based linear analysis of a power system, the nonlinear dynamic equations that describe the power system could be linearized around a desired operating point using Truncated Taylor Series Expansion [3]. A system so linearized can be subjected to a complete eigenvalue analysis. In order to perform model based small signal stability analysis, the full mathematical model and parameters should be known for the power system so that the nonlinear dynamic equations could be linearized. There are commercially available software to linearize a power system with generic components, specified by library models. If a power system consists of components whose models are not included in a generic library, the user must manually linearize the nonlinear equations and derive the linear model.

In measurement based linear analysis of a power system, system identification is used to identify transfer functions between inputs and outputs of a power system by giving a small perturbation to the system. Measurement based analysis provide only

limited insight to the system. There are advanced system identification methods that accurately estimate the low damped modal content (eigenvalues) of a power system at a given operating point. The modal content alone can be used to determine the proximity of a power system to the stability margin, at a given operating point, in applications of dynamic security assessments. Since meaningful system matrices cannot be determined by measurement based methods, the insight one gets from a model based linear analysis, cannot be obtained from measurement based linear analysis. Applications in controller design and finding the root cause of low damped modes (by participation factor analysis) is limited in measurement based analysis. A brief review of measurement based small signal stability of power systems is presented in Chapter 3.

1.3 Absence of Mathematical Models and Parameters

A power system device can be divided into two subsystems, namely, the current injection device and the auxiliary controllers. E.g. in case of a synchronous machine: the turbine-governor, the excitation system and the power system stabilizer (PSS) are the auxiliary controllers, and the machine, consisting of the stator and the rotor, is the current injection device.

Current injection devices (i.e. synchronous machines, induction machines, thyristor bridge inverters and IGBT bridge inverters) have well reviewed mathematical models that were developed over time. Their parameter estimation methods too are well established.

The sensors and actuators of the auxiliary controllers have their own dynamics which are complemented by numerical controller blocks designed by power system engineers to achieve desired performance of the power system. The industry used to adopt generic auxiliary controllers for the dynamic devices. Models for these generic controllers are designed and documented in the public domain by technical standard committees of professional bodies such as Institute of Electrical and Electronic Engineers (IEEE) [4, 5]. These controllers are included in power system simulation programs as library models [6]. The user of the simulation program can easily incorporate them in a simulation study. The design exercise, when using the generic controllers, is to find the suitable parameters. Small signal stability analysis programs often have the linear equivalent models of the said library models and are capable of incorporating them in a small signal stability study [7].

1.3.1 Custom Control Blocks

Instead of using generic control blocks, a power system engineer can design their own user-written control blocks and implement them in the auxiliary controllers. In such instances, not only the parameters, but also the entire controller model needs to be recreated on a simulation software in order to successfully simulate the system.

Most of the EMT simulation software allows the user to design and implement controllers using fundamental control blocks on the software's user interface. Some small signal stability analysis programs too allow incorporating user-written control blocks to a linearized power system. However, the user-written control blocks are not interoperable between different software, as there are no common protocols. Therefore, even if a user-written controller is available for an EMT software, it needs to

be entirely recreated in the small signal stability analysis program (only if the small signal program has the facility).

1.3.2 Black-boxed Models

With the advent of complex control strategies for power system devices, controller structures and parameters of the controllers are not revealed to the public. When a manufacturer produces a power system component (i.e. a generator), a software simulation model of the device, usually in the EMT simulation domain, is released to the customers instead of publishing the mathematical model and its parameters. This simulation model could be incorporated into a larger power system simulation case. Typically, the larger system is the actual power system to which the new device is planned to be connected. The customer (typically the utility) can then run simulation cases and perform power system studies in the time domain. These software simulation models are black-boxed for proprietary reasons [8]. A limited number of output variables are made available to the user in order to observe time domain response. None of the intermediate controller state variables are available to the user.

It should be noted that the current injection device of such a black-boxed model is essentially one of the well-established models (i.e. synchronous machine, induction machine). Therefore, model data of the current injection device can be assumed as *a priori* knowledge of the device. It is the auxiliary controller that is subjected to proprietary restrictions. Therefore we could expect the manufacturer to reveal the parameters of the current injection device (the reactances and time constants of the physical machine) in the simulation model. The focus of this thesis is, conducting

small signal analysis of a power system in the presence of black-boxed power system device models.

1.4 Motivation

As described above, the linear equivalent model of the power system cannot be derived when there is a black-boxed device, as neither its structure nor the parameters are known to the user, even to manually linearize the system. Almost all new power system devices are made available as black-boxed EMT simulation models and it has driven the power system engineers to either omit the small signal stability analysis and entirely rely on detailed EMT simulations, or incorporate a "typical" controller and perform eigenvalue analysis, whose results are not reliable.

Confining to EMT simulations in a power system study, limits the number of operating scenarios that can be studied, as EMT simulations are time consuming. By observing only the time domain outputs, important dynamics of the system may be missed. Authors of [1] reiterate the importance of linear analysis of power systems.

An as-built black-boxed EMT simulation model can be connected to any known power system and be perturbed to observe the variation of certain variables in the time domain. This allows the model to be subjected to system identification, hence the title of this thesis, *Simulation Based Methods to Determine Linear Equivalent Models of Power System Devices*. Authors of [1] also present a conceptual process of identifying data generated with a simulation program, as presented in Fig. 1.2.

Measurement based linear analyses are dependent on the operating point at which the measurements were done and also limited to observing the frequency and the

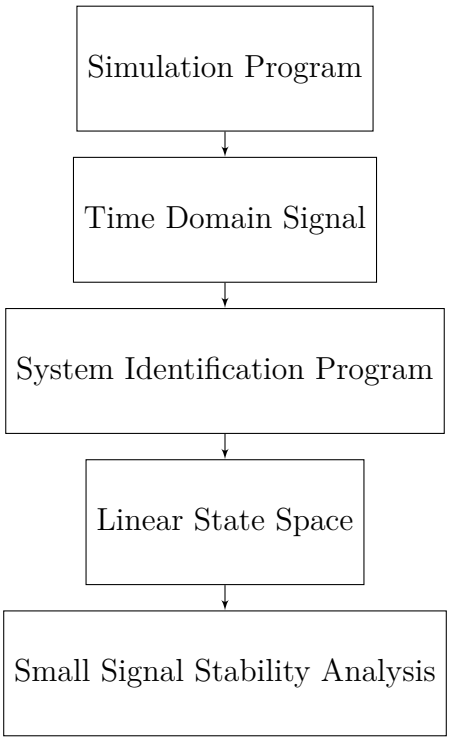

Fig. 1.2: Conceptual process for small signal stability studies from time domain simulations [1]

damping of only the excited modes of the system. The motivation of this research is to explore methods to utilize *a priori* knowledge of a black-boxed power system device and modal information extracted from system identification methods, to develop system matrices of the linear model of the device. Such system matrices may be applied in complete eigenvalue analyses, which give reasonably good insight into a power system.

1.5 System Identification Methods in Power System Applications

Existing system identification methods applied in power systems were closely studied as the research sought to extract advantages of both measurement based and model based linear analysis techniques.

Applications of system identification in power systems found in literature have three main motivations, namely:

1. Deriving a reduced equivalent model for a large power system.
2. Online monitoring of power system modal contents for dynamic security.
3. Validating existing power system models.

In both 1 and 2, the modal content (eigenvalues) of the system is identified at a given operating point. The proposed methods are black-box methods and, utilizing any *a priori* knowledge of the system is minimal.

In 3, the model structure is known and, the focus is to estimate the parameters which may have changed due to aging and undocumented adjustments to the system.

A detailed literature review is presented in Section 3.2.

1.6 Research Goal and Objectives

The goal of this research is to estimate the parameters of a linear equivalent model of a black-boxed power system device, so that the estimated model parameters can be used for small signal stability analysis at any operating point of the device. The

generic schematic of a black-boxed power system model is shown in Fig. 1.3. In order to achieve this, the auxiliary controller transfer functions have to be separately identified. The first approach of anybody trying to solve this problem would be to perform simple system identification between inputs and outputs of each auxiliary controller block. However, the black-boxed EMT simulation models do not always give access to intermediate controller state variables. Therefore such a simple approach would not work.

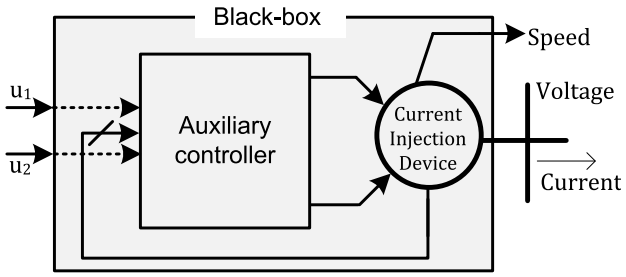

Fig. 1.3: Generic schematic of the black-box model considered in the research

1.6.1 Research Strategy

The strategy followed in this research is of two steps.

1. Identify the modal content (eigenvalues) of a single machine power system.

   The as-built EMT simulation model can be connected to any power system on a simulation software e.g. PSCAD/EMTDC. The dynamics observed by connecting such a model to an infinite bus through a short transmission line are the dynamics of the black boxed model only. The small power system can be brought to a desired steady state operating point by setting the reference

points of active and reactive power (for example), to desired values. The modal content observed by giving a small perturbation to the single-machine-infinite-bus (SMIB) power system would be the composite modal content contributed by the current injection device and the auxiliary controllers at the operating point at which the system was perturbed.

2. Determine an auxiliary controller structure that achieves the same modal content at different operating points.

   Depending on the current injection device, the basic structure of the power system device can be determined, even though the model orders are not known. E.g. for a synchronous machine, it could be concluded that an exciter, a power system stabilizer and a turbine-governor block would constitute the complete auxiliary controller. This knowledge can easily be utilized to simplify the problem. The model orders of each control block differs from each other and their parameters too. The strategy would be to determine the model order and parameters of individual controller block.

The nature of the problem allows the following to be utilized in this strategy.

(i) The ability to perturb the system at multiple operating points

The reference values of active power and reactive power can be changed in the simulation case as desired. Available inputs in the black-boxed model can be used to perturb the system.

(ii) Data of the current injection device

The current injection device is always a well known device whose models are well documented. Their parameters are not subjected to proprietary restrictions.

Therefore, the parameters of the current injection device of the black-box such as, inertia constant, reactances and other time constants of a machine, can be assumed to be available to the user.

1.6.2 Research Goal

Fig. 1.3 is the structure of a power system device, made available as a black-boxed EMT simulation model, that is considered in this thesis. All variables and parameters inside the "black-box" are NOT accessible to the user of the simulation. The model comes with some variables accessible from outside the black-box for time domain analyses. The user has access to some inputs to perturb the model. Parameters of the current injection device inside the black-box are available to the user. Therefore, current injection device transfer functions can be calculated.

The goal of this research is to identify the auxiliary controller transfer functions as shown in the block diagram in Fig. 1.4, so that a complete eigenvalue analysis can be carried out for a power system that includes the given device.

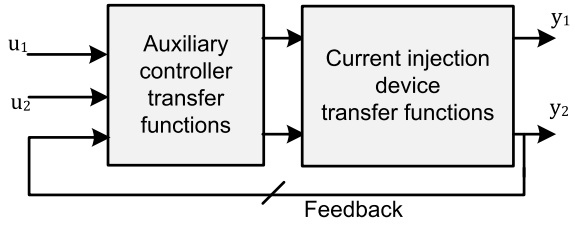

Fig. 1.4: Schematic of linear model of a power system device

1.6.3 Research Objectives

(i) To come up with a system identification procedure incorporating *a priori* knowledge, to identify the equivalent linear model of a single-machine-infinite-bus system of a synchronous machine with auxiliary controllers.

(ii) To come up with a procedure to perform eigenvalue analysis of a multimachine power system which includes a black-boxed synchronous machine, at a given operating point.

(iii) To develop a procedure to accurately identify transfer functions for auxiliary controllers of a synchronous machine i.e. excitation system, governor-turbine block and power system stabilizer.

(iv) To extend the procedure of (iii) to accurately identify transfer functions for auxiliary controllers of a Doubly Fed Induction Generator (DFIG) Wind Turbine i.e. grid-side controllers and rotor-side controllers.

1.7 Thesis Outline

A procedure for determining auxiliary controller transfer functions of a black-boxed power system device has been introduced in this thesis. The procedure focuses on utilizing *a priori* knowledge of the power system device along with system identification results, in order to achieve the goal of determining auxiliary controller transfer functions. The ability of a power system device to be divided into two main subsystems i.e. the operating-point-dependent current injection device, and the auxiliary controller which is operating point independent within a given operating mode, was

also utilized to generate a linear system of polynomial equations that is solved for auxiliary transfer function polynomials using system identification results from multiple operating points. The methodology to achieve the research goal presented in this chapter is developed in the following chapters which have been organized as follow:

Chapter 2 introduces small signal stability assessment of a power system. It describes the importance of carrying out linear analyses in modern power systems and elaborates on advantages and additional insights gained from linear analyses as a compliment to nonlinear power system simulation studies. Chapter 2 also presents the methodology of a software module developed to incorporate small signal stability to RSCAD® EMT simulation software. The software module is capable of reading dynamic data of Library Models used in a simulation case and calculate eigenvalues and eigenvectors of the case.

Chapter 3 reviews existing power system identification methods and explains the advantages of Prony Analysis over other methods. Conventional Prony Analysis is a linear system identification method suitable for modal identification in ringdown situations. Also, conventional Prony Analysis overfits data with spurious modes. Chapter 3 combines a method of using an exogenous input for Prony Analysis with a method to use multiple data windows with expanding lengths, in order to overcome the shortcomings in the conventional method.

Chpater 4 introduces a novel method to utilize *a priori* knowledge of the system to improve the system identification result. Using eigenstructure assignment (ESA), a fictitious controller is designed for the known current injection device subsystem to achieve the modes and mode shapes identified from the method introduced in Chapter 3.

Chapter 5 describes the characteristic of a power system device having an operating-point-dependent current injection device subsystem and an operating-point-independent auxiliary controller subsystem. Mason's Gain Rule is utilized to simplify and decompose a Single Machine Infinite Bus (SMIB) system of a Synchronous Machine into the known and unknown subsystem transfer functions. An important relationship of MIMO system transfer functions has been presented as a theorem, whose proof is presented in Appendix D. The system identification results from multiple operating points, as described in Chapter 4, have been used in the methodology developed in Chapter 5 to solve the linear system of polynomial equations in order to determine the operating-point-independent controller transfer functions.

Chapter 6 extends the methods used in Chapter 5 on a Doubly Fed Induction Generator (DFIG) wind turbine model. The challenges of applying the proposed methods to a system with greater complexity than a synchronous machine model have been presented. A procedure to overcome the challenges, too, has been presented in Chapter 6, suggesting the applicability of the proposed methodology of this thesis to complex power system device models.

The conclusions, contributions and suggestions for future work are presented in Chapter 7.

Chapter 2

Power System Linearization and Linear Analysis

As described in Section 1.2, power system linear analyses fall into two main classes, namely, model based method and measurement based methods. This chapter introduces the concept of linear analysis of power systems and its utility and, focuses on model based linear analysis. The model based methods involve linearization of the nonlinear dynamic equations that describe a power system. The measurement based linear analyses are introduced in Chapter 3

2.1 A Mechanical Analogy

Electromechanical dynamics of a power system are described as analogous to dynamics of a multi-mass pendulum system, shown in Fig. 2.1 [9]. While, in detail, the analogy has many discrepancies, it is a good illustration to grasp the concept of transient stability and small signal stability of a power system.

The pendulum consists of bobs of different masses, suspended from a network of elastic strings. The bobs are analogous to generators of the power system with

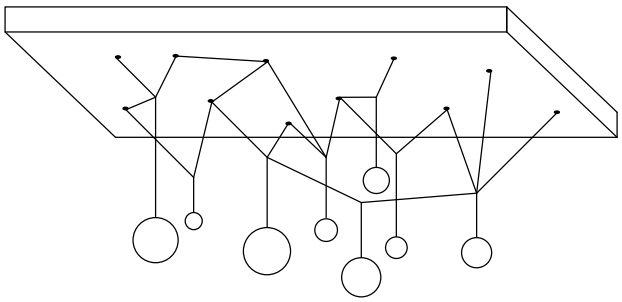

Fig. 2.1: Multimass pendulum

different inertia. The elastic strings represent the transmission lines of the power system. The pendulum system at static steady state represents the power system operating at steady state. Depending on the weights of the bobs and the topology of the string connections, all the strings are loaded with a tension below their respective loading limits, representing the loading of transmission lines of a power system. A disturbance, such as cutting one of the strings, causes the bobs to start moving. Depending on the initial topology of network of strings and the masses of the bobs, the the bobs are subjected to coupled motions. Fluctuations in the tensions of the strings may cause the strings to violate their loading limits, which may cause breakage of one or more strings. The system may settle to another static steady state point or, breakage of strings may cascade until all the bobs are disconnected from the system. This phenomenon is a classic illustration of dynamics of a power system subsequent to a disturbance, including that of a cascading failure. The simplicity of this pendulum system helps to grasp the concept of power system stability.

The bobs have oscillatory motions:

(i) when a relatively small disturbance is given to the system.

(ii) just before settling to a static steady state, subsequent to a large disturbance (post fault).

Accordingly, the tensions of the strings too fluctuate in an oscillatory manner. This motion is analogous to the small signal dynamics of a power system. Motion of each bob contributes to the resultant oscillation with its own frequency and some motions maybe tightly coupled. These oscillations are referred to as oscillatory modes and are represented by pairs of complex eigenvalues of a representative linear model of the system.

The oscillatory modes may be either well-damped (complex eigenvalues with large negative real part), low-damped (complex eigenvalues with small negative real part) or negatively-damped (complex eigenvalues with positive real part). Existence of at least one negatively damped oscillatory mode would cause in an oscillation whose amplitude would grow over time and cause the system to collapse. If the linear mathematical model of the system at the static steady state prior to the small disturbance could be obtained, the eigenvalues of the system can be calculated and the oscillatory dynamics could be predicted. In order to obtain the linear model of the pendulum system, the masses of the bobs, lengths of the strings, spring constants of the strings (dynamic data) and the initial tensions of the strings at the static steady state (operating point data) are required. Similarly, reactances, time constants and model structures of devices and controllers (dynamic data) of the power system and power flow (operating point) data are required to develop the linear system of a power system.

2.2 Linear Analysis of the Swing Equation

The swing equation describes the electromechanical dynamics of a power system. Eq. 2.1 is the swing equation for a single machine power system.

$$P_T - P_G = \frac{2H}{\omega_0}\ddot{\delta} + D\dot{\delta} \tag{2.1}$$

where

P_T = Turbine power (pu)

P_G = Generator power (pu)

H =Inertia constant (s)

ω_0 =Synchronous speed (rad/s)

δ =Rotor angle (rad)

D =Damping constant for the generator (s/rad)

It is fair to assume that the transient turbine power is constant. However the transient generator power is governed by Eq. 2.2.

$$P_G = \frac{|V||E|}{X'_d} sin(\theta) + \frac{|V|^2}{2}\left(\frac{1}{X_q} - \frac{1}{X'_d}\right) sin(2\theta) \tag{2.2}$$

where

V = Terminal voltage of the generator

E = Internal voltage of the generator

X'_d =d-axis transient reactance

X_q =q-axis reactance

θ =Angle between V and E voltage vectors

The angle θ is a function of δ. For example, for the case of a single machine system, $\theta = \delta$. This leads the swing equation to be a coupled nonlinear differential equation. There is no analytical solution to this problem. There are two main methods to analyze this problem, namely the *indirect method* and the *direct method*

2.2.1 Nonlinear Analysis

Indirect method

The indirect method is numerically integrating the differential equations from an initial point. A power system simulation software carries out this function. This is the only practical method to solve a nonlinear coupled dynamic system, especially considering the practical size of power systems. The stability of the system may be determined by visually observing the deviations of state variables in time.

Direct method

The direct method of analyzing a nonlinear coupled dynamic system i.e. a power system, does not *actually solve* the system. Instead, the features of various energy based functions are analyzed to determine the stability of a system. The most popular application of direct methods in power system is the *equal-area-criterion* which is essentially applied to a single machine power system only. Lyapunov method and

Transient Energy Function (TEF) methods are examples for direct methods that have been used in power system applications [10, 11, 12, 13].

2.2.2 Linearization

An autonomous dynamic system of n^{th} order can be described by n first order differential equations given by:

$$\dot{\mathbf{x}} = f(\mathbf{x}, \mathbf{u}) \tag{2.3}$$

where $\mathbf{x} \in \mathbb{R}^n$ is the state vector and $\mathbf{u} \in \mathbb{R}^r$ is the inputs vector.

For a steady state operating point

$$\dot{\mathbf{x}} = f(\mathbf{x_0}, \mathbf{u_0}) = 0 \tag{2.4}$$

where $\mathbf{x_0}$ and $\mathbf{u_0}$ are the steady state state and input vectors respectively.

Let Δ represent a small perturbation to the variables from the steady state values.

$$\mathbf{x} = \mathbf{x_0} + \Delta\mathbf{x} \tag{2.5}$$

$$\mathbf{u} = \mathbf{u_0} + \Delta\mathbf{u} \tag{2.6}$$

From Eq. 2.3:

$$\dot{\mathbf{x}} = f(\mathbf{x_0} + \Delta\mathbf{x}, \mathbf{u_0} + \Delta\mathbf{u}) \tag{2.7}$$

From Truncated Taylor Series Expansion of the i^{th} differential equation, where higher

order terms of the complete Taylor's Series are neglected:

$$\dot{x}_i = \dot{x}_{i0} + \Delta\dot{x}_i \tag{2.8}$$

$$\dot{x}_i = f_i(\mathbf{x}_0, \mathbf{u}_0) + \frac{\partial f_i}{\partial x_1}\Delta x_1 + \frac{\partial f_i}{\partial x_2}\Delta x_2 + ...\frac{\partial f_i}{\partial x_n}\Delta x_n + \frac{\partial f_i}{\partial u_1}\Delta u_1 + \frac{\partial f_i}{\partial u_2}\Delta u_2 + ...\frac{\partial f_i}{\partial u_r}\Delta u_r \tag{2.9}$$

Since $\dot{x}_{i0} = f_i(\mathbf{x_0}, \mathbf{u_0})$, from Eq. 2.8 and 2.9

$$\Delta\dot{x}_i = \frac{\partial f_i}{\partial x_1}\Delta x_1 + \frac{\partial f_i}{\partial x_2}\Delta x_2 + ...\frac{\partial f_i}{\partial x_n}\Delta x_n + \frac{\partial f_i}{\partial u_1}\Delta u_1 + \frac{\partial f_i}{\partial u_2}\Delta u_2 + ...\frac{\partial f_i}{\partial u_r}\Delta u_r \tag{2.10}$$

Such a linearization yields the linearized state space

$$\Delta\dot{\mathbf{x}} = \mathbf{A}\Delta\mathbf{x} + \mathbf{B}\Delta\mathbf{u} \tag{2.11}$$

The outputs of the linear model maybe described by the following state-output relationship.

$$\Delta\mathbf{y} = \mathbf{C}\Delta\mathbf{x} \tag{2.12}$$

Linearizing the Swing Equation: Example

Several simplifications have been considered, for simpler demonstration of applying the above linearization technique to the swing equation in Eq. 2.1 for a single machine system.

Assuming there is no mechanical damping in the system Eq. 2.1 can be written as:

$$P_T - P_G = \frac{2H}{\omega_0}\ddot{\delta} \tag{2.13}$$

Neglecting the effect of saliency of the machine, Eq. 2.2 can be written as:

$$P_G = \frac{|V||E|}{X'_d} sin(\delta) \tag{2.14}$$

From Truncated Taylor's Series Expansion shown in Eq. 2.10, Eq. 2.13 can be linearized as:

$$\Delta P_T - \left(\frac{\partial P_G}{\partial \delta}\right)_0 \Delta\delta = \frac{2H}{\omega_0}\Delta\ddot{\delta} \tag{2.15}$$

Further simplifying the model by assuming the bus voltage magnitude $|V|$ and internal voltage magnitude $|E|$ are constant during the transients:

$$\left(\frac{\partial P_G}{\partial \delta}\right)_0 = \frac{|V||E|}{X'_d} cos(\delta_0) \tag{2.16}$$

$$\Delta P_T - \frac{|V||E|}{X'_d} cos(\delta_0)\Delta\delta = \frac{2H}{\omega_0}\Delta\ddot{\delta} \tag{2.17}$$

Also, for first order differential equation representation:

$$\Delta\dot{\delta} = \omega_r - \omega_0 = \Delta\omega_r \tag{2.18}$$

$$\Delta\ddot{\delta} = \Delta\dot{\omega}_r \tag{2.19}$$

Therefore the complete linearized swing equation, with the simplifications, is:

$$\begin{bmatrix} \Delta\dot{\delta} \\ \Delta\dot{\omega}_r \end{bmatrix} = \begin{bmatrix} 0 & 1 \\ \frac{|V||E|\omega_{r0}}{2HX'_d} cos(\delta_0) & 0 \end{bmatrix} \begin{bmatrix} \Delta\delta \\ \Delta\omega_r \end{bmatrix} + \begin{bmatrix} 0 \\ \frac{\omega_0}{2H} \end{bmatrix} \Delta P_T \tag{2.20}$$

2.3 Complete Small Signal Stability Analysis of a Multimachine Power System

The linear model of the power system takes the form of Eq. 2.11 and 2.12. Given the causal property of a power system, the system is strictly proper. For all power system output variables i.e. generator speeds, voltages and currents, Eq. 2.12 is valid.

2.3.1 Modal Decomposition of the State Space

The system matrix **A** describes the coupling between all state variables in the system. If there exists a matrix **Φ** that diagonalizes **A** by a similarity transform, the resulting similar matrix is the new system matrix of the system with a basis with states that are decoupled from each other. The diagonal similar matrix would be the eigenvalue matrix of the system matrix **A** and, **Φ** would be the corresponding right eigenvector matrix. Such a diagonalization of the system is known as modal decomposition [14]. Each real eigenvalue represents a stationary mode and each pair of complex eigenvalues represent an oscillatory mode of the system.

The modal decomposition of a typical linear model of a power system is given below.

Let the right eigenvector matrix be:

$$\mathbf{\Phi} = [\ \phi_1 \quad \phi_2 \quad ... \quad \phi_n\ ] \tag{2.21}$$

where the right eigenvector ϕ_i and the corresponding eigenvalue λ_i has the relation-

ship:

$$\mathbf{A}\phi_i = \lambda_i \phi_i \tag{2.22}$$

Also, the left eigenvector matrix $\mathbf{\Psi}$ is given by:

$$\mathbf{\Psi} = \mathbf{\Phi}^{-1} \tag{2.23}$$

Let

$$\Delta\mathbf{x} = \mathbf{\Phi}\Delta\mathbf{z} \tag{2.24}$$

Then, from Eq. 2.11 and 2.24

$$\mathbf{\Phi}\Delta\dot{\mathbf{z}} = \mathbf{A}\mathbf{\Phi}\Delta\mathbf{x} + \mathbf{B}\Delta\mathbf{u} \tag{2.25a}$$

$$\Delta\dot{\mathbf{z}} = \mathbf{\Phi}^{-1}\mathbf{A}\mathbf{\Phi}\Delta\mathbf{z} + \mathbf{\Phi}^{-1}\mathbf{B}\Delta\mathbf{u} \tag{2.25b}$$

From the relationship in Eq. 2.22, $\mathbf{\Lambda}$ can be defined as the diagonal matrix of eigenvalues of $\mathbf{A}$.

$$\Delta\dot{\mathbf{z}} = \mathbf{\Lambda}\Delta\mathbf{z} + \mathbf{\Psi}\mathbf{B}\Delta\mathbf{u} \tag{2.26}$$

From Eq. 2.12 and 2.24

$$\Delta\mathbf{y} = \mathbf{C}\mathbf{\Phi}\Delta\mathbf{z} \tag{2.27}$$

where $\mathbf{C}\mathbf{\Phi}$ can be described as the mode observation matrix.

2.3.2 Mode Shape and Participation Factors

Mode shape is defined as the "relative activity of state variables when a particular mode is excited" [3]. From Eq. 2.27 it could be seen that right eigenvector gives the mode shape.

From Eq. 2.24 and 2.23

$$\Delta \mathbf{z} = \mathbf{\Psi} \Delta \mathbf{x} \tag{2.28}$$

From Eq. 2.28 it could be seen that the left eigenvector ψ_i^T identifies the weight of the original state variables displayed in the ith mode. Therefore, p_{ki}, the product of elements of the right and left eigenvectors as given by Eq. 2.29

$$p_{ki} = \phi_{ki} \psi_{ik}^T \tag{2.29}$$

where

ϕ_{ki} = kth element of right eigenvector ϕ_i

ψ_{ik} = ith element of left eigenvector ψ_k^T

gives the measure of the relative participation of the kth state variable in the ith mode, and vice versa. This relative measure is defined as the *participation factor*. Participation factor analysis is an important part of a complete small signal stability analysis. It allows to identify the following:

(i) Contribution of machines to the oscillations

(ii) Interactions between different machines

(iii) Modes contributed by systems other than rotors of the machines

(iv) Modes contributed by controllers and their interactions

2.3.3 Relationship Between Modes and States

Fig 2.2 is a block diagram illustration of a generic dynamic system with feedback control. A set of linearly independent state variables describes the state space of a dynamic system. The plant, the transducers and the actuators are usually modeled using the physics that governs their dynamics. Thus the state variables of the plant have a quantifiable physical interpretation. The controllers maybe digital implementations of algorithms, whose state variables may not have a quantifiable physical interpretation. The system matrix $\mathbf{A}$ describes the interrelationship between different state variables of the system. It is important to note that any similar matrix of $\mathbf{A}$, given by $\mathbf{T^{-1}AT}$ where $\mathbf{T}$ is an arbitrary invertible matrix, also describes the dynamics of the original state space but the state variables do not necessarily have a physical meaning. They are any arbitrary linear relationship of state variables of the original state space.

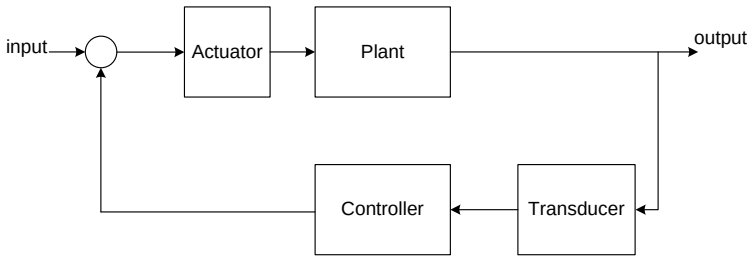

Fig. 2.2: Generic Control System

In a participation factor analysis, it is important to identify which state variable

contributes to which mode. In analyzing the participation of controllers in modes, it is sufficient to identify which controller is participating in what mode. The exact state variable of a controller does not have any significance as controllers are implementations of algorithms where the resulting state variables are fictitious. It is fair to attribute the dynamics of transducers and actuators too to the dynamics of the complete controller. This distinction between plant state variables and controller state variables is utilized in this research.

2.4 Small Signal Stability Analysis Tool for EMT Power System Simulation Software

EMT simulation software like PSCAD and RSCAD do not have the capability of eigenvalue analysis incorporated to them. An attempt to include eigenvalue analysis into PSCAD has been reported in [15]. SSAT by Powertech Labs is a commercially available standalone software that performs eigenvalue analysis of power systems. Input to this software is the power flow data in the RAW file format and dynamic data in the DYR file format. RAW and DYR are well known file formats of the transient simulation software, PSS/E. DYR file contains parameters of standard power system models. This lacks the ability to incorporate user-written models which are not included in the library.

This section presents a demonstration of incorporating small signal stability analysis to the EMT simulation software, RSCAD, developed by RTDS Technologies. It is shown that, it is not essential to access internal workings of the software to perform a complete eigenvalue analysis. A separate software module, which runs on

the MATLAB platform, extracts the network and dynamic data from files generated by RSCAD in the process of compiling the simulation case. The RSCAD user does not need to arrange the simulation case in any special way for the purpose of using this software module. The said software module is referred to as the *SSSA Tool* throughout this Chapter.

2.4.1 Data Extraction from the RSCAD Simulation Case

RSCAD - An Overview

RSCAD comprises of two main modules, namely, the Draft Module and the Runtime Module. The Runtime Module allows the simulation to be controlled either manually by the user or automatically, using scripts. Monitoring of simulation results and data acquisition is also a function of the Runtime Module. The Draft Module is the software where the simulation case is defined. It is a graphical interface where the user can place power system components chosen from the *component-library*. The library includes standard power system device and controller models as well as fundamental circuit components and fundamental control components i.e. integrators and time-delay blocks. An initial power flow calculation included in the software initializes the voltages and angles of all buses. The draft case must be compiled before it is passed to the simulator for real time simulation, which is then controlled and monitored by RSCAD Run-time Module.

Basic Structure of a Draft Case

The Draft Case has current injection devices i.e. synchronous generators, STATCOMs etc, and loads connected to the electrical network. All current injection devices are

connected to buses in the network. Any bus can have one or more current injection devices connected to it. The current injection devices have controllers connected to them. The controllers may be of feedback type with measurements of the own device bus (local signal feedback) or with remote signal feedback. In terms of the control action, each control block can be identified with only one current injection device. Therefore, the control block can be identified using the bus connection of the associated current injection device. The most straightforward way is to place *generic models* on the *canvas* and build the power system to be studied. Instead of using generic models the user can also design custom circuit models and control blocks, on the draft canvas, using the fundamental circuit and controller components available in the library.

RSCAD Files Available to the User

After running the power flow and compiling a draft case in RSCAD, several files are generated, to which the user has access. Among these are the RPT file and the DTP file. These files can be read as text files. The RPT file includes network data in the form of a converged power flow. The DTP file includes all other data related to the draft case, including all dynamic data. The dynamic data is written to the file as clusters of datasets for each component that constitutes the draft case. E.g. data of each synchronous generator in the draft case appears as a single cluster in the DTP file. Also, a simple summation block appears as a single cluster. These data sets include a unique keyword that identifies the power system or controller component. The parameters of each component are organized in an order unique to that component. Identifying the keyword and extracting data clusters of each

component and then identifying the unique order in which the data set is written and storing them in the SSSA Tool software module are the key steps of the data extraction process. The SSSA Tool also writes the extracted data to RAW and DYR formats so the data of RSCAD case can be fed to simulation software like PSS/E, SSAT and TGSSR.

Generic Models

In this chpater, the term *generic model* is used to identify mathematical models of power system components and control blocks whose models are well known and often included in libraries of power system simulation software (e.g. 6th order round rotor synchronous generator model, GENROU). Dataset for a generic model in the RSCAD case can be readily identified in the DTP file by the specific keyword for that model. Datasets of current injection devices and control blocks include the parameters of the model and the bus which it is connected to. Since the structure of the generic model is known, the linearized dynamic equations can be written in state space representation.

Data Extraction

The RPT and DTP files are read word by word, by the file-read function of the SSSA Tool. All *words* are stored sequentially. Then keywords for different types of components are searched for. Upon finding keywords, different functions act upon the extracted sequence of *words*, in order to extract the data from the unique order in which the parameters and the bus number information are written in the DTP file.

Formulation of Linearized State Space from Extracted Data

The current injection device and its controllers together can be identified as the *device*. The devices can be identified with the bus it is connected to. The extracted data is then passed to different functions to determine the coefficients of the device equations i.e. $\mathbf{A}_D$, $\mathbf{B}_D$, $\mathbf{E}_D$, $\mathbf{C}_D$ and $\mathbf{D}_D$. Then the linearized state space for the multi-machine power system is developed.

2.4.2 Prototype Test Results of SSSA Tool

The IEEE benchmark 12-bus test system is used to test the prototype of the software module. The prototype software module is able to extract the network data and dynamic data. The test system is implemented on RSCAD and compiled. The linearized system has 41 states hence 41 eigenvalues are to be calculated. The SSSA Tool was run and the eigenvalues obtained are plotted on Fig. 2.3 against the eigenvalues obtained from SSAT®.

The RAW file and the DYR file generated by PSS/E software for the power system with the same parameters, were identical to the same type of files generated by the SSSA Tool. This validates the data extraction process. As seen on Fig. 2.3, the SSSA Tool calculates the same eigenvalues as SSAT ® does. This validates the SSSA Tool's multi-machine power system small signal stability analysis for the limited number of generic models it can currently handle.

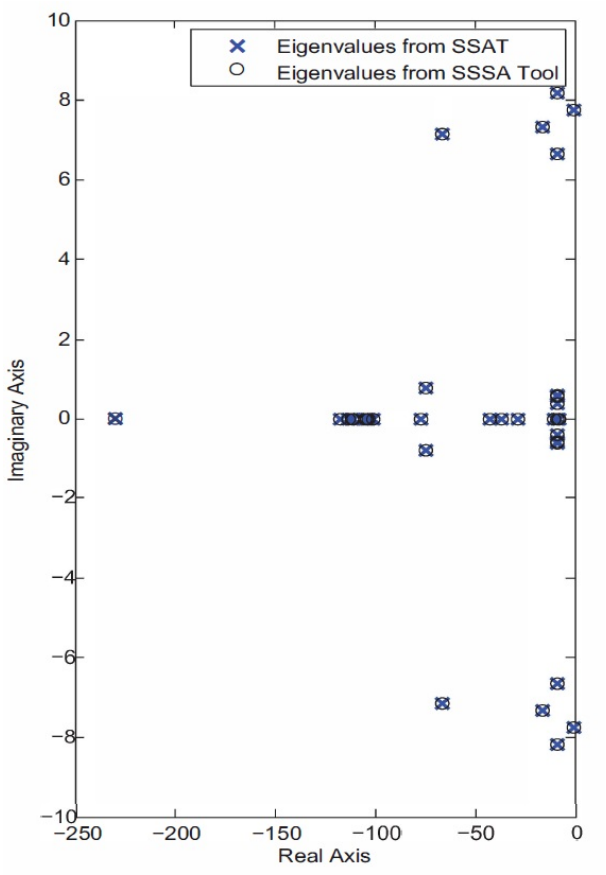

Fig. 2.3: Validation of eigenvalues obtained from SSSA Tool against SSAT®

2.4.3 Inclusion of User-Written Control Blocks to Eigenvalue Analysis

As described earlier, RSCAD users can build custom controllers using fundamental control blocks from the RSCAD library. The prototype of the SSSA Tool has the ability to extract data of fundamental control blocks and include them in the eigenvalue analysis. The prototype software can identify the transfer function components and summing junctions. Unlike generic models, the datasets of these fundamental

control blocks in the DTP file do not identify themselves with the current injection device they are associated with. Instead, the datasets include information of the signal flow. Therefore, it is required to store all the signal variables in the draft case and map them to the state variables to determine the topology of custom control blocks. Signal variables are all the available inputs and outputs of generic models and fundamental control blocks. The signal variable names are assigned, either manually by the user or automatically by RSCAD. In order to incorporate these custom control blocks in the state-space of the linearized power system, dynamic equations related to the fundamental control blocks need to be determined. The procedure followed by SSSA Tool is given in the flowchart in Fig. 2.4. The example provided below shows how custom control blocks are used in place of a generic exciter model found in the library. Fig. 2.5 shows the RSCAD Draft view of using a generic model of an exciter from the Generator Controls Library and Fig. 2.6 shows the same exciter modeled using fundamental control blocks, excluding the nonlinear limiters.

Example

The control system shown in Fig. 2.6 is considered. It has two time-delay blocks and one lead-lag block. Signal variables V_t, p, q, r, V_{ref} and E_fd are shown on the figure.

Eq. 2.30 and 2.31 are included in the SSSA Tool as attributes of the generic functions for Time-Delay Block and Lead-Lag Block respectively. Whenever the simulation case includes any of these control blocks, these equations are used to develop the linearized state-space.

$$\Delta \dot{y_1} = \frac{-1}{T}\Delta y_1 + \frac{G}{T}\Delta u_1 \tag{2.30}$$

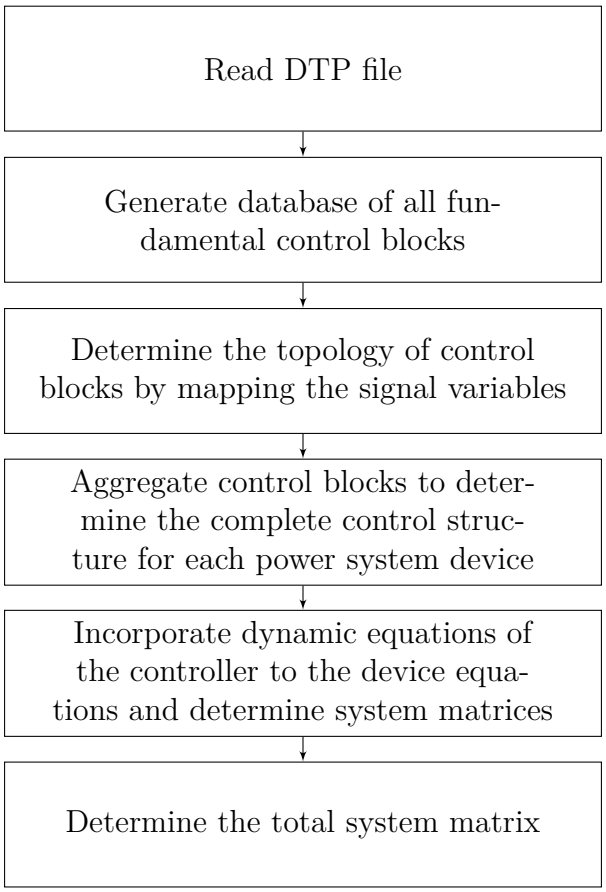

Fig. 2.4: Procedure of incorporating fundamental control blocks to the linearized power system, in SSSA Tool

$$\Delta \dot{y}_2 = \frac{-1}{T_1}\Delta y_2 + \frac{G_2}{T_1}\Delta u_2 + \frac{G_2 T_2}{T_1}\Delta \dot{u}_2 \tag{2.31}$$

where

y_1, y_2 = outputs

u_1, u_2 = inputs

T, T_1, T_2 = time constants

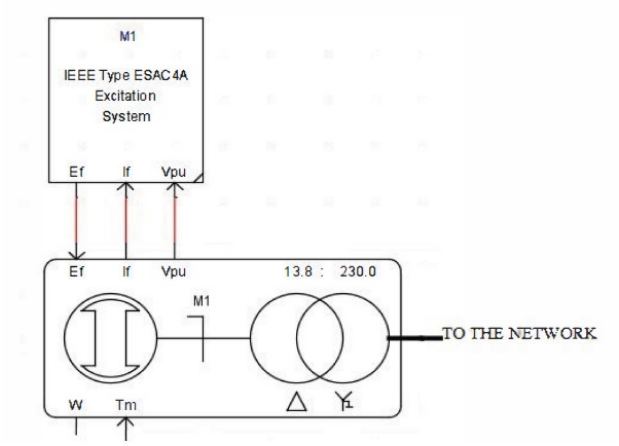

Fig. 2.5: RSCAD Draft view of ESAC4A generic exciter model connected to a synchronous generator

G_1, G_2 = gains

The SSSA Tool uses information in tables 2.1 and 2.2 and apply the appropriate parameters in the Eq. 2.30 and 2.31 and generates the system shown in Eq. 2.32, which is part of the device equations for generator associated with the control system.

$$\begin{bmatrix} \Delta\dot{p} \\ \Delta\dot{p} \\ \Delta\dot{E}_{fd} \end{bmatrix} = \begin{bmatrix} \frac{-1}{T_R} & 0 & 0 \\ \frac{-G_A}{T_R} & \frac{-1}{T_A} & 0 \\ 0 & \frac{G_1}{T_1} - \frac{G_1 T_2}{T_1 T_A} & \frac{-1}{T_1} \end{bmatrix} \begin{bmatrix} \Delta p \\ \Delta r \\ \Delta E_{fd} \end{bmatrix} + \begin{bmatrix} \frac{1}{T_R} & 0 \\ 0 & \frac{G_A}{T_A} \\ 0 & \frac{G_A G_1 T_2}{T_A T_1} \end{bmatrix} \begin{bmatrix} \Delta V_t \\ \Delta V_{ref} \end{bmatrix} \tag{2.32}$$

Subsequently, the device matrices including custom control blocks are processed, to derive the system matrix.

The prototype SSSA Tool was validated for inclusion of custom control blocks, by replacing all generic models of exciters in the test system with their respective

Table 2.1: Database generated for the control system in Fig. 2.6

Component ID	Block 1	Block 1	Block 1	Block 1
Component Type	Time-Delay	Summing	Time-Delay	Lead-Lag
Parameters	$G = 1$ $T = T_R$	-	$G = G_A$ $T = T_A$	$G = G_1$ $T_1 = T_1$ $T_2 = T_2$
No. of States	1	0	1	1
Input Signal Variables	V_t	p, V_{ref}	q	r
Output Signal Variables	p	q	r	E_{fd}

Table 2.2: Signal Variable data for control system in Fig. 2.6

Signal Variable	Associated Bus	External Input	Gain
V_t	Bus 1	-	+1
p	-	-	-1
V_{ref}	-	Yes	+1
q	-	-	+1
r	-	-	+1
E_{fd}	Bus 1	-	+1

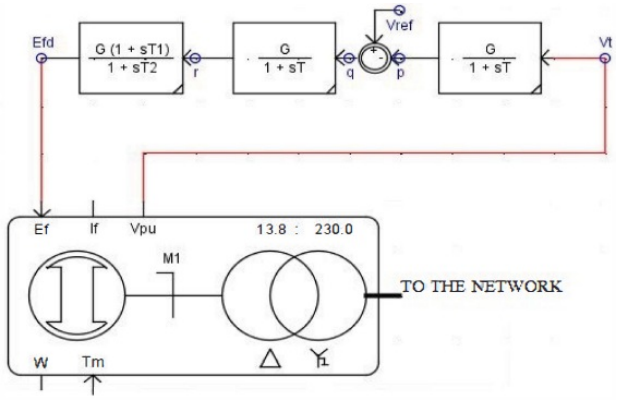

Fig. 2.6: RSCAD Draft view of ESAC4A type exciter (excluding limiters), built using fundamental control blocks, connected to a synchronous generator

custom control blocks (as in Fig. 2.6) and comparing the final system matrices. The exact same system matrix was achieved.

2.4.4 Common Protocol for Further Development of SSSA Tool

In order to include all generic models available in RSCAD in the SSSA Tool, each generic model should be linearized manually and included in the SSSA Tool library. Each component may be added as a function file to the SSSA Tool. The functions need to be written with correct sequence of inputs and outputs.

2.5 Chapter Summary

A mechanical analogy was used in this chapter to explain transients and small signal dynamics of a power system. The methodology to develop the small signal model

is explained. The methodology of a software module developed to incorporate small signal stability analysis to RSCAD EMT simulation software has been presented. The software module can only perform linear analysis of simulation cases that use only generic library models. While the importance of complementing small signal stability analyses with EMT simulations of power systems is elaborated, the exercise demonstrates the usability of an inbuilt small signal stability tool in an EMT simulation software. The software tool's applicability is limited to simulation cases with only generic library models. In the following chapters, a procedure to determine the linear models of black-boxed power system device simulation models is developed.

Chapter 3

Transfer Function Identification by Expanding Window Prony Analysis

3.1 History

History of System Identification Methods (SIM) in power systems and power system components goes to as far as 1930s. Open circuit and short circuit tests were carried out on a synchronous machine to determine its parameters i.e. direct and quadrature axes reactances and time constants, as reported in a classical paper by Wright in 1931 [16]. A large body of literature on system identification of more complex power system components, including controllers, started appearing in late 1960s. Estimation of the transfer function of the excitation system of a synchronous machine, using measurements, is presented in [17]. A pseudo-random binary signal was used as the input in [18], to identify the total transfer function and the subsystem transfer functions of a synchronous machine. These early works were mainly focused on parameter estimation using field measurements. They lacked the use of advanced computing and advanced signal processing algorithms available today.

3.2 Applications of System Identification in Power Systems

In Section 1.5 a list of different motivations for use of system identification in power system applications is given. A literature review of these applications is presented in this section.

3.2.1 Deriving reduced equivalent models for large power systems

When simulating a very large power system of tens of thousands of nodes, the computation burden is very high, hence the long time taken for simulation. Distant or external parts of the power system cannot be neglected because of their contribution to the dynamics of the system i.e. oscillations. A reduced linear model of such a distant or external system may replace the large system. In order to determine the linear equivalent model, two approaches may be used. One is the calculation of the state space model of the external system using Taylor Series Expansion method, which requires all data of the system [19]. The other approach is system identification of the large system which reveals the low-damped modal content in the power system. Authors of [19] have summarized techniques that have been developed and published since the introduction of Prony Analysis to power system application by Dr. J.F. Hauer in 1990, until 2012. (Details of Prony Analysis is given in Section 3.3)

Auto Regressive Moving Average (ARMA) linear identification method [20] and Prony Analysis in power system applications, have been compared in [21]. It concludes that Prony Analysis has more numerical robustness in the algorithm while ARMA is

more simple. It recognizes that both methods identifies spurious modes which need to be carefully removed from the final linear model. This is caused by the "overfitting" done by the two algorithms. In [22], Prony Analysis's superiority over ARMA is presented.

A powerful alternative to Prony Analysis has been presented in [23]. The proposed algorithm has been named as Minimum Realization Algorithm in [23]. In subsequent papers [24, 25] the same algorithm has been referred to as Matrix Minimal Realization and Eigensystem Realization Algorithm (ERA). ERA had previously been applied in aerospace applications [19]. A formal mathematical comparison between ERA and Prony Analysis has not been done as yet. However, observers claim that the difference between the two methods are only *superficial* [23, 24]. The ability to form a Multi-input-Multi-output (MIMO) state space from ERA has been claimed as an advantage over Prony Analysis. However, the modal content identified by both methods are the same [25].

Steiglitz-McBride Algorithm has been used in [26] for identification of low-order linear power system models from EMT simulations. The paper claims that it has similar performance to Prony Analysis. However, in a performance comparison done between Steiglitz-McBride Algorithm, ERA and Prony Analysis in [27], it has been firmly concluded that ERA and Prony are superior identification methods in power system applications over Steiglitz-McBride Algorithm. It has been reported that the performance of ERA and Prony Analysis are similar [27]. Prony Analysis and ERA have been tested in noisy environments and an algorithm has been proposed to remove the effects of noise and to remove spurious modes [28].

In more recent publications, MIMO system identification has gained more at-

tention. The pioneer work related to MIMO linear identification in power systems has been presented in [29]. It is a subspace identification method. In [30], a MIMO transfer function identification based on multichannel ARMAX method is proposed. Authors of [31], a very recent paper, compares the two algorithms, among other things. In more recent publications, methods of utilizing PMU data for MIMO linear system identification has been presented. It should be noted that the MIMO methods require a probing signal to the power system and the state variables in the derived state space does not represent any physical state but fictitious states whose physical meaning cannot be determined. In other words, the basis of the derived state space has no physical meaning.

The nature of the problem addressed in this research can be described as taking the form of recovering the linear state space of a system. The preferred approach for such a problem is subspace identification [32]. Subspace identification methods i.e. N4SID [33] and, recursive stochastic subspace identification [34], have been employed to identify a state space for a power system. Subspace methods only allow to identify the modes and mode shapes of the system at the given operating point. The states realized in subspace methods lack a physical description. All these methods reported in the literature lack the ability to incorporate any a-priori knowledge of the system [35].

3.2.2 Online monitoring of power system modal contents for dynamic security assessment

Most of the recent literature related to system identification of power systems focus on online monitoring of modes in the system. The purpose is to identify insufficiently

damped oscillatory modes, especially, electromechanical modes. Such monitoring requires fast calculation of modes but only the low damped critical modes are of interest.

Prony Analysis, has been proposed for the purpose of oscillation monitoring for dynamic security assessment of power systems[36, 37, 38]. A modified form of Prony Algorithm, used as the candidate System Identification Method in this thesis, is presented in detail, in Section 3.3.

Kalman filter uses an auto-regressive (AR) model to approximate the observed data. The coefficients of the AR model are determined such that the error between the actual value and the predicted value by the model is minimized. This is achieved using a recursive algorithm. Once the coefficients are found, the roots of the characteristic equation give the eigenvalues of the system. Thus, the Kalman filter algorithm can be used to determine the modal content in the output signals of transient simulation programs. A detailed comparison between the Kalman filters and the Prony analysis can be found in [39].

Kalman filter algorithm has been used in [40], to track the most dominant oscillatory mode in the real-time environment. In [41], the algorithm has been improved to track multiple oscillatory modes.

Reference [42] presents an algorithm using the Fourier Transform (FT) to determine the frequencies and damping ratios of the dominant modes present in the outputs of transient simulations. First, the frequency content of a ring-down oscillation is obtained via the frequency spectrum. Based on the dominant frequency, the length of a data window and the gap between the adjacent data windows are determined. FT is applied on these multiple data windows and the real part of the

eigenvalue associated with the oscillation mode is determined by taking the ratio of the FTs at the selected oscillation frequency.

The damping ratio estimations of this approach are sensitive to the length and the separation between the data windows. Furthermore, the presence of multiple modes in the ring-down oscillation interferes on the calculated values. Therefore, it is recommended to eliminate the neighbouring model interactions before the analysis. An improved algorithm using the FT applied on multiple measurements in power systems is proposed in [43] to monitor the power system oscillations in real-time. It is shown in [43] that the damping ratio of an oscillatory mode can be determined as the rate of decay of its energy.

The discrete short time Fourier transform (STFT) is essentially a discrete FT of a sampled signal over a short time data window. Thus, at each time instant, the STFT is related with the FT of the signal in the vicinity of that time instant, which makes it an appropriate tool to determine the time-dependent variation of a spectral content of a signal. The usage of STFT to determine the time-frequency distribution of energy of electromechanical oscillations is given in [44]. The frequencies of the dominant modes are identified by the peaks of the energy spectrum. A scenario of oscillatory instability is represented by an unbounded increase in the kinetic energy determined at the dominant frequency. This method is more suitable to observe the patterns of system dynamic behaviour. Nevertheless, it lacks providing an accurate damping estimation.

3.2.3 Validating existing power system models

One of the main motivations of using system identification in power systems is validating models of the existing power system devices in the system. This can extend to validating the as-built detailed simulation model built to represent a new power system device.

Power system devices, once installed, can be subjected to changes due to aging etc. Their controller parameters too may be changed without proper documentation. When a power system simulation does not agree with the actual dynamic response, the result may be catastrophic. In [45], the discrepancy between the simulation and the actual system response, at the 1996 system outage in the WSCC electric power system, affecting 7.49 million customers in North America, has been reported. The importance of validating the power system models to achieve a good fit with the measured data is elaborated. Report of the IEEE PES Task Force on Wind Generation Model Validation 2011 [46] sets out 3 steps for the model validation process.

Step 1 Define the model and model structure to be used for modeling the device(s) under study - in the case of this research: a wind turbine generator (or an entire wind power plant).

Step 2 Collect recorded/measured data from the actual device(s) to be modeled. Such data is typically collected either from a set of "staged" tests (e.g., purposely injecting a small change in the reference set-point of a controller such as the voltage set-point of a voltage regulator) or through online monitoring of the device to see its response to naturally occurring disturbances (e.g., in the case of this research: to see the response of the wind power plant to disturbances on

the electric power system, etc.).

Step 3 Attempt to simulate the same set of tests/events as occurred/ forced during the data collection process using the model(s) in step 1 and compare the simulated response of the device to the recorded response in step 2. If the two responses match adequately, we have a validated model.

This approach is *prima facie* similar to the research strategy set out in Section 1.6.1. However, defining the model structure (step 1) limits the degree of freedom of the order of the system. Attempting to achieve a good fit (step 3) as suggested is more of a trial-and-error tuning procedure. These 3 steps with Levenberg-Marquardt-Fletcher algorithm have been used to find the parameters of a doubly-fed induction generator [47].

In [48], a method to use wide area measurements to identify the need to re-tune the models is suggested. In [49] a hybrid method to bridge the simulation world and the measurement world is suggested to identify the need to re-tune power system models. In [50] PMU measurements are used to re-tune the models of a practical system. In [51], simulation-measurement hybrid method with PMU measurements are used to re-tune a synchronous machine model.

Given Prony Analysis and its time-tested application in power systems as described above, it was chosen as the candidate system identification method for the purpose of this research. "Prony analysis is a technique for modeling sampled data as a linear combination of exponentials" [52]. An improved system identification method based on Prony analysis has been proposed to identify transfer functions for inputs of a given class. For the purpose of this research, the method proposed in [53] has been further improved using concepts presented in [38].

3.3 Transfer Function Identification from Prony Analysis

Prony Analysis is considered one of the widely used power system identification algorithms. Initial theory of Prony Analysis was presented by G.R.B. Prony in 1795. "Its practical use has awaited the digital computer and means for dealing with some inherent ill-conditioned mathematics", states J.F. Hauer in [54].

3.3.1 Theory of Prony Analysis

Prony Analysis is essentially a curve fitting method that fits a time domain signal $y(t)$ to a weighted sum of exponential terms of the form

$$y(t) = \sum_{i=1}^{n} R_i e^{\lambda_i t} \tag{3.1}$$

In discrete form, 3.1 takes the form

$$y(k) = \sum_{i=1}^{n} R_i z_i^k \tag{3.2}$$

where

$y(k), y(t)$ = Time-domain signal (discrete and continuous time)

R_i = Complex amplitude of the ith exponent

λ_i =Continuous-time mode

z_i =Discrete-time mode

n =Model order

The application of Prony's method in the modal identification of the problem this research is tackling, is developed from Eq. 3.3 to Eq. 3.9.

Let the auto-regressive model be described as:

$$y(k) = a_1 y(k-1) + a_2 y(k-2) + ...a_n y(k-n) \tag{3.3}$$

then, Eq. 3.3 can be applied to form the linear set of equations, where N is the number of sample points.

$$\begin{pmatrix} y(n+0) & y(n-1) & ... & y(1) \\ y(n+1) & y(n+0) & ... & y(2) \\ ... & ... & ... & ... \\ y(N-1) & y(N-2) & ... & y(N-n) \end{pmatrix} \begin{pmatrix} a_1 \\ a_2 \\ ... \\ a_n \end{pmatrix} = \begin{pmatrix} y(n+1) \\ y(n+2) \\ ... \\ y(N) \end{pmatrix} \tag{3.4}$$

Eq. 3.4 is a set of overdetermined linear equations which can be solved for the coefficients vector $[\ a_1 \quad a_2 \quad ... \quad a_n\ ]^T$. The discrete time (z-domain) modes are the roots of the polynomial

$$z^n - a_1 z^{n-1} - ... - a_n = 0 \tag{3.5}$$

From the z-domain modes, continuous time (s-plane) modes can be calculated as follows:

$$\lambda_i = log_e(z_i)/\Delta t \tag{3.6}$$

where Δt is the sampling time of the signal.

Frequency ω_i and damping ratio ζ_i of each mode are given as follows:

$$\omega_i = Im(\lambda_i) \quad rad/s \tag{3.7}$$

$$\zeta_i = \frac{-Re(\lambda_i)}{|\lambda_i|} \times 100\% \tag{3.8}$$

The complex amplitudes R_i can then be calculated by solving the linear set of equations:

$$\begin{pmatrix} z_1^0 & z_2^0 & ... & z_n^0 \\ z_1^1 & z_2^1 & ... & z_n^1 \\ ... & ... & ... & ... \\ z_1^{N-1} & z_2^{N-1} & ... & z_n^{N-1} \end{pmatrix} \begin{pmatrix} R_1 \\ R_2 \\ ... \\ R_n \end{pmatrix} = \begin{pmatrix} y(1) \\ y(2) \\ ... \\ y(N) \end{pmatrix} \tag{3.9}$$

For the best fit, it is recommended to choose the model order $n \approx N/2$, but $n < N/2$.

It is clear that the best fit occurs at a very high model order. Most of the modes calculated from this method do not represent actual modes of the system (spurious modes). It is suggested to choose the modes with large amplitudes $|R_i|$, which represent the mode strengths [22]. Threshold of the mode strength is to be chosen by the user. Using engineering intuition, modes with unlikely frequencies can be omitted. It is observed that many spurious modes have very high frequencies.

3.3.2 Including an Exogenous Input for Transfer Function Identification from Prony Analysis

Prony Analysis presented in Section 3.3.1 above, assumes that the output $y(t)$ is dependent only on past values of the output. A modification to the Prony model has

been proposed in [53] to include a certain class of input signals in the analysis, so that the transfer function can be identified.

The class of input signals is described in Laplace domain by:

$$U(s) = \frac{\left(c_0 + c_1 e^{-sD_1} + c_2 e^{-sD_2} + ... + c_k e^{-sD_k}\right)}{s - \lambda_{n+1}} \tag{3.10}$$

where $D_i < D_{i+1}$ and c_i are real coefficients.

The input is a summation of signals with the same pole and with different delays. The $n+1$ subscript of the pole λ_{n+1} ensures that it is different from the distinct poles in the system that is being identified, as described in Eq. 3.1. An example input signal would be a finite pulse stream with different delays as shown in Fig. 3.1, which could be described by:

$$U(s) = \frac{\left(1 - 2e^{-s\tau} + 2e^{-s2\tau} + ... + 2.(-1)^k e^{-sk\tau}\right)}{s} \tag{3.11}$$

A finite pulse stream is a viable excitation input for system identification in power systems. Governor speed reference and exciter voltage reference are examples of such inputs. Throughout the rest of this subsection, the TFI algorithm is presented with an exogenous input of $\frac{k}{2}$ pulses with a magnitude of $1p.u.$ and a duty cycle of τ.

Let $G(s)$ be the system transfer function, that needs to be identified.

$$Y(s) = G(s)U(s) \tag{3.12}$$

where $U(s)$ is the input defined in Eq. 3.11.

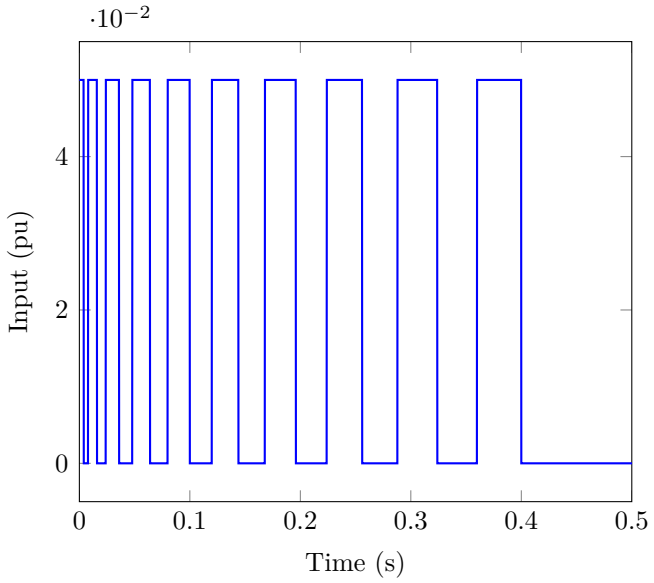

Fig. 3.1: Exogenous Input Signal for Prony Analysis

Partial fraction decomposition yields

$$Y(s) = \left(1 - 2e^{-s\tau} + 2e^{-s.2\tau} + ... + e^{-sk\tau}\right)\left(\frac{Q_{n+1}}{s} + \sum_{i=1}^{n} \frac{Q_i}{s - \lambda_i}\right) \tag{3.13}$$

where

$$Q_i = \frac{R_i}{\lambda_i} \tag{3.14}$$

$$Q_{n+1} = -\sum_{i=1}^{n} Q_i \tag{3.15}$$

Inverse Laplace transform of Eq. 3.13 would be:

$$y(t) = \left(Q_{n+1} + \sum_{i=1}^{n} Q_i e^{\lambda_i t}\right) u(t) - 2\left(Q_{n+1} + \sum_{i=1}^{n} Q_i e^{\lambda_i (t-\tau)}\right) u(t-\tau) + ... + \left(Q_{n+1} + \sum_{i=1}^{n} Q_i e^{\lambda_i (t-k\tau)}\right) u(t-k\tau) \quad (3.16)$$

For causality, $t >= k\tau$, then Eq. 3.16 can be rewritten as:

$$y(t) = Q_1\left(1 + \sum_{i=1}^{k-1} 2.(-1)^i e^{-\lambda_1 . i\tau} + e^{-\lambda_1 . k\tau}\right) e^{\lambda_1 t} + Q_2\left(1 + \sum_{i=1}^{k-1} 2.(-1)^i e^{-\lambda_2 . i\tau} + e^{-\lambda_2 . k\tau}\right) e^{\lambda_2 t} + ... + Q_n\left(1 + \sum_{i=1}^{k-1} 2.(-1)^i e^{-\lambda_n . i\tau} + e^{-\lambda_n . k\tau}\right) e^{\lambda_n t} \quad (3.17)$$

It is not possible to apply Prony analysis described in Section 3.3.1 directly to the output described in Eq. 3.17. However, if we consider the output signal just after the finite input pulse stream, i.e. after a delay of $k\tau$, the delayed output can be described by $v(h)$ as follows.

Let $h = t - k\tau$ and $v(h) = y(h + k\tau)$

$$v(h) = Q_1\left(1 + \sum_{i=1}^{k-1} 2.(-1)^i e^{\lambda_1 \tau (k-i)} + 1\right) e^{\lambda_1 h} + Q_2\left(1 + \sum_{i=1}^{k} 2.(-1)^i e^{\lambda_2 \tau (k-i)} + 1\right) e^{\lambda_2 h} + ... + Q_n\left(1 + \sum_{i=1}^{k} 2.(-1)^i e^{\lambda_n \tau (k-i)} + 1\right) e^{\lambda_n h} \quad (3.18)$$

$$v(h) = Q_1 \left(\sum_{i=0}^{k-1} 2.(-1)^i e^{\lambda_1 \tau (k-i)} \right) e^{\lambda_1 h} + Q_2 \left(\sum_{i=0}^{k} 2.(-1)^i e^{\lambda_2 \tau (k-i)} \right) e^{\lambda_2 h} + \\ ... + Q_n \left(\sum_{i=0}^{k} 2.(-1)^i e^{\lambda_n \tau (k-i)} \right) e^{\lambda_n h} \quad (3.19)$$

For $h >= 0$ Eq. 3.18 can be rewritten as:

$$\hat{v}(t) = \sum_{i=1}^{n+1} B_j e^{\lambda_i k \tau} \quad (3.20)$$

where

$$B_j = Q_j \left(\sum_{i=0}^{k-1} 2.(-1)^i e^{\lambda_i h (k-i)} \right) \quad (3.21)$$

and from Eq. 3.14

$$Q_j = \frac{R_j}{\lambda_j} \quad (3.22)$$

From Eq. 3.21 and Eq. 3.22, the transfer function residues can be obtained as

$$R_j = \frac{B_j \lambda_j}{\sum_{i=0}^{k-1} 2 \cdot (-1)^i e^{\lambda_j h (k-i)}} \quad (3.23)$$

The representation in Eq. 3.20 is the same as the Prony model given in Eq. 3.1. Therefore, B_j and λ_j can be found using the procedure described in Section 3.3.1.

3.3.3 Expanding-Window Prony Analysis with Exogenous Input

In the recent paper [38], a simple improvement to the conventional Prony Analysis is suggested in order to determine true modes of a ringdown power system signal. As shown in Fig. 3.2 the length of the data window, on which Prony Analysis is performed, is extended and Prony Analysis is repeated. This is done for several expanding data window lengths. Each Prony Analysis overfits the signal in the data window. Each overfitting has true modes and spurious modes. While each data window must have the true modes in them repeatedly, the spurious modes do not repeat. Instead of relying on the mode strength calculation, this method ensures identification of all excited true modes in the data window, including those having a low mode strength.

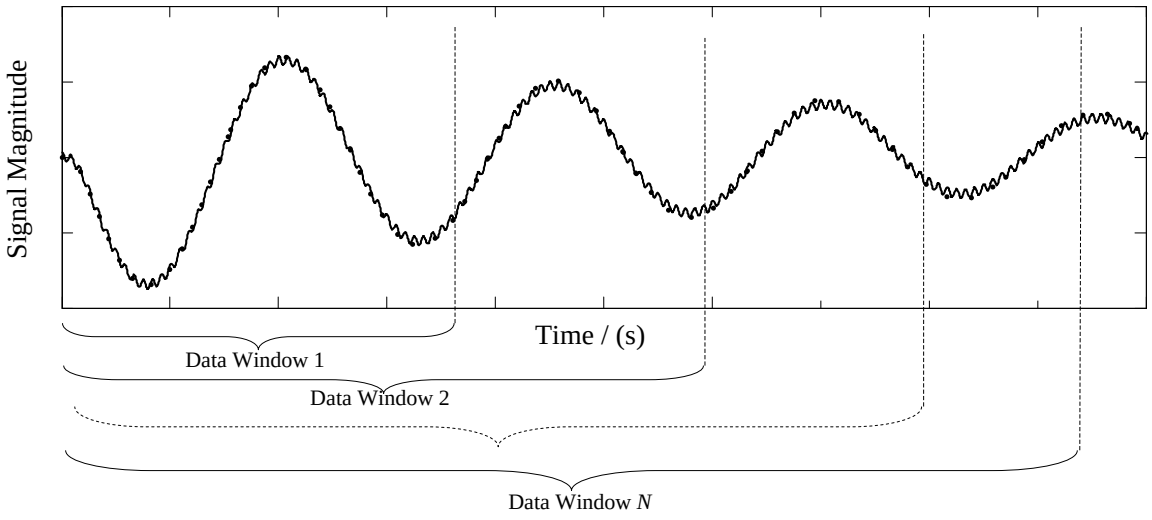

Fig. 3.2: Illustration of a power system signal subjected to multiple Prony Analyses with expanding window lengths

According to the research strategy explained in Section 1.6.1, it is important to identify all modes in the system. Therefore this improved Prony Analysis is suitable to identify all modes including the less excited and the less observed.

The transfer function identification method explained in Section 3.3.2 was tested for the "Expanding Window" method given in [38].

3.3.4 Limitations of Expanding-Window Prony Analysis

Excessive data points in the signal

EMT simulation time step for successful simulation of power systems is in the order of $50\mu s$. Especially when the devices have power electronic switching components, the required simulation time step can be as small as $10\mu s$. An electromechanical mode in the power system can have frequencies as low as 0.1Hz. In order to conform to the Nyquist criterion, the minimum data window length of the system identification process should be half the period of the minimum frequency. Therefore, a data window of at least $5s$ should be chosen for the Prony Analysis. In a general case of the simulation time step being $50\mu s$, the total number of data points for the shortest required data window is 1×10^5 samples. This many data points causes solving Eq. 3.4 and 3.9 very time consuming.

Fast decaying stationary modes

Power system signals have fast decaying stationary modes represented by negative real eigenvalues. These highly damped modes may disappear during the first few data points in the data window. The effect of highly damped stationary modes on stability of a system is minimal. However, their inclusion improves the accuracy of

the reconstructed signal. A priori knowledge of the system was utilized to incorporate some of the fast decaying modes in the system identification, and it is described in Chapter 4.

3.4 Chapter Summary

This chapter reviews existing system identification methods used in power system applications. It identifies merits of Prony Analysis against other available methods. Two short comings of Prony Analysis were overcome by improvements to Prony Analysis proposed in literature. Conventional Prony Analysis is an autoregressive type linear system identification method. It is important to identify transfer functions of the system. A specific type of exogenous input is chosen to perturb the system, as suggested in the literature for successful transfer function identification. Conventional Prony Analysis overfits the signal with spurious modes. In order to identify the true modes of the system, an expanding window algorithm has been chosen along with the exogenous input. However, capturing fast decaying modes is still a challenge. In order to proceed with the research strategy laid out in Chapter 1, it is important that all modes contributed by the current injection device subsystem, including those decaying fast, are in the identified transfer functions. A methodology to utilize a priori knowledge of the system with the use of eigenstructure assignment, that ensures the identification of modes contributed by the current injection device, is presented in the next chapter.

Chapter 4

Utilizing A Priori Knowledge to Improve Modal Identification

4.1 Introduction

As explained in Chapter 1, for a successful small signal stability analysis, all models and parameters of all devices and network elements must be available [3]. If any of the devices has an unknown controller, the conventional model-based small signal stability assessment procedure fails.

A power system consists of a large number of devices and network elements that have been incrementally installed over decades. Data of these devices are usually well documented. With the increased interest in renewable energy sources, distributed energy sources are being added to the existing network i.e. wind power plants and solar power plants. These distributed generators have new control schemes which are generally not made public. However, the current injection element of these new devices, especially in the case of wind turbines, is still a well-known machine, i.e. an induction machine. Even if the manufacturers have proprietary concerns over the

controllers, the name plate data and the dynamic data of the machine can be made available to the customer.

Out of the large body of previous work on system identification of power systems, only a limited number of work attempt to identify an unknown device i.e. a black boxed model, in a way that it could be included in a model-based small signal stability study [55].

As laid out in Chapter 1, the first part of the research strategy is to identify all modes of a black-boxed device utilizing *a priori* knowledge of the black boxed device, namely, data of the current injection device. The Expanding Window Prony Analysis with an Exogenous Input presented in Chapter 3 ensures that the overfitting spurious modes are omitted from the system identification result. However, Prony Analysis method alone does not capture highly damped modes. It is important to capture all modes contributed by the current injection device subsystem, as current injection device transfer functions calculated from available dynamic data are used as *a priori* knowledge of the system in the latter stages of the proposed procedure.

This chapter proposes a method that involves designing a fictitious controller to the known current injection device in such a way the modes identified by the Expanding Window Prony Analysis are achieved. The fictitious controller is designed using Eigenstructure Assignment (ESA). ESA is a controller tuning procedure that allows to place eigenvalues almost at any point on the *s-plane*. However, in order to match the system identification results, the parameter selection for ESA has to be done within strict constraints which leads to a highly nonlinear optimization problem, as explained in the following sections. A meta-heuristic optimization method is proposed for the nonlinear optimization required in the process and the candidate

algorithm chosen is Simulated Annealing.

4.2 Application of Eigenstructure Assignment

The eigenstructure of a linear system is the combination of its eigenvalues and eigenvectors. A set of eigenvalues and corresponding eigenvectors uniquely defines the system matrix of a linear state space system. Therefore, if the eigenstructure of a system can be determined, the system matrix of the system can be calculated.

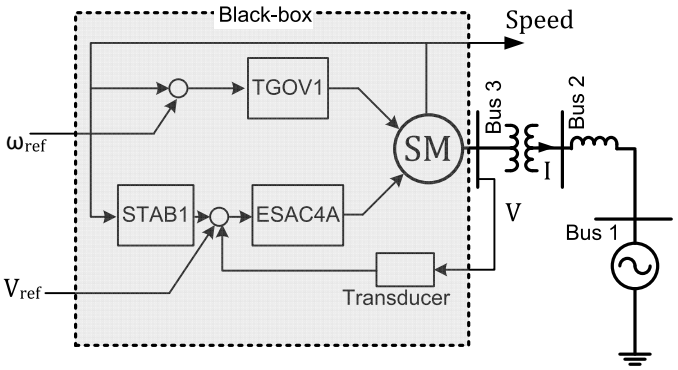

Fig. 4.1: Single Machine Infinite Bus (SMIB) test system of synchronous machine (SM)

Let us consider a synchronous machine single machine infinity bus (SMIB) system with auxiliary controllers as shown in Fig. 4.1. The linearized system of the test system, with machine states and the controller states separated, can be derived as follow:

Let

$\mathbf{x}_g \in \mathbb{R}^{n_g}$ =Vector of machine state variables

$\mathbf{i} \in \mathbb{R}^2$ =Current injection from the machine

$\mathbf{u}_g \in \mathbb{R}^{r_g}$ =Input vector to the machine

$\mathbf{v} \in \mathbb{R}^2$ =voltage of the machine bus

$\mathbf{x}_c \in \mathbb{R}^{n_c}$ =Vector of controller state variables

$\mathbf{u}_c \in \mathbb{R}^{r_c}$ =Input vector to the controller

$\mathbf{Y}_{eq} \in \mathbb{R}^{2\times 2}$ =Equivalent admittance matrix

$\mathbf{A}_g \in \mathbb{R}^{n_g\times n_g}, \mathbf{E}_g \in \mathbb{R}^{n_g\times 2}, \mathbf{B}_g \in \mathbb{R}^{n_g\times r_g}, \mathbf{C} \in \mathbb{R}^{2\times n_g}, \mathbf{D} \in \mathbb{R}^{2\times 2}, \mathbf{A}_c \in \mathbb{R}^{n_c\times n_c}, \mathbf{E}_c \in \mathbb{R}^{n_c\times 2}$ =Corresponding coefficient matrices.

$\mathbf{A}_D \in \mathbb{R}^{n_g\times n_g}$ =System matrix for machine-only

$\mathbf{M_1} \in \mathbb{R}^{n_g\times n_c}, \mathbf{M_2} \in \mathbb{R}^{n_c\times n_g}$ =Coefficient submatrix with interconnections between the controller and machine

Δ denotes small variations

$$\Delta\dot{\mathbf{x}}_g = \mathbf{A}_g\Delta\mathbf{x}_g + \mathbf{E}_g\Delta\mathbf{i} + \mathbf{B}_g\Delta\mathbf{u}_g \tag{4.1a}$$

$$\Delta\mathbf{i} = \mathbf{C}\Delta\mathbf{x}_g + \mathbf{D}\Delta\mathbf{v} \tag{4.1b}$$

$$\Delta\mathbf{y}_g = \mathbf{C}_g\Delta\mathbf{x}_g \tag{4.1c}$$

$$\Delta\mathbf{i} = \mathbf{Y}_{eq}\Delta\mathbf{v} \tag{4.1d}$$

$$\Delta\dot{\mathbf{x}}_c = \mathbf{A}_c\Delta\mathbf{x}_c + \mathbf{E}_c\Delta\mathbf{i} + \mathbf{B}_c\Delta\mathbf{u}_c \tag{4.1e}$$

$$\Delta\mathbf{y}_c = \mathbf{C}_c\Delta\mathbf{x}_c \tag{4.1f}$$

$$\mathbf{A}_D = \mathbf{A}_g + \mathbf{E}_g(\mathbf{C} + \mathbf{D}(\mathbf{Y}_{eq} - \mathbf{D})^{-1}\mathbf{C}) \tag{4.1g}$$

From equations 4.1

$$\Delta\dot{\mathbf{x}}_g = \mathbf{A}_D\Delta\mathbf{x}_g + \mathbf{B}_g\Delta\mathbf{u}_g \tag{4.2a}$$

$$\Delta\dot{\mathbf{x}}_c = \mathbf{A}_c\Delta\mathbf{x}_c + \mathbf{E}_c(\mathbf{C} + \mathbf{D}(\mathbf{Y}_{eq} - \mathbf{D})^{-1}\mathbf{C})\Delta\mathbf{x}_g + \mathbf{B}_c\Delta\mathbf{u}_c \tag{4.2b}$$

The complete state space shall be written as

$$\begin{bmatrix} \Delta\dot{\mathbf{x}}_g \\ \Delta\dot{\mathbf{x}}_c \end{bmatrix} = \begin{bmatrix} \mathbf{A}_D & \mathbf{M}_1 \\ \mathbf{M}_2 & \mathbf{A}_c \end{bmatrix} \begin{bmatrix} \Delta\mathbf{x}_g \\ \Delta\mathbf{x}_c \end{bmatrix} + \mathbf{B}_c\Delta\mathbf{u}_c \tag{4.3}$$

If the model data of the machine and the network data are known, the sub matrix $\mathbf{A}_D$ is known. All other elements of the system matrix are unknown. If the order of the controller is unknown, the order of complete system matrix is unknown.

If the complete eigenstructure of the system is known, all elements of the system matrix can be calculated. If only the eigenvalues are known, a set of fictitious controllers with states $\mathbf{x}_c$ can be designed to achieve the same eigenvalues. Such knowledge of eigenvalues can be obtained from system identification procedure proposed in Section 3.3.3. One of the controllers in the set of fictitious controllers is the actual controller in the system, exactly as modeled. Such a controller gives the eigenstructure that can calculate the basis on which the system was originally modeled.

Due to limitations in the Prony Analysis method presented in Section 3.3.4, all the eigenvalues of a power system device cannot be identified. The motive of this section is to use an optimization procedure to design a fictitious controller that best matches the combination of *a priori* knowledge of submatrix $\mathbf{A}_D$ and the knowledge of

modes and mode shapes obtained from Prony Analysis. The preferred control design method is Parametric Eigenstructure Assignment which is a control design procedure that assigns a limited number of eigenvalues and eigenvectors to a system.

4.2.1 Parametric Eigenstructure Assignment

Eigenstructure assignment has been developed since 1960s as a linear control design method. The focus is to assign preferred eigenvalues to a system by choosing suitable eigenvectors. Choice of eigenvectors is usually not unique. In [56], a parametric approach has been proposed. The theory behind parametric eigenstructure assignment is given in Section 4.3.

In short, parametric eigenstructure assignment calculates a feedback gain matrix $\mathbf{K}(\mathbf{F}_P)$ using a matrix of arbitrary parameter vectors $\mathbf{F}_P$ as given in Eq. 4.11.

4.3 Parametric Right Eigenstructure Assignment

When the open loop system is given by

$$\dot{\mathbf{x}} = \mathbf{A}\mathbf{x} + \mathbf{B}\mathbf{u} \tag{4.4a}$$

$$\mathbf{y} = \mathbf{C}\mathbf{x} \tag{4.4b}$$

Where $\mathbf{x} \in \mathbb{R}^n$, $\mathbf{u} \in \mathbb{R}^r$ and $\mathbf{y} \in \mathbb{R}^m$ are the state vector, input vector and output vector respectively, where:

n = order of the system

r = number of inputs to the system

m = number of outputs available for feedback

$\mathbf{A}$ = system matrix

$\mathbf{B}$ = input matrix

$\mathbf{C}$ = output matrix

A feedback control law $\mathbf{K} \in \mathbb{R}^{r \times m}$ can be defined as:

$$\mathbf{u}(t) = \mathbf{K}\ \mathbf{y}(t) \tag{4.5}$$

Then the closed loop system is:

$$\dot{\mathbf{x}} = (\mathbf{A} + \mathbf{BKC})\mathbf{x} \tag{4.6}$$

Let $\mathbf{v}_i$ be a right eigenvector corresponding to the eigenvalue λ_i. Then:

$$(\mathbf{A} + \mathbf{BKC})\mathbf{v}_i = \lambda_i \mathbf{v}_i \tag{4.7}$$

By defining a parameter vector $\mathbf{f}_i$ as:

$$\mathbf{f}_i = \mathbf{KCv}_i \tag{4.8}$$

$\mathbf{v}_i$ can be presented in terms of free parameters as follows:

$$\mathbf{v}_i = (\lambda_i \mathbf{I} - \mathbf{A})^{-1}\mathbf{Bf}_i \tag{4.9}$$

Let:

p = number of eigenvalues to be assigned

When the number of eigenvalues that need to be assigned is less than the number of outputs available for feedback i.e. $p < m$, the eigenvalues can be assigned by merely choosing a feedback matrix $\mathbf{K}$.

Let:

$$\begin{aligned} \mathbf{V}_P &= [\mathbf{v}_1, \mathbf{v}_2, ...\mathbf{v}_p] \\ \mathbf{F}_P &= [\mathbf{f}_1, \mathbf{f}_2, ...\mathbf{f}_p] \end{aligned}$$

Then $\mathbf{K}$ can be calculated as:

$$\mathbf{K} = \mathbf{F}_P(\mathbf{C}\mathbf{V}_P)^{-1} \tag{4.11}$$

In order to determine $\mathbf{K}$, the parameter vectors, $\mathbf{f}_1, \mathbf{f}_2, ...\mathbf{f}_p$ should be chosen under three mild conditions, namely:

(i) $|\mathbf{C}\mathbf{V}_P| \neq 0$

(ii) $\mathbf{f}_i \in \mathbb{R}^r$ if $\lambda_i \in \mathbb{R}$

(iii) $\mathbf{f}_j = \mathbf{f^*}_i \in \mathbb{C}^r$ if $\lambda_i \in \mathbb{C}$ where i and j represent the complex conjugate pair indices

However, if the number of eigenvalues that needs to be assigned is more than the number of available outputs for feedback, an additional controller known as a

dynamic compensator has to be introduced. Schematic of a Dynamic Compensator feedback control system is given in Fig. 4.2.

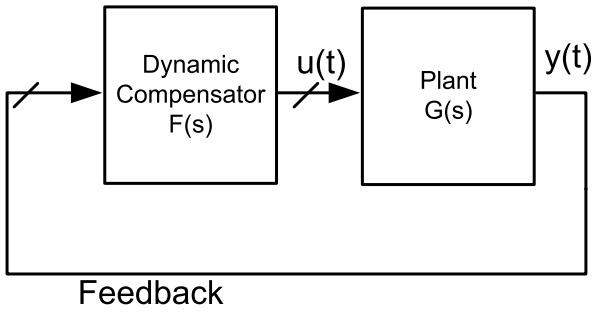

Fig. 4.2: Schematic of a Dynamic Compensator Feedback Control System

The dynamic compensator is defined as:

$$\mathbf{z}(t) = \mathbf{D}\ \mathbf{z}(t) + \mathbf{E}\ \mathbf{y}(t) \tag{4.12a}$$

$$\mathbf{u}(t) = \mathbf{F}\ \mathbf{z}(t) + \mathbf{G}\ \mathbf{y}(t) \tag{4.12b}$$

Where $\mathbf{z}(t)$ is the state vector of the dynamic compensator.

It should be noted that the equivalent input vector to the state space of the dynamic compensator is $\mathbf{y}(t)$, which represents the outputs of the plant that goes in to the dynamic compensator as inputs. The equivalent outputs of the state space is $\mathbf{u}(t)$, which represents the output of the dynamic compensator that goes in to the plant according to the control law.

$$\dot{\bar{\mathbf{x}}} = \bar{\mathbf{A}}\bar{\mathbf{x}} + \bar{\mathbf{B}}\bar{\mathbf{u}} \tag{4.13a}$$

$$\bar{\mathbf{y}} = \bar{\mathbf{C}}\bar{\mathbf{x}} \tag{4.13b}$$

Where:

$$\bar{\mathbf{A}} = \begin{pmatrix} \mathbf{A} & \mathbf{0} \\ \mathbf{0} & \mathbf{0} \end{pmatrix}$$

$$\bar{\mathbf{B}} = \begin{pmatrix} \mathbf{B} & \mathbf{0} \\ \mathbf{0} & \mathbf{I} \end{pmatrix}$$

$$\bar{\mathbf{C}} = \begin{pmatrix} \mathbf{C} & \mathbf{0} \\ \mathbf{0} & \mathbf{I} \end{pmatrix}$$

$$\bar{\mathbf{K}} = \begin{pmatrix} \mathbf{G} & \mathbf{F} \\ \mathbf{E} & \mathbf{D} \end{pmatrix}$$

The choice of parameters for $\mathbf{F}_P$ determines the feedback matrix $\bar{\mathbf{K}}$ hence the closed loop system matrix.

$$\mathbf{A*} = \bar{\mathbf{A}} + \bar{\mathbf{B}}\bar{\mathbf{K}}\bar{\mathbf{C}} \tag{4.15}$$

4.3.1 Choosing candidate parameter vectors for eigenstructure assignment

Theoretically, the choice of the parameter vectors $\mathbf{f}_i$, for successful eigenstructure assignment, is only constrained by the three constraints given above. From Eq. 4.9, it is evident that resulting eigenvectors from distinct parameter vectors may not be distinct. In order to limit the search space to the unit hypersphere of eigenvectors, the following manipulation is done to the parameter vectors.

For all real valued eigenvalues to be assigned let:

$$\mathbf{f}_{i\ real} = \boldsymbol{\theta_i}$$

and for all complex valued eigenvalue pairs let the parameter vector pairs be:

$$\begin{aligned} \mathbf{f}_{i\ complex} &= \boldsymbol{\alpha_i} + j.\boldsymbol{\beta_i} \\ \mathbf{f^*}_{i\ complex} &= \boldsymbol{\alpha_i} - j.\boldsymbol{\beta_i} \end{aligned}$$

where, $\boldsymbol{\alpha_i} \in \mathbb{R}^r, \boldsymbol{\beta_i} \in \mathbb{R}^r$ and $\boldsymbol{\theta_i} \in \mathbb{R}^r$ and $j = \sqrt{-1}$.

Therefore,

the total number of parameters (number of elements in $\mathbf{F}_P$***)*** $= r \times p$

The initial values for these $r \times p$ parameters can be randomly chosen from a uniform distribution. The following steps were followed.

Step 1

Generate random numbers for vectors $\boldsymbol{\theta_i}, \boldsymbol{\alpha_i}$ and $\boldsymbol{\beta_i}$ for $i = 1, 2, ...p$ between 0 and 1 with a resolution of 1×10^{-4}.

The randomly chosen initial parameters within the mild constraints described in Section 4.3 above, still achieve the target eigenvalues in the system. The range and resolution of the distribution, from which the parameters are chosen, limit the number of solutions in the search domain.

Step 2

Calculate the candidate eigenvector for each parameter vector $\mathbf{f}_i$ from Eq. 4.9

Step 3

Convert the eigenvector to its unit eigenvector by dividing by the norm of the eigenvector.

$$\frac{\mathbf{v}_i}{||\mathbf{v}_i||} = (\lambda_i \mathbf{I} - \mathbf{A})^{-1}\mathbf{B}\left(\frac{\mathbf{f}_i}{||\mathbf{v}_i||}\right) \tag{4.17}$$

Step 4

Candidate parameter vector $\bar{\mathbf{f}}_i$ is given by

$$\bar{\mathbf{f}}_i = \left(\frac{\mathbf{f}_i}{||\mathbf{v}_i||}\right) \tag{4.18}$$

Choosing $\mathbf{f}_i$ from a set of uniformly distributed random numbers within limits, as described in **Step 1** ensures that the vector $\bar{\mathbf{f}}_i$ is a randomly chosen vector from the hypersphere, which is the search domain for the optimization problem described in Section 4.4

4.3.2 Non-uniqueness of the Solution of the Optimization Problem

Let us consider an analytically derived linear dynamic system given by Eq 4.4. When developing a state space model of a dynamic system, every state has a physical meaning. The derived linear state space can be described by a state space of a different

basis. The change of basis can be done by any invertible matrix $\mathbf{T}$ as given in Eq 4.19.

Let $\tilde{\mathbf{x}} = \mathbf{T}\mathbf{x}$

$$\dot{\tilde{\mathbf{x}}}(t) = \mathbf{T}^{-1}\mathbf{A}\mathbf{T}\tilde{\mathbf{x}}(t) + \mathbf{T}^{-1}\mathbf{B}\mathbf{u}(t) \tag{4.19a}$$

$$\mathbf{y}(t) = \mathbf{C}\mathbf{T}\tilde{\mathbf{x}}(t) \tag{4.19b}$$

and

$$\dot{\tilde{\mathbf{x}}}(t) = \tilde{\mathbf{A}}\tilde{\mathbf{x}}(t) + \tilde{\mathbf{B}}\mathbf{u}(t) \tag{4.20a}$$

$$\mathbf{y}(t) = \tilde{\mathbf{C}}\tilde{\mathbf{x}}(t) \tag{4.20b}$$

where

$$\tilde{\mathbf{A}} = \mathbf{T}^{-1}\mathbf{A}\mathbf{T}$$

$$\tilde{\mathbf{B}} = \mathbf{T}^{-1}\mathbf{B}$$

$$\tilde{\mathbf{C}} = \mathbf{C}\mathbf{T}$$

In order to calculate the system matrix $\mathbf{A}$ with the same basis with physical meaning, the exact normalized eigenvector matrix $\mathbf{\Phi}$ (or $\mathbf{\Psi}$ for that matter) has to be known. In the eigenstructure assignment procedure presented above, the eigenvector $\mathbf{v}_i$ is determined by the choice of the parameter vector $\mathbf{f}_i$ as given in Eq 4.9. When calculating the system matrix using the procedure, basis of the states of the plant are preserved, but the basis of the controller states cannot be preserved. Therefore, physical meanings of controller states that were considered during the analytical

derivation of the linear system are no longer valid for the new controller states. Controller states are mostly signals and their physical meanings are not very important in a small signal analysis, other than the information about which controller subsystem it belongs to i.e. exciter, governor etc. The fact that there is no unique basis that has to be achieved makes the optimization problem in Eq. 4.27 to have multiple solutions. Finding any one of these solutions is successfully solving the optimization problem.

4.3.3 Choosing Free Parameters Using Optimization

The choice of free parameters in the above procedure is the discretion of the user. Any set of parameters chosen under the given mild conditions results in a system that has the preferred eigenvalues. Apart from the assigned eigenvalues, the system has other eigenvalues too. In order to choose from all possible sets of free parameters, further constraints should be imposed.

If the user has knowledge of the mode shapes of the modes he is assigning using eigenstructure assignment, such mode shapes can be translated in to the objective function of an optimization procedure.

4.4 Objective Function

The rationale of choosing the objective function is that the mode shapes of the identified modes should be the same as the mode shapes of the system with the fictitious controller.

The residues of the p number of modes identified by system identification are the mode shapes. Mode shape has the magnitude (strength) and the angle (phase) of

each mode.

Let R_{ik} be the residue of the ith mode of the kth output. Then $|R_{ik}|$ is the mode strength and $arg(R_{ik})$ is the mode phase.

Mode strengths of all identified modes at output k, from $i = 1, 2, \ldots p$ can be represented by a normalized vector γ_k.

$$\gamma_k = \frac{[|R_{1k}|, |R_{2k}|...|R_{pk}|]}{||[|R_{1k}|, |R_{2k}|...|R_{pk}|]||} \tag{4.22}$$

When a fictitious controller assigns identified eigenvalues to the system using eigenstructure assignment, the closed loop eigenvalue can be categorized into three categories as follow:

(i) Eigenvalues identified and assigned (denoted by Λ_1)

(ii) Eigenvalues that are more damped than the assigned eigenvalues (denoted by Λ_2)

(iii) Eigenvalues that are less or as equally damped as the assigned eigenvalues(denoted by Λ_3)

The modal decomposition of the system can be given by the following partitioned representation

$$\dot{\bar{\mathbf{z}}} = \begin{bmatrix} \Lambda_1 & 0 & 0 \\ 0 & \Lambda_2 & 0 \\ 0 & 0 & \Lambda_3 \end{bmatrix} \bar{\mathbf{z}} + \Psi \mathbf{B} \mathbf{u} \tag{4.23a}$$

$$\bar{\mathbf{y}} = \bar{\mathbf{C}} \begin{bmatrix} \boldsymbol{\Phi_1} & \boldsymbol{\Phi_2} & \boldsymbol{\Phi_3} \end{bmatrix} \bar{\mathbf{z}} \tag{4.23b}$$

Where $\mathbf{\Psi}$ and $\mathbf{\Phi}$ are the left and right eigenvector matrices respectively and $\bar{\mathbf{z}}$ is the modal state vector. $\mathbf{\Phi}$ is partitioned appropriately in Eq 4.23.

Normalized mode strength vector of the assigned eigenvalues in the jth output can be given by a similar vector as γ_k.

$$\zeta_k = \frac{[|\bar{\mathbf{c}}_k\phi_{11}|, |\bar{\mathbf{c}}_k\phi_{12}|...|\bar{\mathbf{c}}_k\phi_{1p}|]}{|||\bar{\mathbf{c}}_k\phi_{11}|, |\bar{\mathbf{c}}_k\phi_{12}|...|\bar{\mathbf{c}}_k\phi_{1p}|]||} \tag{4.24}$$

For the designed system to have the same behaviour as the identified system, a necessary condition would be, the two vectors γ_k and ζ_k to coincide. For the minimum Euclidean distance between the two vectors the following minimization should be achieved.

$$\min_{\mathbf{F_P}} \left\{ \sum_{i=1}^{m} ||\gamma_k - \zeta_k|| \right\} \tag{4.25}$$

where $\mathbf{F}_P$ is the matrix of free parameters which are the decision variables of the optimization problem.

The objective function should also account for the additional modes introduced to the system. If these additional modes have more strength than those assigned modes, the controllers that caused to result in such systems should be avoided. The rationale of this measure is that the modes with the greatest strength must be identified in the identification procedure. In order to avoid such fictitious controllers, a penalty function is proposed.

$$P = \begin{cases} h, & \text{if } \ max(real(\Lambda_2)) > min(real(\Lambda_1)) \\ 0, & \text{otherwise} \end{cases} \tag{4.26}$$

Where h is a relatively large number e.g. 100.

Therefore, the complete proposed objective function is

$$\min_{\mathbf{F_P}} E = \min_{\mathbf{F_P}} \left\{ \sum_{i=1}^{m} ||\gamma_i - \zeta_i|| + P \right\} \tag{4.27}$$

The relationship between E and elements of $\mathbf{F}_P$ is nonlinear and the problem is non-convex. Therefore, a meta-heuristic optimization method has to be chosen to solve the minimization problem. The subject of non-convex optimization is a developing one and numerous algorithms have been developed. There are many algorithms that mimic natural processes. (e.g. genetic evolution, swarming movements of animal species and metal annealing process.) The efficiency of the algorithm depends on the problem it is applied to. Each algorithm has room for variations and choice of parameters that will further improve its efficiency in solving a given problem. This research does not investigate methods and parameters to improve the efficiency of solving the given optimization problem. The time it takes to achieve a feasible solution is not considered as a major constraint. Simulated Annealing was chosen as a candidate meta-heuristic optimization procedure. Theory and application of Simulated Annealing is given in Appendix A.

4.5 Application to Synchronous Machine SMIB System

In setting up the test case we assume that the EMT simulation model of the device is provided by the vendor as a black box with a limited number of output and inputs.

Such a model is connected to an infinite bus in the EMT program and time-domain outputs are observed. Schematic of the simulated test system is given in Fig. 4.10. Components inside the dashed-line box are considered to be in a black box. The generator speed and other terminal measurements such as voltage, current and power are available to the user as output signals. Voltage reference input to the exciter and the speed reference input to the governor are also available to the user.

The proposed method was applied to the test system. Fig. 4.3 summarizes the procedure that was followed. The network and dynamic data for the test system are given in the Appendix C.

The system was simulated on PSCAD/EMTDC software with an integration time step of $50\mu s$. A small disturbance was given to the system by giving a 0.25pu pulse for 30 ms to the V_{ref} input of the exciter. The speed of the generator and the terminal voltage were the only outputs observed. The output signals was decimated to a sampling time of $10ms$. The smallest data window was $1.7s$ and five expanding data windows were chosen with an increment of $0.2s$. Thus the largest data window was $2.5s$. The identification procedure was carried out on both output signals and the union of sets of modes identified from the two different outputs were accepted as true modes of the system.

Outcome of Step 1 is the first column of Table 4.1. In Step 2, the synchronous machine is modeled as shown in Fig. 4.4. Known parameters of the synchronous machine are included in the subsystem labeled as "SM". All the unknown dynamics are modeled by the dynamic compensator. The goal is to ensure that the closed loop system has the eigenvalues identified in Step 1. Simulated annealing algorithm, described in Appendix A, was performed multiple times with varying initial temper-

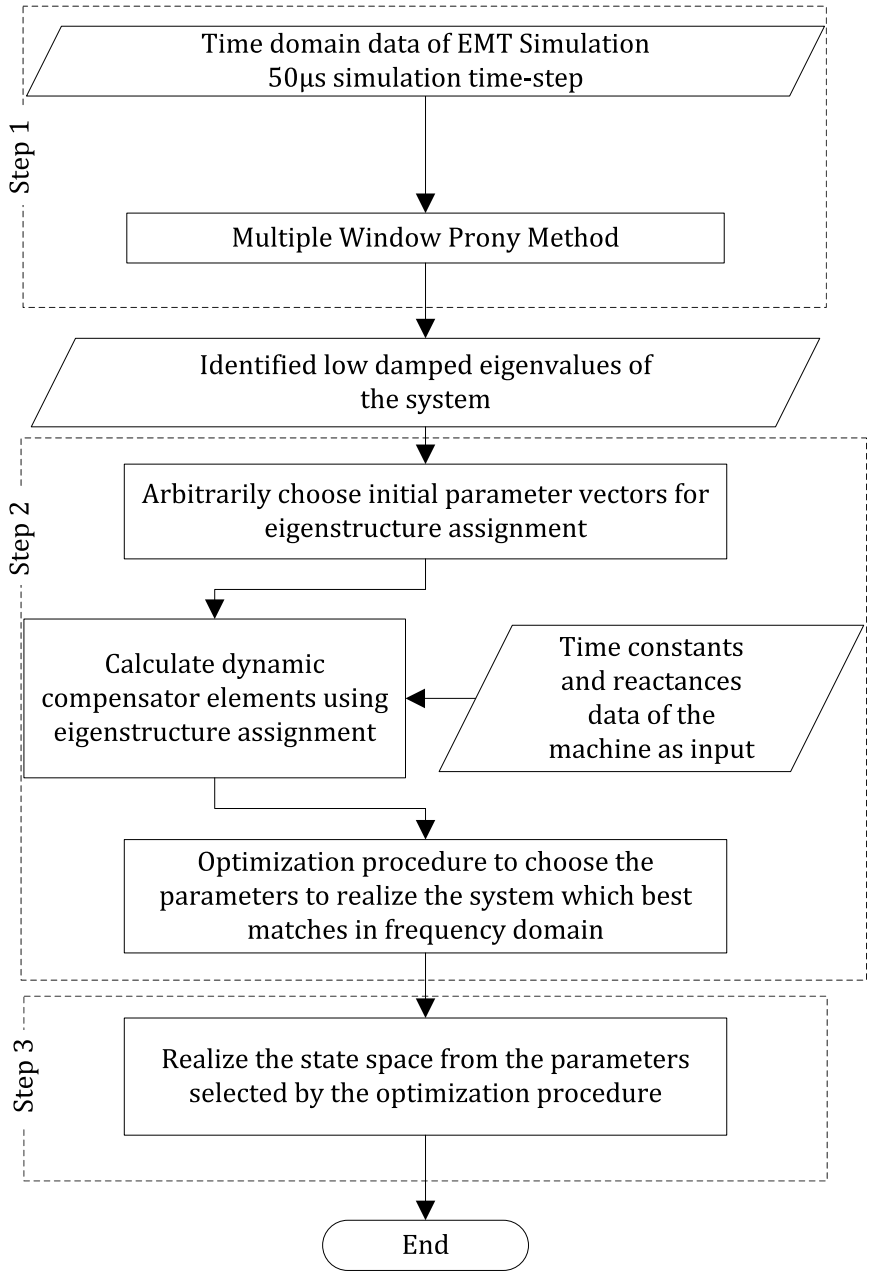

Fig. 4.3: Procedure to identify highly damped modes of a SMIB system incorporating *a priori* knowledge of the current injection device

atures between 1000 and 10000 with varying maximum number of iterations as the stopping criteria to minimize the objective function given in Eq. 4.27. The most efficient convergence was shown at the intial temperature 2000 with a maximum allowed iterations 6000 as shown in Fig. 4.5.

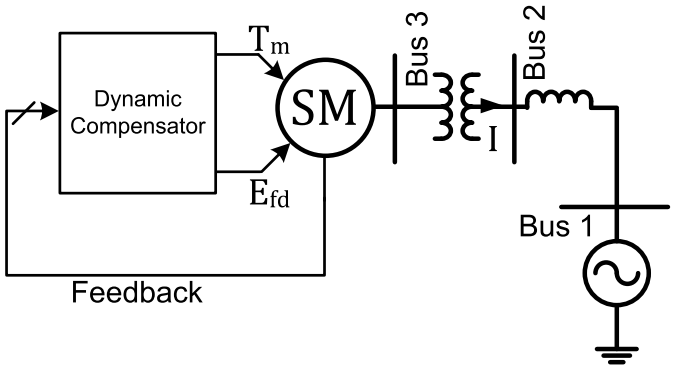

Fig. 4.4: Single Machine Infinite Bus (SMIB) test system of synchronous machine with the designed controller

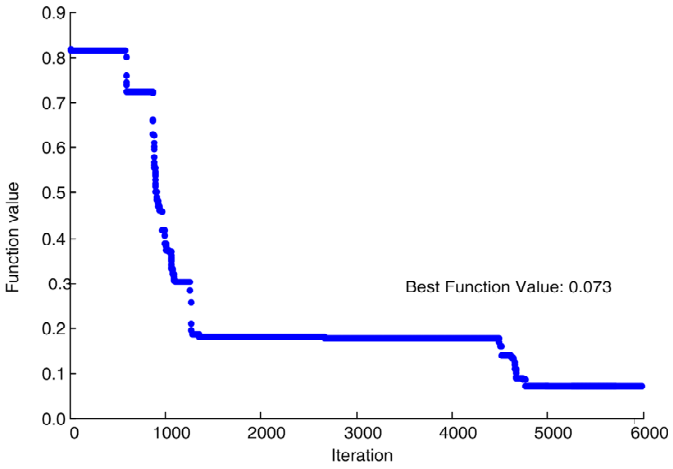

Fig. 4.5: Variation of the objective function value of the simulated annealing optimization procedure in Step 1

Calculated eigenvalues of the state space realized using eigenstructure assignment

Table 4.1: Eigenvalues identified from the time domain simulation and eigenvalues determined by the proposed method

Identified Modes	Modes Determined by Prony+ESA Method
$-0.6356 \pm j12.6332$	$-0.6356 \pm j12.6332$ - Mode A
-3.529	-3.529 - Mode B
-0.5018	-0.5018 - Mode C
-0.1989	-0.1989 - Mode D
-0.9721	-0.9721 - Mode E
$-0.3747 \pm j0.5850$	$-0.3747 \pm j0.5850$ - Mode F
	-37.3402 - Mode G
	-28.1941 - Mode H
	-43.7292 - Mode I
	-3.6404 - Mode J

are reported in the 2^{nd} column of Table 4.1.

For the purpose of comparison, the actual system was linearized using the data given in the Appendix C. The calculated eigenvalues and their participating dominant states are shown in Table 4.2.

Comparing the eigenvalues shown in Tables 4.1 and 4.2 it can be seen that the eigenvalues of the realized system are of 3 types:

(i) Modes identified by the Prony method - Modes A to F.

(ii) Modes that were not identified by the identification process but are numerically close to theoretically calculated eigenvalues of the original system - Modes G and H.

Table 4.2: Theoretical modes in the system

Mode No.	Mode	Dominant States
1	-100.2823	Exciter
2	-49.855	Exciter
3	-36.9351	D-axis damper winding
4	-28.2409	Q-axis damper winding 2
5, 6	$-0.6392 \pm j12.5693$	Rotor speed and rotor angle
7	-3.4893	Q-axis damper winding 1
8	-2.0000	Governor turbine
9	-0.9763	Governor turbine
10	-0.5002	Stabilizer
11, 12	$-0.1999 \pm j0.0047$	Stabilizer
13, 14	$-0.3696 \pm j0.5729$	Exciter and generator field winding

(iii) Modes that are not found in the original linearized system - Modes I and J.

The state space realized by eigenstructure assignment has 12 states. According to the partitioning in Eq. 4.2 the first 6 states are the states of the synchronous machine. The rest are those of the dynamic compensator. Table 4.3 gives the list of states of the realized state space.

Fig. 4.6 shows state participation in modes described by above (ii) and (iii).

The following deductions can be made by observing Fig. 4.6.

a Participation of modes categorized by above (ii) are very close to that of the original system and are highly damped modes participated by the generator.

b Modes categorized in above (iii) are mainly participated by the dynamic com-

Table 4.3: States of the state space realized using eigenstructure assignment

State No.	Description
1	Rotor speed
2	Rotor angle
3	Field winding
4	D-axis damper winding
5	Q-axis damper winding 1
6	Q-axis damper winding 2
7-12	Dynamic compensator states

pensator states and can be treated as spurious modes realized by the eigenstructure assignment procedure.

Thus, modes described in above (a) are accepted as true modes along with the modes identified by the identification process. The user has the discretion either to accept or decline modes described in (b). Residues of these true modes are recalculated using Eq. 3.9.

Fig. 4.7 presents comparison between speed deviations of the theoretical linear system and that of the nonlinear EMT simulation response. The responses are almost perfectly matching. Therefore the theoretical linear system response is used to compare the Multiple-Window Prony Analysis and the proposed method.

In conventional Prony analysis, the time domain signal is overfit by fictitious modes. The multiple-window Prony method extracts less damped true modes as described in Section 3.3.3. As a result of missing highly damped modes that exist in the system, the comparison between the time domain responses of the system

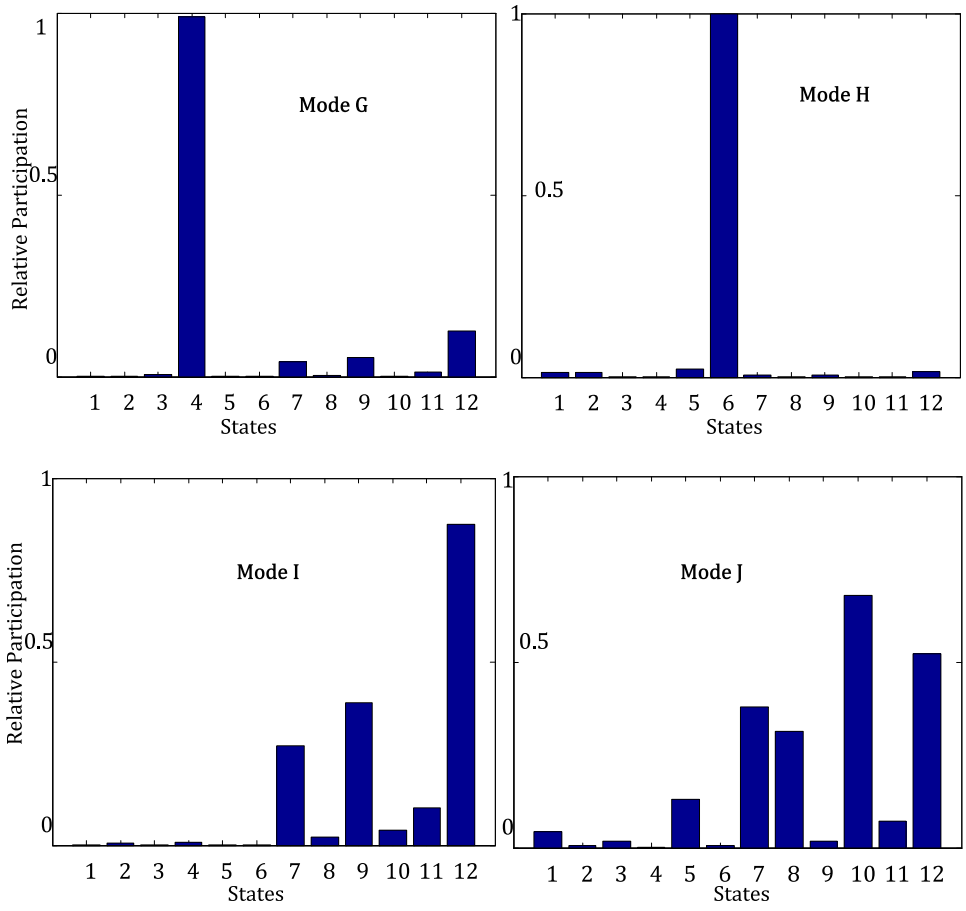

Fig. 4.6: Participation of each state of the realized state space in modes that were not initially identified by the Prony Method (*States 1-6: generator states, States 7-12: controller states; Modes (G)-(J) ref. Table 4.1*)

realized by multiple-window Prony method and the theoretically linearized system is not perfectly matching. (See Fig. 4.8-a). The method proposed in this chapter determines additional true modes (Modes G and H) and results in a better match in time domain responses. (See Fig. 4.8-b).

Fig. 4.9 presents the voltage deviation response comparison for theoretical linear system and the response of the system determined by the proposed method.

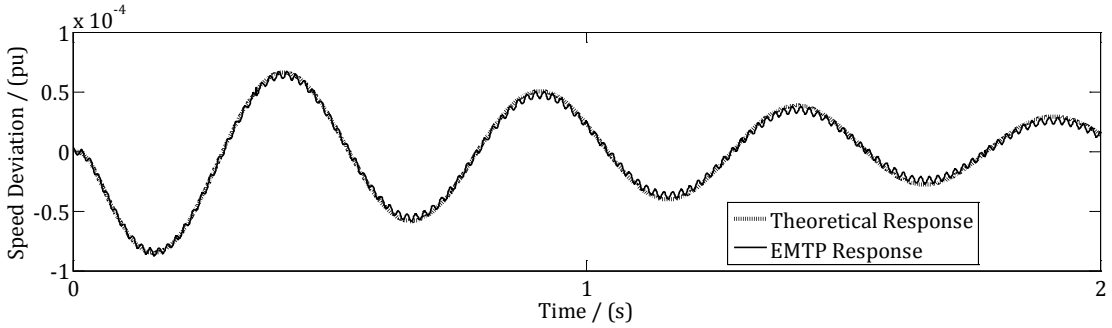

Fig. 4.7: Comparison of EMT simulation time domain output with the response of theoretical linear system

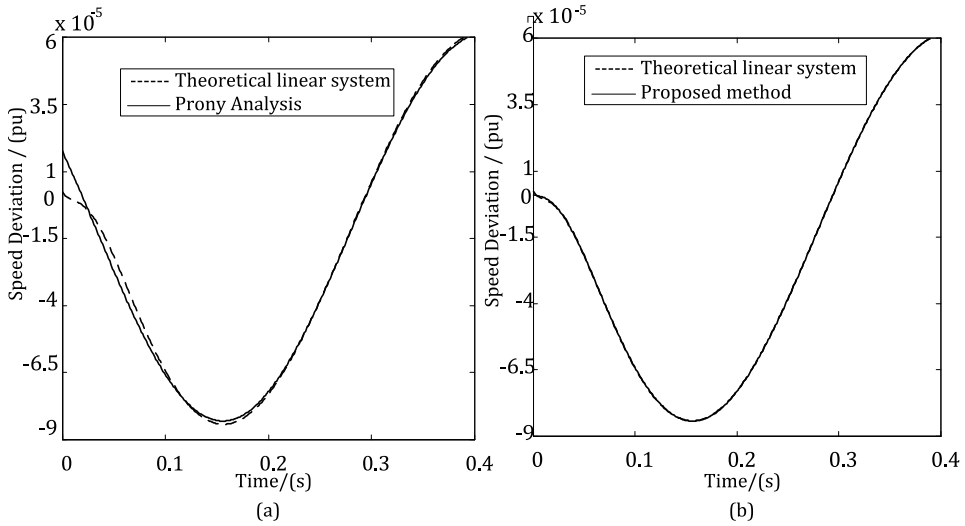

Fig. 4.8: Comparison of (a) Multiple-Window Prony Method and (b) the proposed method responses against the theoretical linear system response

4.6 Incorporating a Black Boxed Device to a Linear Analysis of a Power System

This section extends the concepts of Section 4.5 to a multi-machine system. The same three step procedure was carried out. In the first step, time domain output signals

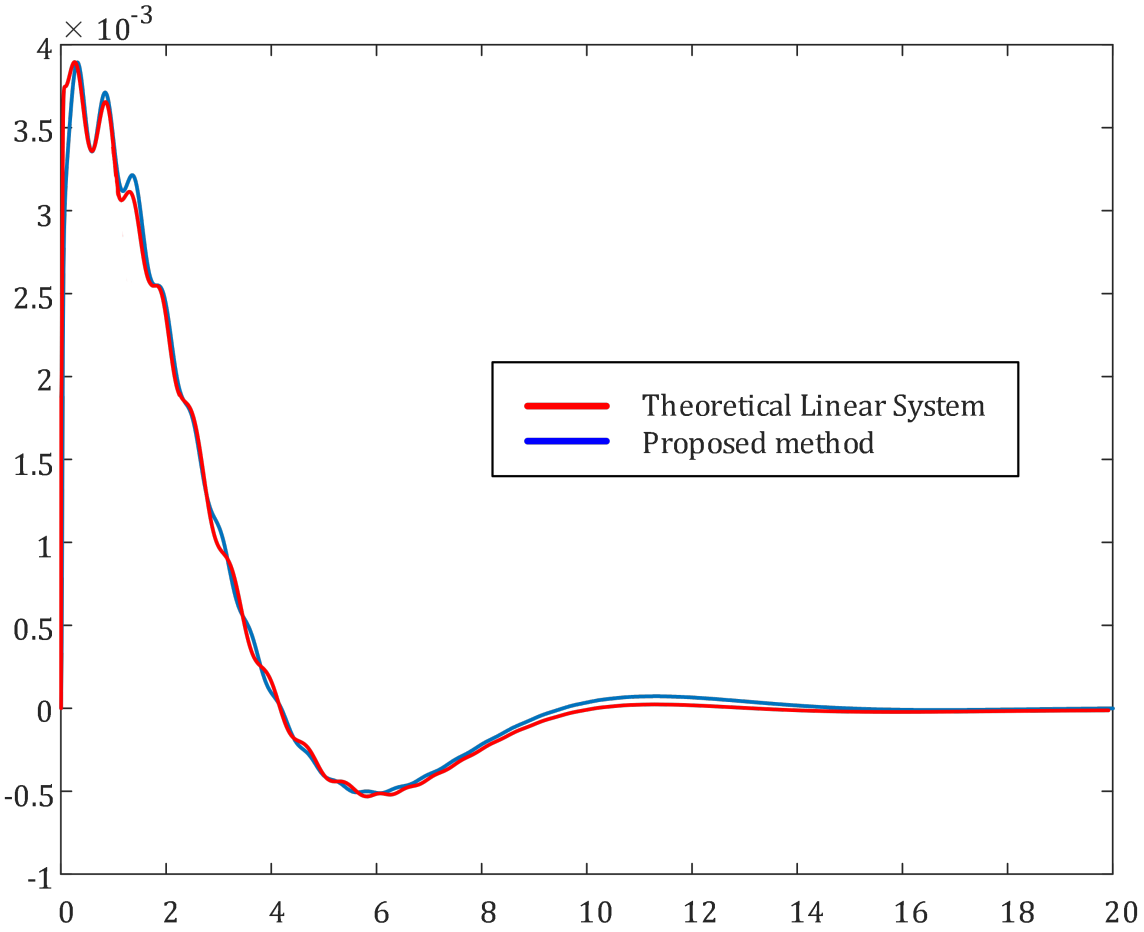

Fig. 4.9: Comparison of voltage deviation response of theoretical linear system with the the proposed method response

from generator buses of an EMT simulation of the multimachine power system are subjected to a multiple window Prony method presented in Section 3.3.3 and low damped modes of the system are identified. In the second step, a fictitious controller is designed using Eigenstructure Assignment (ESA). In the third step a state space is realized for the full system.

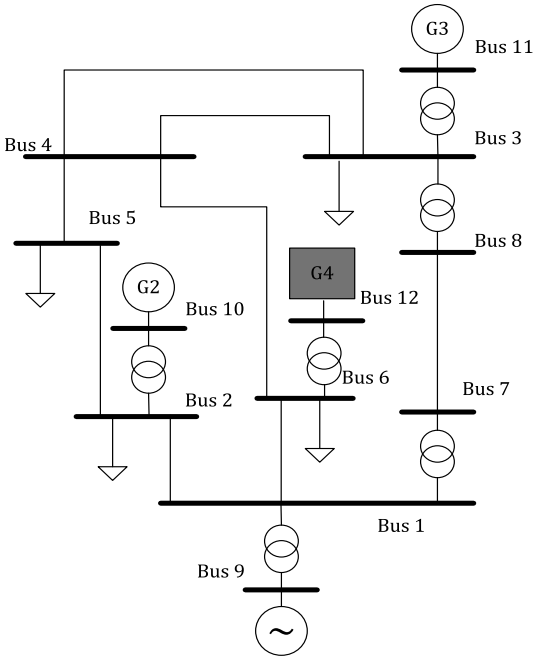

Fig. 4.10: IEEE 12-bus test system with bus 12 generator black-boxed

4.6.1 System Identification

In setting up the test case we assume that the EMT simulation model of the device is provided by the vendor as a black box with a limited number of outputs and inputs. Generator 4, connected to bus 12 of the IEEE 12-bus system [57], is considered to be a black-box. The generator speed (ω) and other terminal measurements such as voltage (V), current (I) and power of the black-box model are available to the user as output signals. The system is simulated in the EMT program and time-domain outputs at its three generator buses, 10, 11 and 12, are observed. Schematic of the simulated test system is shown in Fig. 4.10.

The system was simulated on PSCAD/EMTDC software with an integration time step of $50\mu s$. A $0.1pu$ pulse of 20ms duration was given to the mechanical torque input

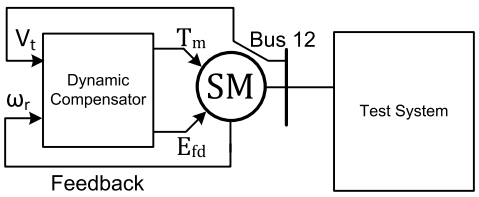

Fig. 4.11: Black box modeled as a synchronous machine with a dynamic compensator, connected to the larger system

of generator 3 (G3). Generator speeds and voltages at all three generator buses were observed. The smallest data window was $1.7s$ and five expanding data windows were chosen with an increment of $0.2s$. Thus the largest data window was $2.5s$

As the first step of the methodology, the Expanding-Window Prony method described in Section 3.3.3 was performed on the time domain signals of the test system. The method identifies the true modes of the system and their relative strength at each measuring point (generator buses). Outcome of Step 1 is reported in Table 4.4.

4.6.2 Eigenstructure Assignment

In Step 2, the test system, including the black-box synchronous machine, is modeled as shown in Fig. 4.11. Known parameters of the synchronous machine are included in the subsystem labeled as “SM". All the unknown dynamics are modeled by the dynamic compensator. The goal is to ensure that the closed loop system has the eigenvalues identified in Step 1.

Eigenstructure Assignment procedure with optimization proposed in Sections 4.3 and 4.4 was used to achieve this controller design goal. The most efficient convergence

of the Simulated Annealing used, was achieved with an initial temperature of 9000 with 10000 maximum iterations as the stopping criterion.

4.6.3 Results

Table 4.4: Eigenvalues and mode strengths identified from the time domain simulation

Eigenvalue	Relative Mode Strength in Signals					
	Speed Measurements			Voltage Measurements		
	Bus10	Bus11	Bus12*	Bus10	Bus11	Bus12*
$-0.313 \pm j8.60$	0.047	1	0.219	0.566	1	0.043
$-0.342 \pm j5.96$	0.188	0.182	0.587	0.261	0.377	0.134
$-0.285 \pm j5.03$	0.563	0.344	0.433	0.334	0.31	0.083
-2.913	0.047	0.027	0.029	0.338	0.179	0.047
-2.595	0.006	0.026	0.044	0.023	0.142	0.078
-2.267	0.01	0.031	0.011	0.013	0.321	0.036
-1.698	0.009	0.077	0.003	0.001	0.255	0.007
-0.645	0.021	0.038	0.128	0.002	0.003	0.006

*Measurements of the black-box generator bus

Mode identification results reported in Table 4.4 were used for the *Step 2* described above. Eigenvalues and participation factors can be conveniently evaluated from the system realized in *Step 3*. All electromechanical modes so calculated are reported in Table 4.5 along with their mode shapes in each generator speed output.

For the purpose of comparison, the actual system was linearized using the actual data including the system inside the black box . The calculated electromechanical

Table 4.5: Electromechanical modes evaluated for the system realized from the proposed method

Frequency (Hz)	Damping (%)	Participation	Mode Shapes					
			Bus10 (G2)		Bus11 (G3)		Bus12 (G4*)	
			Mag.	Ang.	Mag.	Ang.	Mag.	Ang.
1.37	3.63	G3, G4	0.047	94.738	1	-67.973	0.219	111.14
0.95	6.93	G2, G4	0.188	50.958	0.182	-85.196	0.587	-103.973
0.80	5.09	G2, G4	0.563	79.713	0.344	82.891	0.433	71.939

*Mode shapes for the black-box generator bus

Table 4.6: Electromechanical modes analytically evaluated from the actual system

Frequency (Hz)	Damping (%)	Participation	Mode Shapes					
			Bus10 (G2)		Bus11 (G3)		Bus12 (G4)	
			Mag.	Ang.	Mag.	Ang.	Mag.	Ang.
1.33	3.58	G3, G4	0.047	93.61	1	-72.72	0.22	110.7
0.93	5.79	G2, G4	0.189	50.79	0.19	-91.90	0.63	-103.97
0.78	5.90	G2, G4	0.579	78.27	0.34	78.06	0.45	71.93

modes, their participating states and mode shapes are shown in Table 4.6.

Comparing the eigenvalues shown in Tables 4.5 and 4.6 it can be seen that the the realized system represents the actual system with sufficient accuracy.

4.7 Discussion

It is not possible to linearize a power system if complete model data of all devices in the system are available. In case of a black-boxed synchronous machine model, even if the auxiliary controller model data are concealed due to proprietary reasons, the physical

parameters of the synchronous generator can be requested from the manufacturer. This data is utilized in the proposed method as *a priori* knowledge of the system. Using assumed or typical parameters for the unknown auxiliary controller may not result in the actual modes in the system, especially when the unknown auxiliary controller is responsible for damping certain modes in the system.

The black-boxed EMT model of the synchronous machine can be connected to the multi-machine system and perform time domain simulations. Some of the low damped modes of the system can be identified using the system identification procedure. A fictitious controller is designed to represent the auxiliary controller, using eigenstructure assignment, to achieve the identified modes for the system and the complete linear system can be realized. The fictitious controller is valid only for the operating point at which the modes were identified. The realized system gives the same modes and mode strengths identified in the EMT simulation. A modal analysis of the realized system gives participation factors for actual states in the system. This is in contrast to the subspace methods described in the introduction.

The subspace identification methods only give the participating locations of the identified modes, but not the actual states of the system. Subspace methods may be effective in case none of the model data is available. However, power systems are usually well documented and most of the model data pertaining to the system are available. Subspace methods are not capable of incorporating any *a priori* knowledge of the system.

4.8 Chapter Summary

This chapter introduced a novel method to incorporate *a priori* knowledge of a power system device to improve its transfer function identification. The expanding window Prony Analysis described in Chapter 3 was used to identify low damped modes a SMIB system of a synchronous machine. It was assumed that the current injection device data are available to the user but the auxiliary controller parameters are not. Then a fictitious controller was designed for the current injection device. The design objective was to achieve the same eigenstructure (modes and mode shapes) of the identified system. This was achieved by eigenstructure assignment (ESA). The choice of free parameter of the ESA is to be done within constraints which leads to a highly nonlinear optimization problem. Simulated Annealing was chosen as the candidate meta heuristic optimization method for the purpose. The realized system so realized includes all modes, including highly damped modes, of the current injection device along with the identified low damped modes.

This chapter also dealt with the problem of performing eigenvalue analysis of a multi-machine power system in the absence of complete model data of one of the synchronous machines, which is available only as a black boxed EMT simulation model. The specific case where the generator time constants and reactances are known but information of the auxiliary controllers are unknown, has been considered.

Chapter 5

Determining Auxiliary Controller Transfer Functions of a Synchronous Machine Model

5.1 Introduction

In small signal stability programs, the power system is modeled as a network with current injection devices connected to it. Each current injection device can be separated into two subsystems, namely, the device characteristics and the auxiliary controllers. The device characteristics are usually described by the time constants and reactances (in case of generators). Auxiliary controllers can be assumed to be linear and operating-point-independent in the normal operating region of the power system device. If the transfer functions for each auxiliary controller and the transfer functions for the current injection device can be separately determined, the complete linear system can be aggregated into a state-space and complete eigenvalue analysis is possible for the complete system. Given the dynamic data and the operating point data of the machine, the transfer functions for machine can be obtained. Section 5.1

describes the challenge of identifying an operating-point-independent model even if the machine transfer functions are known and describes how to utilize the distinct dynamics at distinct operating points to obtain operating-point-independent auxiliary controller transfer functions.

In this chapter, a black boxed EMT simulation model of a synchronous machine is considered. Modes from a finite number of operating points of the system, are identified using a Prony Analysis method augmented with eigenstructure assignment, presented in Chapter 4 [58, 59]. Mason's Gain Rule is used to separate the subsystems in the simulation case. A linear system of polynomial equations are generated using data from multiple operating points and they are solved for the auxiliary controller transfer function polynomials.

5.2 Utilizing the Operating Point Dependency of Power System Devices

Consider a simple single-input-single-output (SISO) feedback system given in Fig. 5.1.

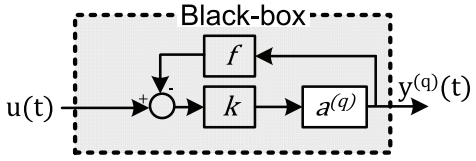

Fig. 5.1: Simple SISO system with feedback

Let $a^{(q)}$ be a known scalar gain at the qth operating point. $y^{(q)}(t)$ is the output obtained at the qth operating point for input $u(t)$. k and f are unknown scalar gains

that need to be estimated. The user can observe $y^{(q)}(t)$ and can control $u(t)$. $y^{(q)}(t)$ and $u(t)$ are the only signals the user has access to. Using system identification, the transfer relationship between inputs and outputs can be found as:

$$y^{(q)}(t) = \theta^{(q)} u(t) \tag{5.1}$$

where

$$\theta^{(q)} = \frac{k a^{(q)}}{1 + k f a^{(q)}} \tag{5.2}$$

$\theta^{(q)}$ is dependent on the operating point. k and f cannot be separately determined by estimating $\theta^{(q)}$ at only one operating point, even if $a^{(q)}$ is known. The operating-point-dependency of gain $a^{(q)}$ allows to obtain the following linear relationship for two operating points for $q = 1, 2$.

$$\begin{bmatrix} \theta^{(1)} \\ \theta^{(2)} \end{bmatrix} = \underbrace{\begin{bmatrix} a^{(1)} & -a^{(1)}\theta^{(1)} \\ a^{(2)} & -a^{(2)}\theta^{(2)} \end{bmatrix}}_{\mathrm{M}} \begin{bmatrix} k \\ kf \end{bmatrix} \tag{5.3}$$

If $\mathbf{M}$ is well conditioned, a unique solution for $\begin{bmatrix} k & kf \end{bmatrix}^T$ exists.

A power system device has the special feature of having some subsystems operating-point-dependent (e.g. the machine), while other subsystems are operating-point-independent (e.g. auxiliary controllers). This Section presents a novel approach, utilizing the said feature, to determine operating-point-independent transfer functions of individual subsystems. The model structure of a power system device is more complex than the example presented in Fig. 5.1. Therefore, Mason's Gain Rule has been carefully used to decompose a complex system into known and unknown

subsystems, in order to apply the simple principle presented above.

5.3 Mathematical Preliminaries

Let there be a linear combination of polynomials $A_i(s)$, $X_i(s)$ and $B_i(s)$ of variable s:

$$\begin{bmatrix} A_1(s) & A_2(s) & ... & A_p(s) \end{bmatrix} \begin{bmatrix} X_1(s) \\ X_2(s) \\ ... \\ X_p(s) \end{bmatrix} = B(s) \tag{5.4}$$

where

$$A_i(s) = \sum_{k=0}^{m} a_{ik} s^k \; ; \quad B_i(s) = \sum_{k=0}^{n} b_{ik} s^k \; ; \text{and} \quad X_i(s) = \sum_{k=0}^{n-m} x_{ik} s^k$$

If orders of $A_i(s)$ and $B_i(s)$ are known to be m and n respectively, order of $X_i(s)$ is $n-m$. The polynomial relationship in Eq. 5.4 can be given by convolution matrices and vectors as follows:

$$\begin{bmatrix} \mathbf{A_1} & \mathbf{A_2} & ... & \mathbf{A_p} \end{bmatrix} \begin{bmatrix} \mathbf{x_1} \\ \mathbf{x_2} \\ ... \\ \mathbf{x_p} \end{bmatrix} = \mathbf{b} \tag{5.5}$$

where:

$\mathbf{A_i}$ = the convolution matrix of $A_i(s)$ of appropriate dimensions

$\mathbf{x_i}$ = the vector of coefficients of the polynomial $X_i(s)$

$\mathbf{b}$ = the vector of coefficients of the polynomial $B(s)$

Similarly, a set of linear equations of polynomials such as:

$$\begin{bmatrix} A_1^{(1)} & A_2^{(1)} & ... & A_p^{(1)} \\ A_1^{(2)} & A_2^{(2)} & ... & A_p^{(2)} \\ ... & ... & ... & ... \\ A_1^{(q)} & A_2^{(q)} & ... & A_p^{(q)} \end{bmatrix} \begin{bmatrix} X_1 \\ X_2 \\ ... \\ X_p \end{bmatrix} = \begin{bmatrix} B^{(1)} \\ B^{(2)} \\ ... \\ B^{(q)} \end{bmatrix} \tag{5.6}$$

can be represented by vectors and convolution matrices, as an extension of Eq. 5.5, as follows.

$$\underbrace{\begin{bmatrix} \mathbf{A_1^{(1)}} & \mathbf{A_2^{(1)}} & ... & \mathbf{A_p^{(1)}} \\ \mathbf{A_1^{(2)}} & \mathbf{A_2^{(2)}} & ... & \mathbf{A_p^{(2)}} \\ ... & ... & ... & ... \\ \mathbf{A_1^{(q)}} & \mathbf{A_2^{(q)}} & ... & \mathbf{A_p^{(q)}} \end{bmatrix}}_{\mathrm{A}} \underbrace{\begin{bmatrix} \mathbf{x_1} \\ \mathbf{x_2} \\ ... \\ \mathbf{x_p} \end{bmatrix}}_{\mathrm{x}} = \begin{bmatrix} \mathbf{b^{(1)}} \\ \mathbf{b^{(2)}} \\ ... \\ \mathbf{b^{(q)}} \end{bmatrix} \tag{5.7}$$

If $\mathbf{A}$ is well conditioned, then, a unique solution for $\mathbf{x}$ can be found.

In the following sections, we show that a linearized power system at q operating points, can be represented by a system of Laplacian Polynomials as in Eq. 5.6, where $X_i(s)$ represents unknown, operating-point-independent subsystems; $A_i^{(j)}(s)$ represents known, operating-point-dependent subsystems, and $B^{(j)}$ represents the known characteristic polynomial of the system at the jth operating point. The unknown subsystems can be determined by solving Eq. 5.7.

5.4 Problem Statement

In this chapter a black-boxed EMT simulation model of a synchronous machine with a limited number of inputs and outputs, is considered. As shown in Fig. 5.2, the EMT simulation model is connected to an infinite bus through a transformer and a short transmission line. Outputs such as generator speed $\omega(t)$ and other terminal measurements such as voltage $V(\mathrm{t})$, current $I(\mathrm{t})$, active power $P(\mathrm{t})$ and reactive power $Q(\mathrm{t})$, and voltage reference input to the exciter $V_{\mathrm{ref}}(\mathrm{t})$ and speed reference input to the governor $\omega_{ref}(t)$ are available to the user. All time constants and reactances of the synchronous machine (SM) included in the model are also available to the user.

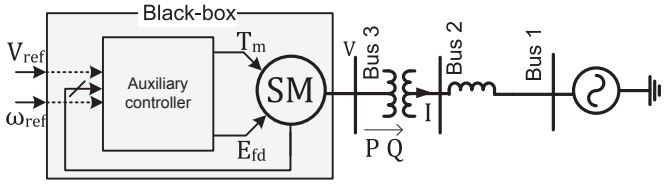

Fig. 5.2: Test power system with the black boxed synchronous machine connected

Parameters of the open-loop synchronous machine (SM) are known. Therefore its MIMO transfer function matrix can be determined by linearizing the nonlinear equations that describe synchronous machines, as described in [3]. The input/output transfer relationship of the MIMO block of Fig. 5.3 is given by Eq. 5.8. Note that the denominator of all transfer functions in the MIMO system are the same.

$$\begin{bmatrix} \Delta\omega(t) \\ \Delta V(t) \end{bmatrix} = \begin{bmatrix} \frac{N_{M1}(s)}{D_M(s)} & \frac{N_{M2}(s)}{D_M(s)} \\ \frac{N_{M3}(s)}{D_M(s)} & \frac{N_{M4}(s)}{D_M(s)} \end{bmatrix} \begin{bmatrix} \Delta T_m(t) \\ \Delta E_{fd}(t) \end{bmatrix} \tag{5.8}$$

A generic auxiliary controller structure as shown in Fig 5.3 is considered. The system consists of an exciter, a power system stabilizer (PSS) and a turbine-governor.

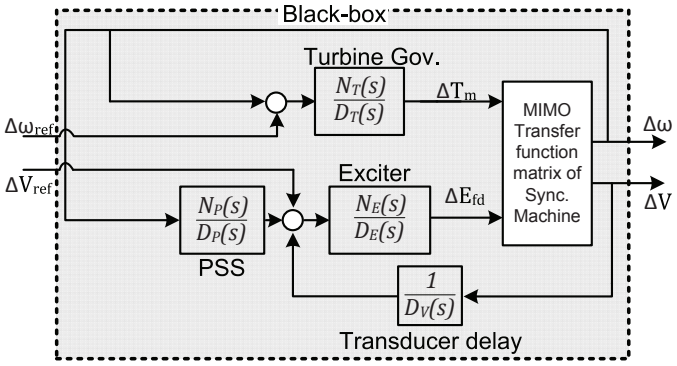

Fig. 5.3: Assumed model structure for the black-boxed device

The objective is to determine the unknown transfer functions $\left(\frac{N_E}{D_E}\right)$, $\left(\frac{N_T}{D_T}\right)$, $\left(\frac{N_P}{D_P}\right)$ and $\left(\frac{1}{D_V}\right)$, in such a way that their parameters could be used in a complete eigenvalue analysis of a power system consisting of the black-boxed synchronous machine model.

5.5 Subsystem Transfer Functions of a Synchronous Machine

5.5.1 Application of Mason's Gain Rule

All variables in this section, unless defined, refer to the Section 5.4, specifically Fig. 5.3 and Eq. 5.8.

Let $G_\omega(s)$ be the transfer function that describes the rotor speed response of the closed loop SMIB synchronous machine system, to a small perturbation of the speed reference input to the governor. The block diagram of the closed loop system is given in Fig.5.3. Applying Mason's Gain Rule [60, 61], $G_\omega(s)$ can be expressed in terms of numerator and denominator polynomials of subsystem transfer functions (denoted

by N and D with subscripts) as shown in Eq 5.9.

$$G_\omega = \frac{N_\omega}{D_{total}} \tag{5.9}$$

where

$$\begin{aligned} N_\omega &= N_T N_{M1} D_V D_E D_P \\ &\quad + N_E N_T D_P U \end{aligned} \tag{5.10}$$

$$\begin{aligned} D_{total} &= D_M D_T D_V D_E D_P \\ &\quad + N_T N_{M1} D_V D_E D_P \\ &\quad - N_T N_E D_P U \\ &\quad - N_P N_E N_{M2} D_T D_V \\ &\quad + N_E N_{M4} D_T D_P \end{aligned} \tag{5.11}$$

Polynomial U in Eq. 5.10 and Eq. 5.11 is defined as:

$$U = \frac{N_{M1} N_{M4} - N_{M3} N_{M2}}{D_M} \tag{5.12}$$

Eq. 5.12 takes the form of the determinant of a square transfer function matrix. This is according to the following Theorem 1, of which the proof is given in Appendix D.

Theorem 1 *For a state space described by* $\mathbf{A} \in \mathbb{R}^{n \times n}$, $\mathbf{B} \in \mathbb{R}^{n \times r}$ *and* $\mathbf{C} \in \mathbb{R}^{r \times n}$,

$$\dot{\mathbf{x}} = \mathbf{A}\mathbf{x} + \mathbf{B}\mathbf{u} \tag{5.13}$$

$$\mathbf{y} = \mathbf{C}\mathbf{x} \tag{5.14}$$

With the transfer function matrix:

$$\mathbf{W} = \mathbf{C}(\mathbf{I}s - \mathbf{A})^{-1}\mathbf{B} \tag{5.15}$$

we have:

$$\det(\mathbf{W}) = \frac{p(s)}{\det(s\mathbf{I} - \mathbf{A})} \tag{5.16}$$

where $p(s)$ is a polynomial in s of order $n - r$.

Numerator and denominator polynomials of transfer function G_ω, can be written as a set of polynomial equations in terms of subsystem transfer functions.

From Eq. 5.10 to Eq. 5.11:

$$\mathbf{H}(s)\mathbf{v}(s) = \begin{bmatrix} N_\omega \\ D_{total} \end{bmatrix} \tag{5.17}$$

where

$$\mathbf{H}(s) = \begin{bmatrix} 0 & N_{M1} & U & 0 & 0 \\ D_M & N_{M1} & -U & -N_{M2} & N_{M4} \end{bmatrix} \tag{5.18}$$

$$\mathbf{v}(s) = \begin{bmatrix} X_1 \\ X_2 \\ X_3 \\ X_4 \\ X_5 \end{bmatrix} = \begin{bmatrix} D_T D_V D_E D_P \\ N_T D_V D_E D_P \\ N_T N_E D_P \\ N_P N_E D_T D_V \\ N_E D_T D_P \end{bmatrix} \tag{5.19}$$

For the considered model structure, there are five unknowns in the polynomial equations derived from Mason's Gain Rule. Each X_k, for $k = [1, 2, ...5]$, is a polynomial. If the order of polynomials in $\mathbf{H}(s)$ is m and the order of the characteristic polynomial D_{total} is n, then the order of each element in $\mathbf{v}(s)$ is $n - m$. Polynomial equation in Eq. 5.17 can be represented by the corresponding convolution matrices and vectors as:

$$\begin{bmatrix} \mathbf{0} & \mathbf{N_{M1}} & \mathbf{U} & \mathbf{0} & \mathbf{0} \\ \mathbf{D_M} & \mathbf{N_{M1}} & \mathbf{-U} & \mathbf{-N_{M2}} & \mathbf{N_{M4}} \end{bmatrix} \mathbf{x} = \mathbf{b^{(k)}} \tag{5.20}$$

This is analogous to Eq. 5.5. The system can be solved for $\mathbf{x}$ by developing a system as given in Eq. 5.7, from data for q operating points, where q is the least number of operating points required to obtain a full rank system of equations. From the solutions for $\mathbf{x}$, elements of $\mathbf{v}(s)$ can be determined.

Let $\Gamma(.)$ be the operator that minimally realizes a rational polynomial function and then normalizes it to the highest order term of the denominator polynomial. By operating $\Gamma(.)$ on elements of $\mathbf{v}(s)$, as shown in Eq. 5.21, an intermediate set of

transfer functions can be calculated.

$$\frac{N_a(s)}{D_a(s)} = \Gamma\left(\frac{X_2}{X_1}\right) \tag{5.21a}$$

$$\frac{N_b(s)}{D_b(s)} = \Gamma\left(\frac{X_3}{X_2}\right) \tag{5.21b}$$

$$\frac{N_c(s)}{D_c(s)} = \Gamma\left(\frac{X_4}{X_1}\right) \tag{5.21c}$$

From Eq. 5.17 and Eq. 5.21 the numerator and denominator polynomials of auxiliary controller transfer functions can be uniquely calculated as presented in Eq. 5.22.

$$N_T = N_a \tag{5.22a}$$

$$D_T = D_a \tag{5.22b}$$

$$N_E = N_b \tag{5.22c}$$

$$D_P = \frac{X_5}{N_b D_a} \tag{5.22d}$$

$$D_E = \frac{D_c}{D_P} \tag{5.22e}$$

$$D_V = \frac{D_b}{D_E} \tag{5.22f}$$

$$N_P = \frac{N_c}{N_b} \tag{5.22g}$$

5.5.2 Transfer Function Identification

To solve Eq. 5.7, the coefficient matrix **A**, is calculated from the machine parameters that are assumed to be available. Vector **b** is determined by the numerator and

denominator polynomials of the total system transfer function. TheProny analysis procedure augmented with eigenstructure assignment *(ESA Prony Method)* presented in Chapter 4 was used to identify the transfer function of the system shown in Fig. 5.2. The reasons for selecting this procedure over others are as follow:

- The procedure assures identifying true modes in the system and avoid over-fitting fictitious modes.
- The procedure assures that all modes dominantly contributed by the machine, including the highly damped machine-modes, are identified.

The ESA Prony Method may still fail to identify modes contributed by the auxiliary controller. The effect of failure to identify modes is discussed in Section 5.7.

The proposed procedure has been summarized by a flowchart given in Fig. 5.4.

5.6 Test System and Results

The system in Fig. 5.2, which is the same as the test system in Fig. 4.1, was simulated on PSCAD/EMTDC software with an integration time step of $50\mu s$. Parameters for the test system are given in Appendix C. It is assumed that the components and signals inside the grayed box in Fig. 5.2, are not accessible to the user. Terminal quantities and rotor speed are accessible outputs. Exciter voltage reference and governor speed reference are accessible inputs. A small disturbance was given to the system by giving a $0.25pu$ pulse for $25ms$ to the ω_{ref} input of the governor. The speed of the generator and the terminal voltage were observed. The output signals was decimated to a sampling time of $10ms$. The multiple window Prony Analysis

augmented with eigenstructure assignment presented in Chapter 4 was used to determine the transfer functions of the system at operating points given in Table 5.1. These candidate operating points were randomly chosen from a uniformly distributed set of operating points, within the operating region of the machine.

Table 5.1: Data of candidate operating points at which modes of the system were identified

Operating Point	1	2	3	4	5	6	7	8	9	10	11
Active Power (pu)	0.81	0.21	0.39	0.37	0.27	0.71	0.66	0.28	0.33	0.65	0.64
Reactive Power (pu)	0.22	0.66	0.66	0.09	0.48	0.12	0.37	0.38	0.08	0.40	0.02

The change in the identified system poles at the first five operating points are visible in the eigenvalue plot in Fig. 5.5.

Polynomials N_{M1}, N_{M2}, N_{M3} N_{M4} and D_M of machine transfer functions were calculated using system data for the chosen set of operating points. The machine transfer functions are of order 6 as a sixth order round rotor synchronous machine model was used in the test system.

The system identification procedure yields 11^{th} order transfer functions for the complete system. Hence the order of the complete auxiliary controller is 5. The calculated machine transfer function polynomials and identified closed loop system transfer function polynomials were used to populate matrix $\mathbf{A}$ and vector $\mathbf{b}$ of Eq. 5.7, respectively, in the form of appropriately dimensioned convolution matrices and coefficient vectors as explained in Section 5.3. Data from five distinct operating points were sufficient to obtain a full rank $\mathbf{A}$ matrix, and a solution for $\mathbf{x}$ was obtained by Moore-Penrose Inversion method. The initial solution for $\mathbf{v}(s)$ in Eq. 5.17 obtained from solution for $\mathbf{x}$ is given in Table 5.2.

Table 5.2: Coefficients of Polynomials of Initial Solution for $\mathbf{v}(s)$

$\mathbf{v}(s)$	Coefficients					
	s^5	s^4	s^3	s^2	s^1	s^0
X_1	0.9953	1.5052	1.3454	0.4983	0.0777	0.0017
X_2	-0.0016	-16.88	-16.36	-5.618	-0.7094	-0.0343
X_3	-0.9582	163.3	309.8	188.7	43.33	3.329
X_4	-37.59	-316.4	-814.6	-833.3	-236.1	-0.647
X_5	-20.68	-30.35	-27.00	-12.53	-2.635	-0.2014

Table 5.3: Coefficients of Polynomials of Refined Solution for $\mathbf{v}(s)$

$\mathbf{v}(s)$	Coefficients					
	s^5	s^4	s^3	s^2	s^1	s^0
X_1	0.9998	1.9207	1.2154	0.3401	0.0433	0.0020
X_2	0	-16.99	-15.45	-5.027	-0.6935	-0.0342
X_3	0	178.3	301.8	162.3	34.95	2.610
X_4	-47.46	-344.2	- 846.1	-840.2	-290.8	-0.002
X_5	-10.49	-28.37	-27.52	-11.72	-2.234	-0.1554

The very small high order terms of X_2 and X_3 in Table 5.2 were eliminated and $\mathbf{v}(s)$ was recalculated. The recalculated solutions for $\mathbf{v}(s)$ is given in Table 5.3.

Application of the operation introduced in Eq. 5.21 yields the intermediate transfer functions given in Eq. 5.23.

Table 5.4: Comparison of Auxiliary Controller Transfer Functions Realized from the Proposed Method with the Actual Transfer Functions

Auxiliary Controller	Realized Transfer Function	Actual Transfer Function
Turbine-Governor $\frac{N_T(s)}{D_T(s)}$	$\frac{-17.05}{s+1.012}$	$\frac{-16.67}{s+1}$
Exciter $\frac{N_E(s)}{D_E(s)}$	$\frac{-10.49s-9.531}{s+0.1099}$	$\left(\frac{-10s-10}{s+0.1}\right)\left(\frac{100}{s+100}\right)$
PSS $\frac{N_P(s)}{D_P(s)}$	$\frac{4.524s^3+24.13s^2+30.16s}{s^3+0.7842s^2+0.198s+0.01611}$	$\frac{4.826s^3+24.13s^2+30.16s}{s^3+0.9s^2+0.24s+0.02}$
Voltage Transducer $\frac{1}{D_V(s)}$	1	$\frac{50}{s+50}$

$$\Gamma\left(\frac{X_2}{X_1}\right) = \frac{-17.05}{s+1.012} \tag{5.23a}$$

$$\Gamma\left(\frac{X_3}{X_2}\right) = \frac{-10.49s-0.9531}{s+0.1099} \tag{5.23b}$$

$$\Gamma\left(\frac{X_4}{X_1}\right) = \frac{47.45s^4+296.2s^3+546.3s^2+287.4s}{s^4+0.9213s^3+0.3034s^2+0.0422s+0.002} \tag{5.23c}$$

The realized controller transfer functions, by application of the simplification given in Eq. 5.22, are presented in Table 5.4. The third column 'Actual Transfer Function' has been included in Table 5.4 for comparison against the realized transfer functions.

The response of each realized transfer function to a 25ms pulse of 0.25pu magnitude are plotted in Fig. 5.6 to Fig. 5.8.

Realizing the auxiliary controller transfer functions is equivalent to obtaining the complete set of dynamic data of the black-boxed synchronous machine. When the dynamic data of a black-boxed machine is available to the user, a linear state space can be obtained for any known power system that includes the black-boxed machine,

at any operating point. The realized transfer functions were incorporated in an SMIB system at a different operating point than that was used for system identification. Operating Point 11 from Table 5.1 was used for the validation. The realized linear system was perturbed and the resulting speed change plot is given in Fig. 5.9. It can be observed that the frequency of the response is matching and the peaks of the first four cycles are slightly different. Given that the system was realized without the knowledge of the auxiliary controller parameters, it can be concluded that the realized model reproduces the dynamics of the actual system with sufficient accuracy, using data from the minimum required number of operating points.

From the time-domain responses in Fig. 5.7 to Fig. 5.8, it is evident that, by utilizing only five operating points for system identification, the time constants of the transfer functions were realized with a reasonable accuracy. However, there are small discrepancies in the gains and zeros in the realized systems for the exciter and PSS that causes the mismatch in damping in the response in Fig. 5.9.

The process was repeated using data from more operating points than the minimum required operating points, and the realized system was tested against Operating Point 11 as before. Fig. 5.10 presents the responses of systems realized, using extra operating points. It was observed that, using data from more operating points, improves the accuracy of the realized system.

5.7 Effects of errors in system identification

5.7.1 Not identifying modes

The system identification procedure proposed in [58] ensures that all modes contributed by the machine are identified as the method utilizes known data of the machine. However, modes contributed by the auxiliary controllers may be missed due to the following reasons.

- Modes are highly damped
- Poles are canceled out with zeros
- Complex modes with very low frequencies may be identified as real modes.

The effect of missing highly damped modes on the Eq. 5.7 is minimal. By performing the system identification on multiple outputs with different perturbations ensures that poles canceled out by zeros for one input/output pair, are made visible by another.

However, if a complex pole with very low frequency and small negative real part was identified as a real mode, a significant error is introduced to the solution of Eq. 5.17. Such an error can be identified by the inconsistency of elements of $\mathbf{v}(s)$ in Eq. 5.17, in the sense that Eq. 5.24 is not satisfied by the obtained solutions.

$$X_1 X_3 - X_2 X_5 = 0 \tag{5.24}$$

5.7.2 Mitigating misidentification of complex modes with very low frequencies

A situation where two eigenvalues are very closely located was created by changing the PSS parameters of the test system given in Table C.4 in Appendix cha:Linearizing. Two parameters were changed as $T_2 = 0.4s$ and $T_4 = 5s$. The change causes the system to have a complex eigenvalue pair $-0.199 \pm j0.005$ which is misidentified by the system identification as a single decaying mode (-0.199). This causes the solutions for $\mathbf{v}(s)$ to not satisfy Eq. 5.24 and the resulting auxiliary controller transfer function responses do not match with the actual responses. In order to mitigate this, all real eigenvalues with magnitudes less than a threshold value Γ, were replaced with pairs of complex eigenvalues with the same real part and very small imaginary part, in different combinations. Criterion for choosing Γ is given by Eq. 5.25.

$$\Gamma = 10 \times \min |\Re\{all\ eigenvalues\}| \tag{5.25}$$

Eq. 5.24 was evaluated for all such combinations and the combination that satisfies the equation the best is chosen as the suitable correction to be introduced to the system identification result. The modified PSS transfer function response, realized by the proposed procedure is given in Fig. 5.11. All other auxiliary controller responses are identical to result obtained in Section 5.6.

5.8 Summary of the Proposed Procedure

Mason's Gain Rule was used to decompose the generic model structure of a synchronous machine into its subsystem transfer functions. The black-boxed simulation model was connected to an infinite bus and was subjected to an enhanced system identification procedure at a limited number of operating points. Data of identified transfer functions of the system and, dynamic data of the synchronous machine were used to generate a polynomial equation. The distinction of poles and zeros of the system at distinct operating points has been utilized to generate a full rank system of polynomial equations whose solutions are the auxiliary controller transfer function polynomials. The realized auxiliary controller transfer functions can be used to include the black-boxed synchronous machine in small signal stability analysis at any operating point, connected to any power system.

5.9 Chapter Summary

This chapter introduced a methodology to decompose a power system device mode into known-operating-point-dependent subsystems and unknown-operating-point-independent subsystems, using results from Mason's Gain Rule. A linear system of polynomial equations was developed. It can be solved for unknown auxiliary controller polynomials by using system identification results (identified transfer functions) from multiple operating points. Such identified transfer functions essentially requires to include all modes contributed by the known current injection device subsystem. Application of the Prony Analysis method augmented with eigenstructure assignment, presented in Chapter 4 ensures that the identified transfer functions meet this condition. The pro-

cedure has been successfully demonstrated for the case of a black-boxed synchronous machine with controllers, to determine operating-point-independent linear auxiliary controller transfer functions. Transfer functions so realized can be easily incorporated into a small signal stability analysis of a power system that includes the black-boxed synchronous machine.

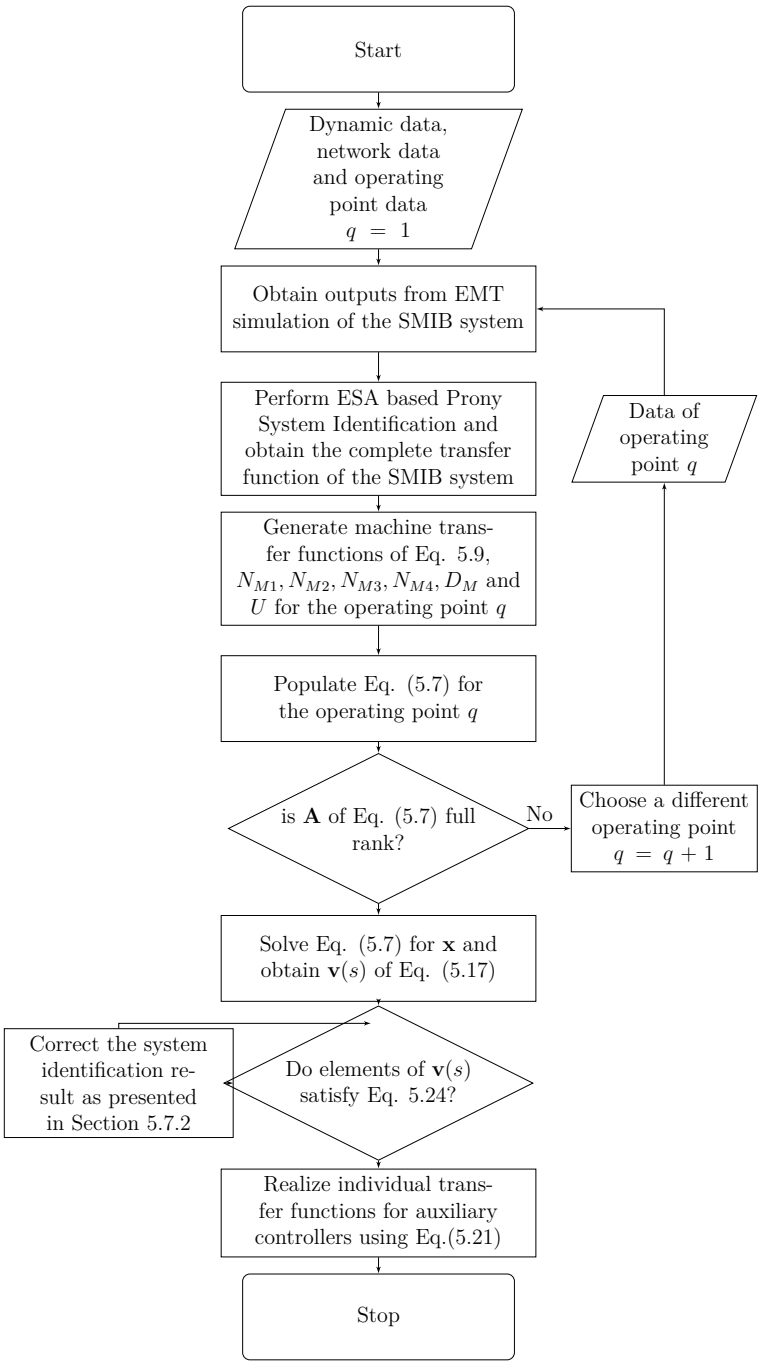

Fig. 5.4: Proposed procedure flow chart

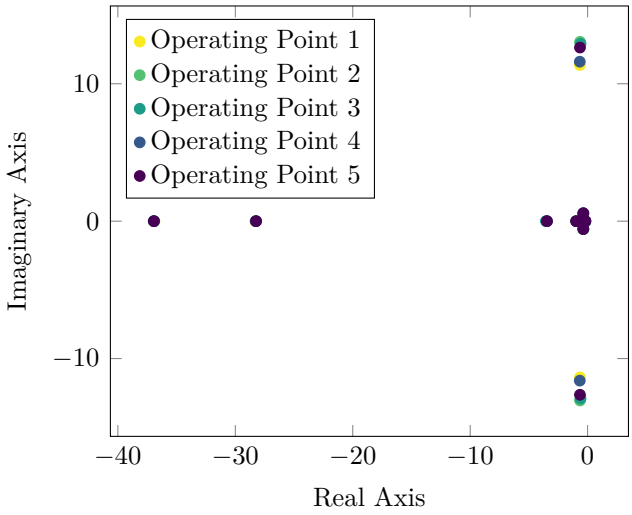

Fig. 5.5: Identified eigenvalues of the system at five distinct operating points

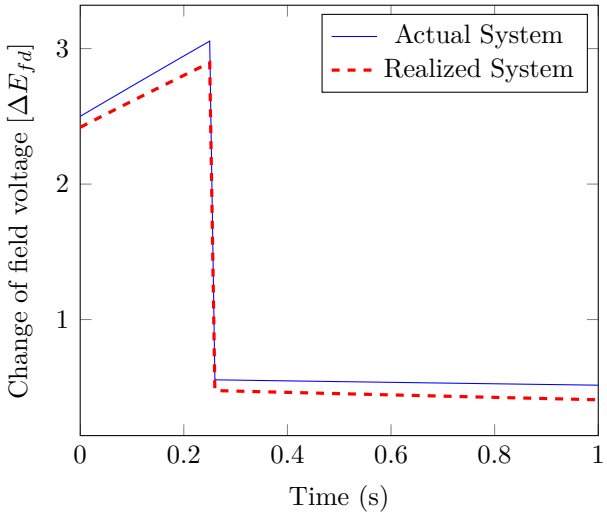

Fig. 5.6: Time responses of realized and actual exciter transfer functions

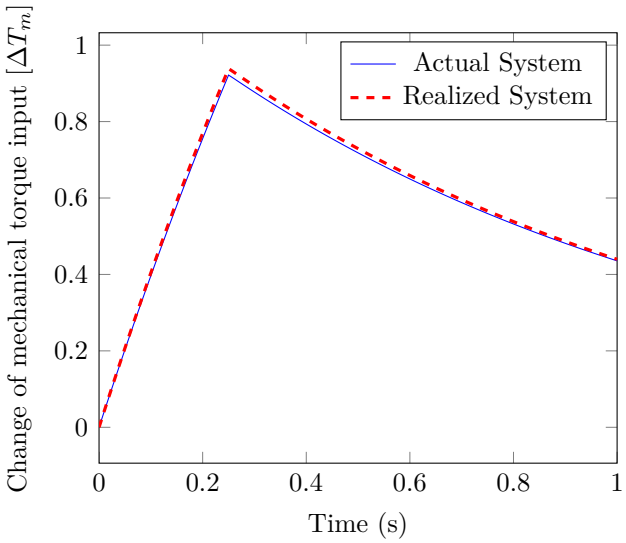

Fig. 5.7: Time responses of realized and actual governor transfer functions

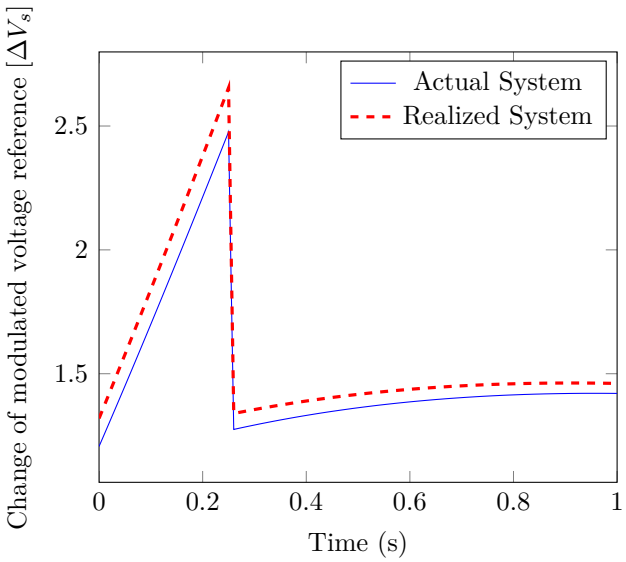

Fig. 5.8: Time responses of realized and actual PSS transfer functions

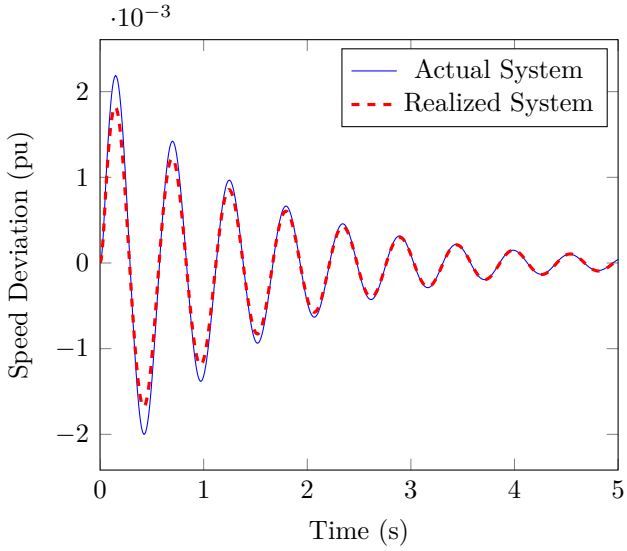

Fig. 5.9: Comparison of realized and actual system responses at Operating Point 11

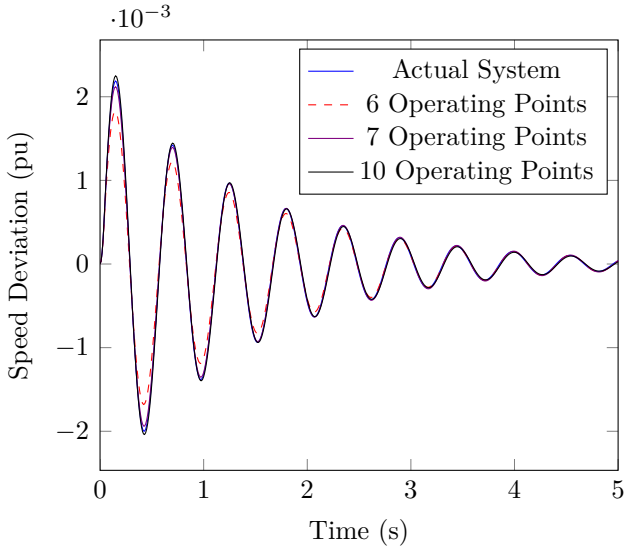

Fig. 5.10: Comparison of system responses realized using data from additional operating point

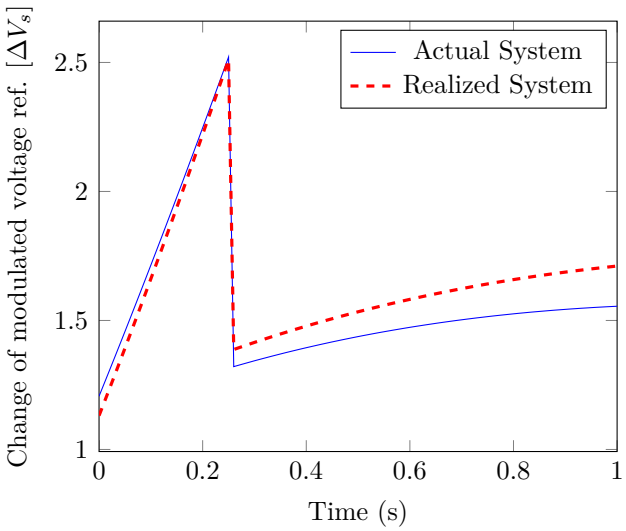

Fig. 5.11: Time responses of realized and actual PSS transfer functions in the presence of two real modes very close to each other

Chapter 6

Determining Auxiliary Controller Transfer Functions of a Black-Boxed DFIG

In the preceding chapters, a procedure for determining auxiliary controller transfer functions of a power system device has been established. The procedure starts with a Prony Analysis method that incorporates *a priori* knowledge of the system by using eigenstructure assignment. Modes so identified at multiple operating points are used to determine subsystem transfer functions of a black-boxed power system device. The power system device was divided into two main subsystems, namely, the operating point dependent current injection device and the auxiliary controller which is operating point independent within a given operating mode. By solving a linear set of polynomial equations, the unknown auxiliary controller transfer functions of a synchronous machine were realized as presented in Chapter 5. The knowledge of the structure of the auxiliary controller was utilized in decomposing the complete system into subsystems using the result of Mason's Gain rule. The real application of determining auxiliary controller transfer functions are in more modern power system

devices. The controller architecture of these modern devices are much more complex than that of a synchronous machine. Doubly-Fed Induction Generator (DFIG) was chosen as a candidate device to apply the procedure proposed in this thesis.

6.1 Overview of DFIGs

Doubly-Fed Induction Generator (DFIG), also known as *Type 3* Wind Turbine Generator (WTG), is a popular technology with converters rated at 25% - 30% of the generator rating. Four-quadrant active and reactive power operation with variable speed is the major advantage of DFIGs over fixed speed induction generators. The cost advantage over the Full Converter Type 4 WTG makes DFIG a popular candidate in the rapid drive for the expansion of wind power generation [62]. Small signal stability analysis of power systems with DFIG wind turbine penetration has been a topic of great interest in the past decade [63]. In planning the expansion of the power grid with modern devices, it is important to pay attention to possible interactions between control systems of the existing power system and those of the planned additions.

The general architecture of a DFIG is given in Fig. 6.1.

Decoupled control architecture is the most common control strategy for DFIG. The generic control structure of a DFIG is given in Fig. 6.2.

It has been identified that DFIGs are the most vulnerable type of WTG to subsynchronous oscillations, especially where there are series compensated lines [63]. There has been a debate in recent papers on the root cause of the subsynchronous oscillations; whether it is due to self excitation or due to controller interactions. Eigenvalue

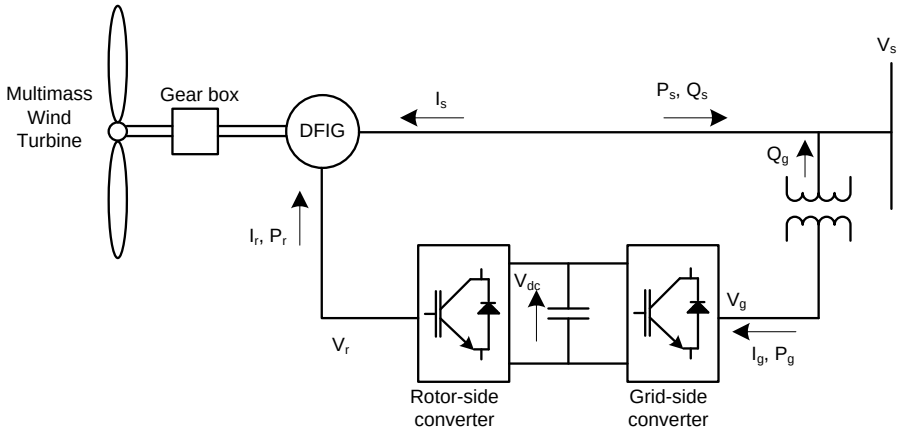

Fig. 6.1: Generic schematic of the Doubly Fed Induction Generator (DFIG)

analysis has been the main tool used in these studies and they all assume that the DFIG of the study case is fully known. The importance of linear analysis has been reiterated especially to find the root cause of oscillatory issues as well as to determine the mitigatory measures.

Manufacturers of DFIGs, almost always, conceal the controllers of their product and make available an as built electromagnetic transient (EMT) simulation model for the users. The common practice in the industry is to connect the black-boxed simulation model to the user's test system and perform time-domain simulations for a limited number of study cases. Unavailability of the complete mathematical model forces the power system engineers to forgo small signal stability analysis of the system, which also closes the door to apply methodologies to investigate root causes of stability issues.

The DFIG control architecture proposed in [64] and, very descriptively presented in [65] was used in the simulation model. For the purpose of this study, the controller blocks and signals of a black boxed EMT model of a DFIG that have been contained in

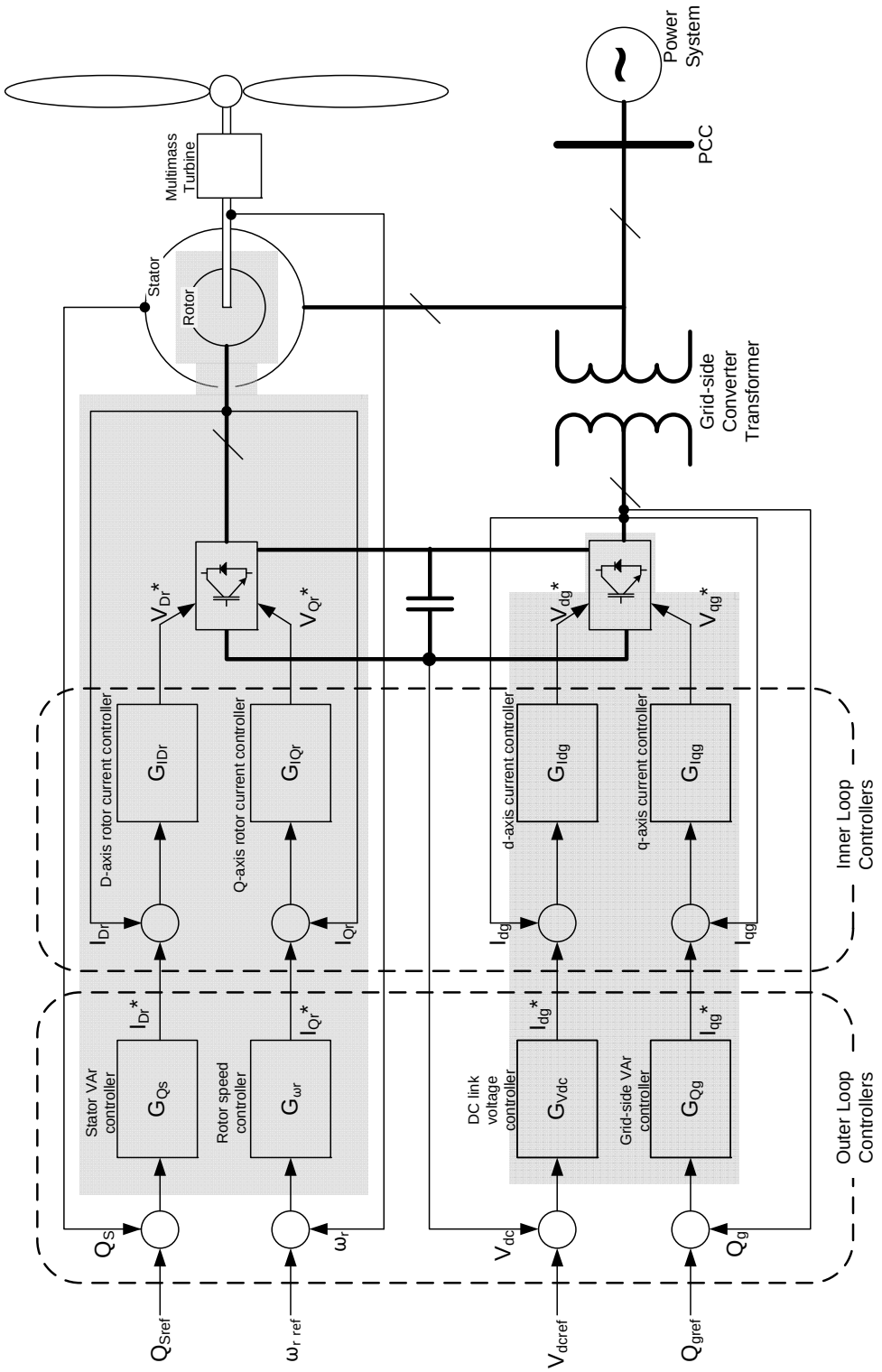

Fig. 6.2: Decoupled control architecture of DFIG

the darkened areas in Fig. 6.2 are considered inaccessible to the user. The induction generator parameters and stator measurements, converter transformer parameters and terminal measurements, DC capacitor voltage measurement and input references are assumed to be accessible to the user.

The problem at hand is to identify transfer functions that describe the inner loop current controllers of both converters and outer loop controllers for speed, stator reactive power, grid reactive power and DC link voltage, separately.

6.2 Applicability of the Proposed Procedure to DFIG

For the case of a synchronous machine with an exciter, power system stabilizer and turbine-governor block, in Chapter 5, a minimum of only 5 operating points were required to solve the linear system of polynomial equations. By increasing the number of operating points to 10, the accuracy of the transfer function determination process increased. It is clear that, as the black-boxed system gets more complex, the number of required operating points increases.

Fig. 6.3 is the block diagram of transfer functions of a DFIG connected to an infinite bus through a short transmission line. Definitions of symbols used in the Fig. 6.3 are given in Table C.7 in Appendix C. The transfer function matrix shown in Fig. 6.3 represents the transfer functions between each input/output pair of the machine subsystem. The transfer functions were calculated based on the linearized model of the wound rotor induction generator presented in [65], based on the detailed model presented in [3]. All signal paths and signal names shown in green colour are reference inputs determined by the user of the simulation. Perturbations to the

system are made through those inputs. All signal paths and signal names shown in blue represent observable signals in the simulation. Transfer functions shown in blue are also fully known. The subsystems and signals shown in black are inside the black box.

The corresponding Signal Flow Graph (SFG) of the block diagram shown in Fig. 6.3 consists of 26 nodes and 72 edges. Applying Mason's Gain Rule between the inputs and outputs of the system and separating the known and unknown subsystem polynomials reveals that there are 139 unknown polynomials that require data from at least 178 operating points to solve. Obtaining distinct modal identification data for a large number of operating points is a challenge as the actual change in poles and zeros from one operating point to another may be smaller than the error in the system identification. Also, very small changes may cause the linear system of polynomial equations to be ill-conditioned.

Due to the requirement of very high number of operating points, some subsystems are required to be identified separately, so that the order of the problem is reduced to a manageable magnitude. The grid-side converter controllers are more accessible than those of the rotor-side. If the grid-side converter controllers and turbine transfer functions are known, the system can be represented by a set of polynomial equations that has 15 unknowns, and data from 8 operating points are required to solve the system. The grid-side converter system is more accessible. Therefore by a conventional system identification exercise, its controller parameters could be estimated as presented in Section 6.3.1 that follows. MATLAB Symbolic Toolbox was used to manipulate the very large amount of variables and equations.

The known and unknown subsystems were separated by applying Mason's Gain

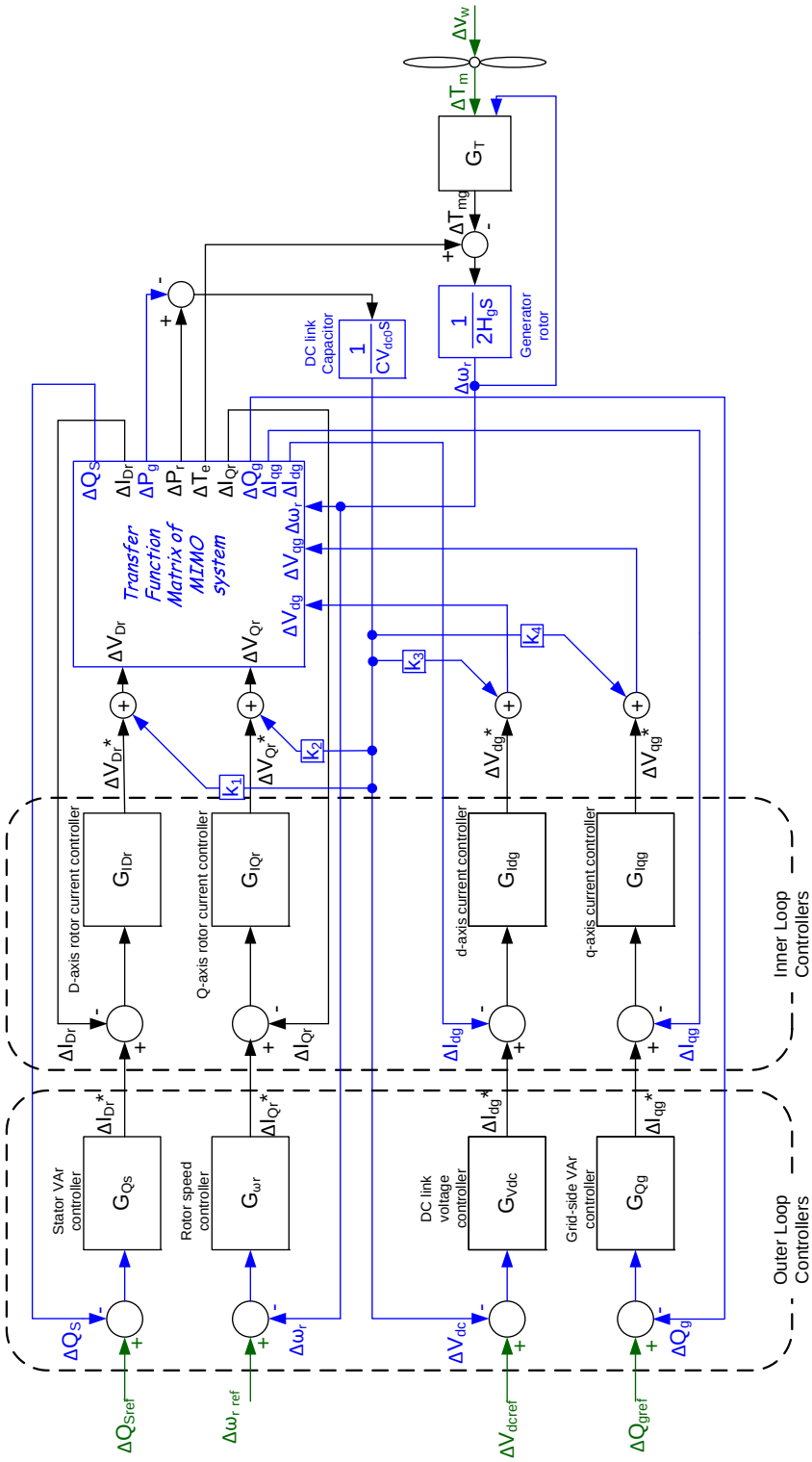

Fig. 6.3: Decoupled control architecture of DFIG

Rule as proposed in Section 5.5 and the linear system of polynomial equations similar to Eq. 5.17 was obtained.

Due to the relative complexity of the system, each element in **H** (in Eq. 5.17) is a summation of a large number of terms. In this specific case, the maximum number of polynomials aggregated in a single element is 64. Each and every element of this matrix can be calculated, as all the polynomials involved are known. The theorem proven in Chapter 5 is used to calculate the polynomials that are in the form of determinants of transfer function matrices. This conditioning ensures that the elements of **H** are numerically accurate, despite the arithmetic summation of a large number of terms.

The unknown vector of polynomials obtained from Mason's Gain Rule reduction is:

$$\mathbf{v}(s) = \begin{bmatrix} X_1 \\ X_2 \\ X_3 \\ X_4 \\ X_5 \\ X_6 \\ X_7 \\ X_8 \\ X_9 \\ X_{10} \\ X_{11} \\ X_{12} \\ X_{13} \\ X_{14} \\ X_{15} \end{bmatrix} = \begin{bmatrix} D_{I_{Dr}} D_{I_{Qr}} D_{Q_s} D_{\omega_r} D_T \\ N_{I_{Dr}} N_{I_{Qr}} N_{Q_s} N_{\omega_r} D_T \\ D_{I_{Dr}} D_{I_{Qr}} D_{Q_s} D_{\omega_r} N_T \\ D_{I_{Dr}} D_{Q_s} D_T N_{I_{Qr}} N_{\omega_r} \\ D_{I_{Dr}} D_{Q_s} D_{\omega_r} D_T N_{I_{Qr}} \\ D_{I_{Dr}} D_{Q_s} D_{\omega_r} N_T N_{I_{Qr}} \\ D_{I_{Qr}} D_{Q_s} D_{\omega_r} D_T N_{I_{Dr}} \\ D_{I_{Qr}} D_{Q_s} D_{\omega_r} N_{I_{Dr}} N_T \\ D_{I_{Qr}} D_{\omega_r} D_T N_{I_{Dr}} N_{Q_s} \\ D_{I_{Qr}} D_{\omega_r} N_{I_{Dr}} N_{Q_s} N_T \\ D_{Q_s} D_T N_{I_{Qr}} N_{\omega_r} N_{I_{Dr}} \\ D_{Q_s} D_{\omega_r} D_T N_{I_{Dr}} N_{I_{Qr}} \\ D_{Q_s} D_{\omega_r} N_{I_{Dr}} N_{I_{Qr}} N_T \\ D_{\omega_r} D_T N_{I_{Dr}} N_{I_{Qr}} N_{Q_s} \\ D_{\omega_r} N_{I_{Dr}} N_{I_{Qr}} N_{Q_s} N_T \end{bmatrix} \tag{6.1}$$

An intermediate set of transfer functions can be realized by Eq. 6.2, where $\Gamma(.)$ is the function for minimum realization.

$$\frac{N_a(s)}{D_a(s)} = \Gamma\left(\frac{X_3}{X_1}\right) \tag{6.2a}$$

$$\frac{N_b(s)}{D_b(s)} = \Gamma\left(\frac{X_5}{X_1}\right) \tag{6.2b}$$

$$\frac{N_c(s)}{D_c(s)} = \Gamma\left(\frac{X_7}{X_1}\right) \tag{6.2c}$$

$$\frac{N_d(s)}{D_d(s)} = \Gamma\left(\frac{X_5}{X_1}\right) \tag{6.2d}$$

Numerator and denominator polynomials of the controllers can be uniquely determined by the following relationships:

$$N_T = N_a \tag{6.3a}$$

$$D_T = D_a \tag{6.3b}$$

$$N_{I_{Qr}} = N_b \tag{6.3c}$$

$$D_{I_{Qr}} = D_b \tag{6.3d}$$

$$N_{I_{Dr}} = N_c \tag{6.3e}$$

$$D_{I_{Dr}} = D_c \tag{6.3f}$$

$$N_{Q_s} = N_d \tag{6.3g}$$

$$D_{Q_s} = D_d \tag{6.3h}$$

$$\frac{N_{\omega_r}}{D_{\omega_r}} = \frac{X_4 D_{I_{Qr}}}{X_1 N_{I_{Qr}}} \tag{6.3i}$$

$$\tag{6.3j}$$

6.3 Test Results

A DIFIG SMIB as shown in Fig. 6.1 was simulated on PSCAD/EMTDC software with an integration time step of $50\mu s$. Test system data are given in the Appendix C. The improved Prony Analysis presented in Chapter 4 was used to identify the modes of the system. The DFIG was opereated at constant Tip-Speed-Ratio (TSR). Constant TSR ensures maximum power tracking by changing the speed reference.

6.3.1 Identification of the Grid-side Converter Controllers

Identification of the grid-side converter controllers was carried out as a system identification exercise between inputs and outputs. Steady state values of all terminal quantities were obtained. The angle between the infinite bus voltage and the transformer terminal voltage is α. Transformer terminal voltage was compared with the reference sinusoidal waveform of steady state voltage and was decomposed into d and q frames and V_{dg} and V_{qg} were obtained, and they are the output signals for the system identification. Transformer terminal current, phase angle of the current, grid-side converter reactive power output Q_g, DC link voltage V_{dc} and input references Q_{gref} and V_{dcref} are the input signals. External current injections along d-axis and q-axis at the converter transformer bus have been introduced to improve the identifiability of the systems.

Identification of DC link Voltage Controller

DC capacitor voltage controller of the grid-side converter controller is shown in Fig. 6.4. The input considered for the transfer function identification, U_1, shown in the

figure, is the difference between the V_{DC-ref} input and measured DC link voltage. The transfer functions between the inputs and outputs are given by Eq. 6.4. A current source is connected to the converter transformer bus and a second transfer function identification was carried out using a current injection along the d-axis. The transfer function between Δi_{dg-ext} and Δv_{dg} is given by Eq. 6.5. It should be noted that N and D denote the numerator and denominator polynomials of the transfer functions shown in the block diagrams.

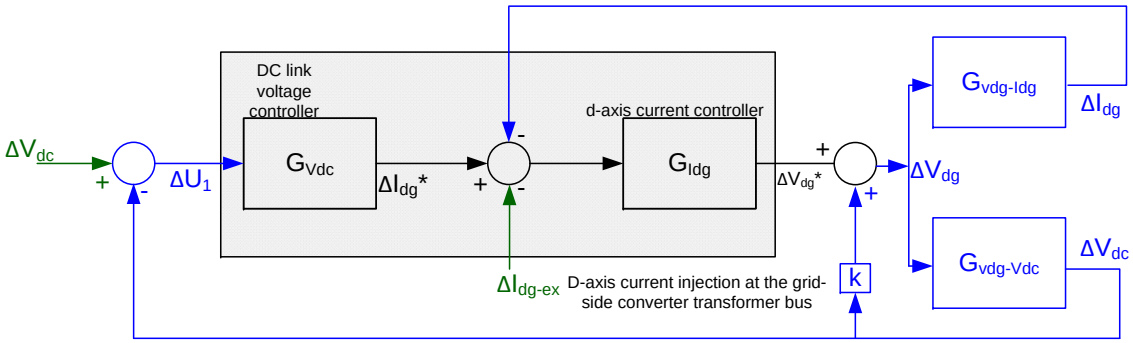

Fig. 6.4: Block diagram of DC link voltage controller

$$\frac{\Delta v_{dg}(s)}{\Delta U_1(s))} = \frac{N_{V_{dc}} N_{i_{dg}} D_{v_{dg}-V_{dc}} D_{v_{dg}-i_{dg}}}{D_{V_{dc}}(D_{i_{dg}} D_{v_{dg}-V_{dc}} D_{v_{dg}-i_{dg}} + N_{v_{dg}-i_{dg}} N_{i_{dg}} D_{v_{dg}-V_{dc}} - k N_{v_{dg}-V_{dc}} D_{v_{dg}-i_{dg}} D_{i_{dg}})} \tag{6.4}$$

$$\frac{\Delta v_{dg}(s)}{\Delta i_{dg-ext}(s)} = \frac{N_{i_{dg}} D_{V_{dc}} D_{vdg-Vdc} D_{vdg-idg}}{D_{i_{dg}}(D_{V_{dc}} D_{vdg-Vdc} D_{vdg-idg} + N_2 D_{vdg-Vdc} D_{V_{dc}} - k N_{vdg-Vdc} D_{vdg-idg} D_{V_{dc}})} \tag{6.5}$$

The transfer functions realized from the two system identification exercises are

given in Table 6.1.

Table 6.1: Identified transfer functions of grid-side converter DC link voltage controller

Transfer Function	System Identification Result
$\frac{\Delta v_{dg}(s)}{\Delta U_1(s))}$	$\frac{-2.43(s+202.35)(s+51.33)(s^2+17.6s+3.176\times10^4)}{(s+93.54)(s+0.43)(s^2+522s+1.321\times10^5)}$
$\frac{\Delta v_{dg}(s)}{\Delta i_{dg-ext}(s)}$	$\frac{0.47(s+204.6)(s^2+18.7s+3.2847\times10^4)}{(s+0.51)(s^2+506s+1.599\times10^5)}$

It should be noted that the response of transfer functions between Δv_{dg} and the output variables ΔV_{dc} and Δi_{dg} are very fast. This can be observed in roots of the numerator of the realized transfer functions. This suggests that the relatively small zeros are those of the DC link voltage controller. This suggests that in determining auxiliary controller transfer functions of complex systems requires engineering intuition, as in the case of any system identification exercise. Further validation of system identification results can be obtained by repeating the transfer function identification of grid-side controllers at different operating points.

By observing the zeros and poles of the realized transfer functions between inputs and outputs, the numerator and denominator polynomials of each auxiliary controller transfer function was realized. The determined parameters have been compared with the actual PI controller parameters in the system, in Table 6.3.

Identification of Grid-Side Converter Reactive Power Controller

The same exercise as above, was carried out for the reactive power controller. The system for which transfer function identification was applied is shown in Fig. 6.5. It

is assumed that v_{qg} has minimal sensitivity to variations in V_{dc} for perturbations to Q_{g-ref} and i_{qg-ext}.

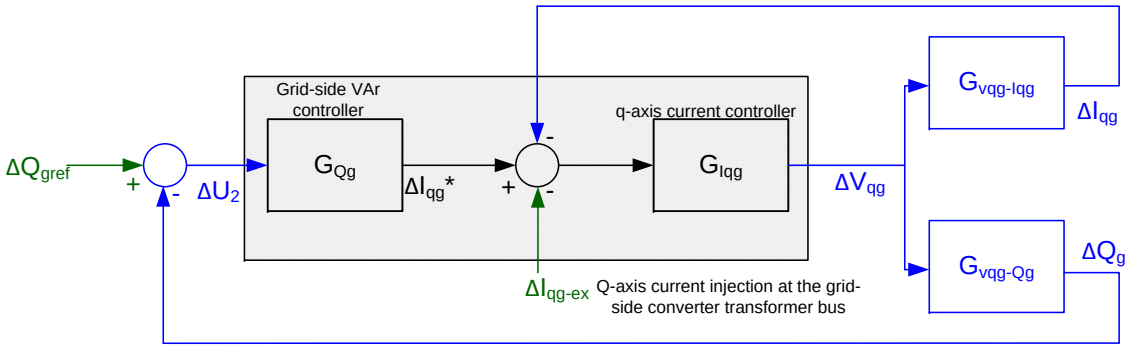

Fig. 6.5: Block diagram of DC link voltage controller

$$\frac{\Delta v_{qg}(s)}{\Delta U_2(s)} = \frac{N_{Q_g} N_{i_{qg}} D_{vqg-iqg}}{D_{Q_g}(D_{vqg-iqg} D_{i_{qg}} + N_{i_{qg}} N_{vqg-iqg})} \tag{6.6}$$

$$\frac{\Delta v_{qg}(s)}{\Delta i_{qg-ext}(s)} = \frac{N_{i_{qg}} D_{Q_g} D_{vqg-Qg} D_{vqg-iqg}}{D_{i_{qg}}(D_{Q_g} D_{vqg-Qg} D_{vqg-iqg} + N_{vqg-iqg} D_{vqg-Qg} D_{Q_g} + N_{vqg-Qg} D_{vqg-iqg} N_{Q_g})} \tag{6.7}$$

The transfer functions realized from the two system identification exercises are given in Table 6.2. Estimated controller transfer function parameters are presented in Table 6.3 along with actual PI controller parameters.

Table 6.2: Identified transfer functions of grid-side converter reactive power controller

Transfer Function	System Identification Result
$\frac{\Delta v_{qg}(s)}{\Delta U_2(s))}$	$\frac{8.89(s+92.82)(s+11.32)(s^2+407.7s+4.101\times10^5)}{(s+87.32)(s+0.93)(s^2+619.3s+3.491\times10^5)}$
$\frac{\Delta v_{qg}(s)}{\Delta i_{qg-ext}(s)}$	$\frac{0.79(s+89.83)(s^2+607.02s+5.861\times10^5)}{(s+0.32)(s^2+643.2s+561.32\times10^5)}$

Table 6.3: Comparison of realized grid-side auxiliary controller transfer functions with the actual transfer functions

Auxiliary Controller	Realized Transfer Function	Actual Transfer Function
$G_{V_{dc}}$	$\frac{-5.17s-16.54}{s+0.43}$	$\frac{-5s-10}{s}$
$G_{I_{dg}}$	$\frac{0.47s+96.162}{s+0.51}$	$\frac{0.5s+100}{s}$
G_{Q_g}	$\frac{11.25s+127.4}{s+0.93}$	$\frac{10s+100}{s}$
$G_{I_{qg}}$	$\frac{0.79s+96.70}{s+0.32}$	$\frac{s+100}{s}$

6.3.2 System Identification of the Total System

The only unknown subsystems left to be determined are the outer-loop and inner loop controller transfer functions of the rotor-side converter and the transfer function

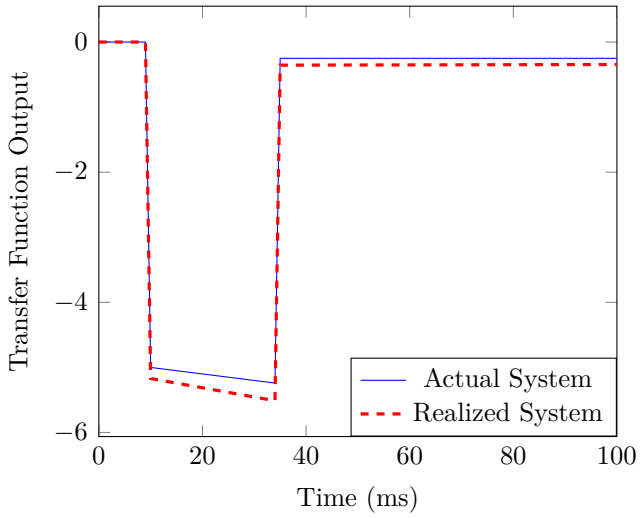

Fig. 6.6: Time responses of realized and actual $G_{V_{dc}}$ transfer functions

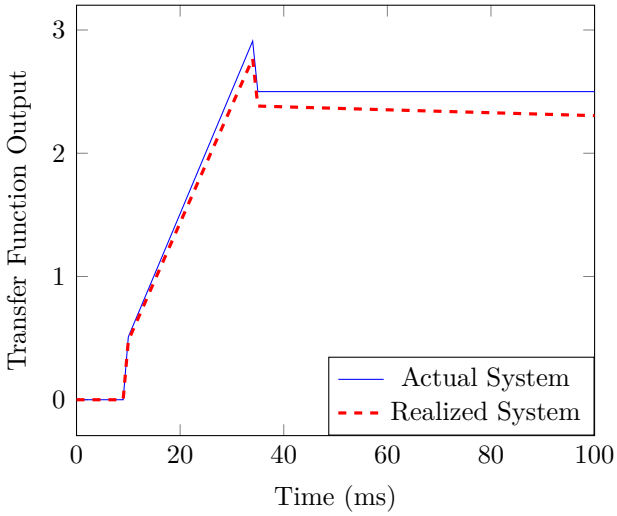

Fig. 6.7: Time responses of realized and actual $G_{I_{dg}}$ transfer functions

of the multimass turbine.

The system was subject to modal identification at 20 operating points. The system was independently perturbed using the DC link voltage reference (V_{dc-ref}) and the stator reactive power reference input (Q_s) to achieve the respective transfer

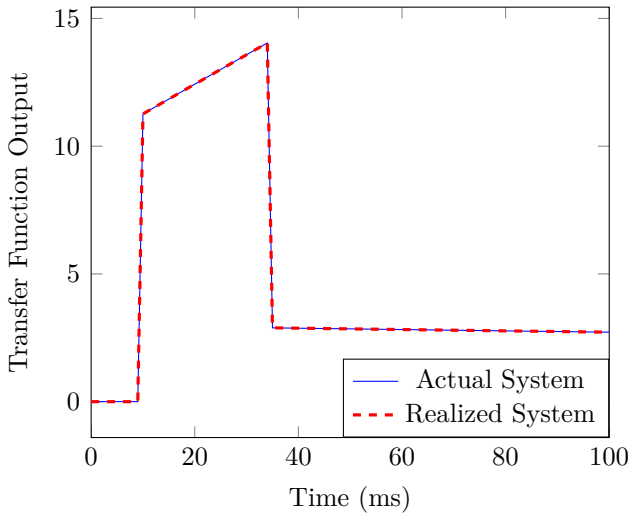

Fig. 6.8: Time responses of realized and actual G_{Q_g} transfer functions

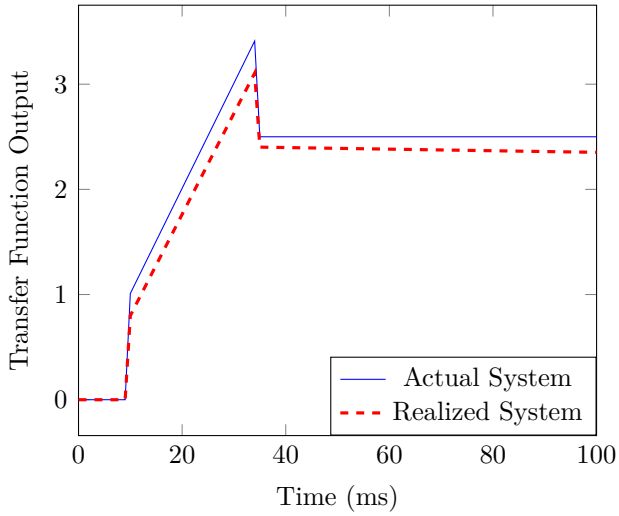

Fig. 6.9: Time responses of realized and actual $G_{I_{qg}}$ transfer functions

functions between the inputs and outputs. In order to maintain a constant torque input to the multimass turbine, the wind speed was modulated using the speed of the rotor. The performance coefficient of the wind turbine was assumed to be constant. It should be noted that parameters of grid-side controller transfer functions were

considered as *a priori* knowledge of the system in application of the methods presented in Chapter 4 to identify the modes.

Variation of the identified modes at varying operating points are shown in Fig. 6.10.

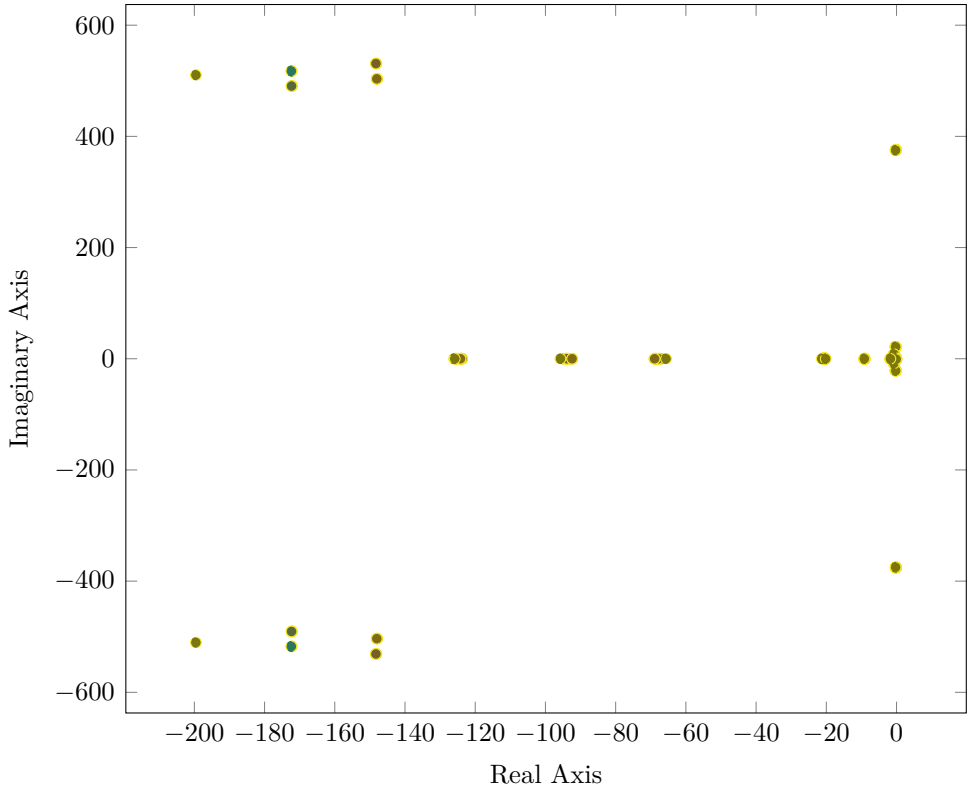

Fig. 6.10: Identified eigenvalues of the system at five distinct operating points

6.3.3 Results for the Rotor-Side Converter Controllers

By applying the system identification data to Eq. 6.1 to 6.3, the auxiliary controllers of the rotor-side converter could be determined. The realized transfer functions and the actual controller transfer functions are shown in Table 6.4.

Table 6.4: Comparison of auxiliary controller transfer functions realized from the proposed method with the actual transfer functions

Auxiliary Controller	Realized Transfer Function	Actual Transfer Function
G_{Q_s}	$\frac{0.39s+1.96}{s+0.21}$	$\frac{0.5s+2.5}{s}$
G_{ω_r}	$\frac{-1.08s-0.69}{s+0.94}$	$\frac{-1.5s-0.75}{s}$
$G_{I_{D_r}}$	$\frac{0.74s+12.45}{s+0.04}$	$\frac{0.5s+10}{s}$
$G_{I_{Q_r}}$	$\frac{0.29s+8.92}{s+0.31}$	$\frac{0.5s+10}{s}$

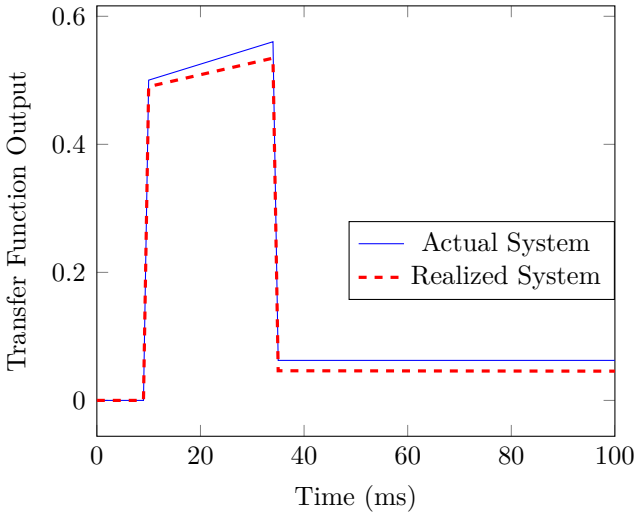

Fig. 6.11: Time responses of realized and actual G_{Q_s} transfer functions

6.3.4 Determining Multimass Turbine Transfer Function

The proposed procedure yields the multimass turbine transfer function as shown in Table 6.5. The transfer function realized is the one between rotor speed deviation, $\Delta\omega_r$, and input torque to the generator rotor ΔT_{mg} (output torque of the multimass turbine). The test system assumes zero mechanical damping in the multimass turbine.

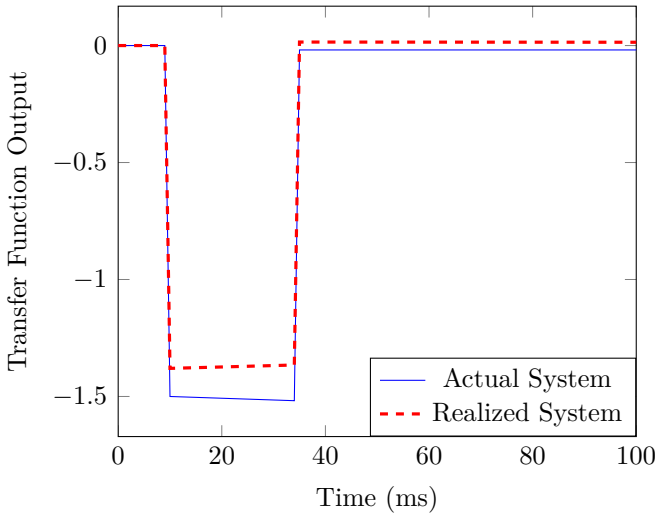

Fig. 6.12: Time responses of realized and actual G_{ω_r} transfer functions

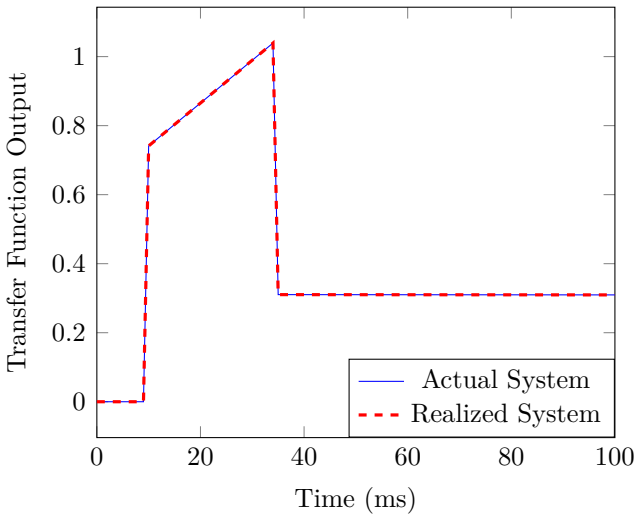

Fig. 6.13: Time responses of realized and actual $G_{I_{D_r}}$ transfer functions

However, the realized transfer function for the turbine shows some damping.

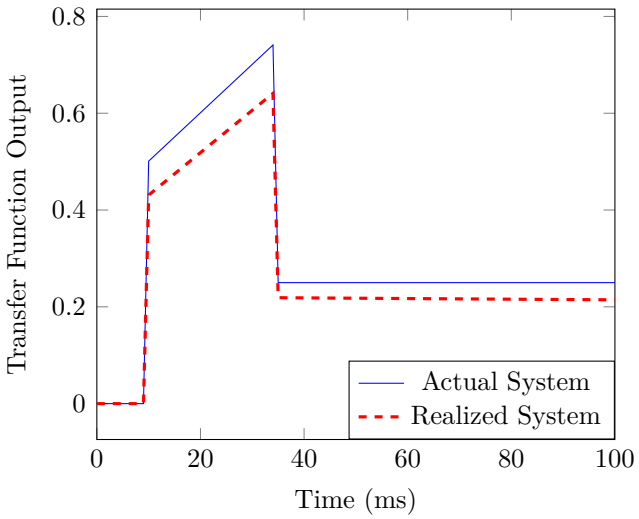

Fig. 6.14: Time responses of realized and actual $G_{I_{Q_r}}$ transfer functions

Table 6.5: Comparison of realized multimass turbine transfer function with the actual transfer function

Realized Transfer Function	Actual Transfer Function
$\frac{112s^3+111.15s^2+2.269\times10^4 s+1.247\times10^4}{s^4+1.334s^3+391.69s^2+430.35s+2784}$	$\frac{113.1s^3+2.29\times10^4 s}{s^4+391.1s^2+2665}$

6.3.5 Limitations and Challenges of Application in a DFIG System

It was observed that the sensitivity of modes to some reference point changes, are less than it is to the others. Modes are more sensitive to change of DC link voltage reference and change of stator reactive power reference. In order to achieve the required distinct modes, additional time-domain simulations had to be run. However, this knowledge of the sensitivity of modes to the change of operating points helps reduce the number of operating points at which the EMT simulations should be run for identification of DFIG systems.

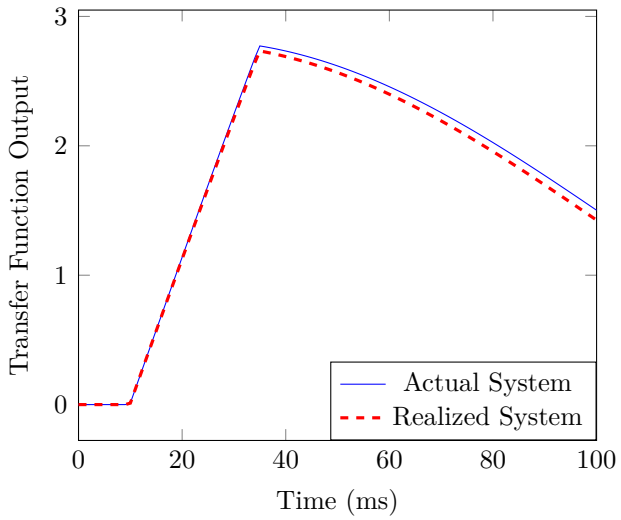

Fig. 6.15: Time responses of realized and actual multimass turbine transfer functions

In order to avoid the effects of converter harmonics, the signals were pre-conditioned using a low pass filter. Signals were decimated to reduce the number of data points for system identification procedures.

More user intervention was required to the minimum realization operation $\Gamma(.)$ as the tolerance of minimum realization of different transfer functions were different.

6.4 Chapter Summary

A black-boxed DFIG has been successfully identified for the purpose of linear analysis with reasonable *a priori* knowledge of the system and reasonable access to measurements of the system states. Compared to the synchronous machine example presented in Chapter 5, the system of a DFIG poses additional challenges due to its complexity. Available access to grid-side converter states was utilized to simplify the system,

by identifying grid-side converter controllers as a separate exercise of conventional system identification. The Prony Analysis method augmented with eigenstructure assignment, presented in Chapter 4 has been used to identify modes of the complete system. Then the results derived from Mason's Gain Rule, in Chapter 5, were used to construct a linear system of polynomial equations in the same way it was applied for a synchronous machine SMIB system. Using system identification results from multiple operating points and *a priori* knowledge of the current injection device subsystem, the linear system of polynomial equations was solved for unknown auxiliary controller polynomials of the rotor-side converter. The application of methods proposed in Chapter 5, in a relatively complex system was successful as it could determine the controller transfer function parameters with reasonable accuracy.

Chapter 7

Conclusions, Contributions and Future Work

7.1 Conclusions

A procedure to identify the operating-point-independent linear auxiliary controller transfer functions of a black-boxed power system device model, has been proposed. The procedure utilizes system identification results at multiple operating points and dynamic data of the current injection device subsystem of the power system device model. A procedure has been proposed to augment the Prony Analysis system identification method with an eigenstructure assignment based controller tuning procedure to enhance the system identification results.

It has become the trend of the power system device manufacturers to make available a detailed EMT simulation model of their devices. Such simulation models are usually black-boxed and cannot be accommodated in a small signal stability analysis. It can be assumed that the time constants and reactances of the current injection device is available.

The proposed procedure requires the user to connect the black-boxed EMT sim-

ulation model to an ideal voltage source through a short transmission line to build a Single Machine Infinite Bus (SMIB) simulation case on the EMT programme. Dynamic data of the current injection device of the black boxed system (e.g. induction generator data of a DFIG system) are available to the user. The user runs time-domain simulations of the SMIB case at a chosen set of distinct operating points. At each operating point, the system is perturbed by a pulse stream of a specific class through inputs available in the black-boxed model. Then the observed output variables are used to estimate system modes at each operating point using a Prony Analysis algorithm with Exogenous Input and with different data window lengths. The identification results are further augmented with a proposed eigenstructure assignment (ESA) controller tuning method, so that the *a priori* knowledge of the current injection device is utilized to improve it. It could be seen that the modes of the system change with the operating point.

A result derived from Mason's Gain Rule was used to to decompose a complex power system model into known-operating-point-dependent subsystems and unknown-operating-point-independent subsystems, to formulate a linear system of polynomial equations of the form $\mathbf{Ax} = \mathbf{b}$, where $\mathbf{A}$ consists of transfer function polynomials of the current injection device calculated using *a priori* knowledge, $\mathbf{x}$ is a vector of unknown auxiliary controller transfer function polynomials and $\mathbf{b}$ consists of system identification results. The system can be made overdetermined by populating it with data from multiple operating points and can be solved for $\mathbf{x}$ and, the auxiliary controller transfer functions can be calculated. Auxiliary controller transfer functions so determined and the current injection device data can be used for complete linear analysis of any power system the black-box is connected to, at any operating point.

The scope of the research is limited to linear auxiliary controllers and operating points that do not cause controller saturation. It is important that the SMIB operating points chosen for system identification cause in distinct modes so that the linear system of polynomial equations is consistent.

The procedure was first applied to a synchronous machine model with controllers. It required a minimum of 5 operating point data to successfully determine the auxiliary controllers. In order to test the application of the method to more complex systems, a Doubly Fed Induction Generator (DFIG) model was chosen. Due the complexity of the system, data from a minimum of 139 operating points were required. Out of the two converters of the DFIG, the grid-side converter state variables are more accessible. A more conventional transfer function identification exercise was carried out to determine the grid-side converter controllers. The problem was reduced to one that requires data from a minimum of only 11 operating points. Data from 20 operating points were used to successfully determine the auxiliary controller transfer functions of rotor-side converter controllers.

It has been shown that the proposed procedure can be generally applied to complex power system models. When the order of the problem increases due to the complexity of the system, it can be made simpler by utilizing other data of the system.

7.2 Contributions

The main contributions of this thesis are summarized below,

- A methodology to decompose a complex power system model into known-

operating-point-dependent subsystems and unknown-operating-point-independent subsystems was formulated to allow to use system identification data from multiple operating points and *a priori* knowledge of the system to solve for unknown auxiliary controller transfer functions. In order to make this formulation possible, a novel result from Mason's Gain Rule has been presented as a theorem with proof.

- The system identification results used in the method proposed above essentially requires to include all modes contributed by the known current injection device subsystem. An Eigenstructure Assignment (ESA) based method has been proposed to incorporate *a priori* knowledge of the current injection device subsystem to linear system identification results. The method involves designing a fictitious controller to the known subsystem, i.e. current injection device model of a power system device, using ESA, to achieve the same modes and mode shapes identified from a linear system identification. A meta heuristic optimization problem has been formulated to choose free parameters of ESA. The method was successfully used with Single Machine Infinite Bus system.

- The system identification method augmented with eigenstructure assignment has been extended to a multimachine power system with black-boxed devices. This application allows the user to perform complete eigenvalue analysis to a system with black-boxed devices at a given operating point.

The main contributions of this thesis have been published in reputed journals and conference proceedings.

Journal Papers

1. B. W. H. A. Rupasinghe, U. D. Annakkage and C. Karawita, "A Procedure to Identify the Linear Models of Auxiliary Controllers of a Synchronous Machine," in *IEEE Transactions on Power Systems*, vol. 33, no. 5, pp. 5006-5015, Sept. 2018.

Conference Proceedings

1. B. W. H. A. Rupasinghe and U. D. Annakkage,"Incorporating a black-boxed synchronous machine model into a linear analysis of a power system," *2017 IEEE Manchester PowerTech*, Manchester, 2017, pp. 1-6.

2. B. W. H. A. Rupasinghe and U. D. Annakkage, "A procedure to identify an accurate linear model of a synchronous machine," *2017 IEEE Power and Energy Conference at Illinois (PECI)*, Champaign, IL, 2017, pp. 1-7.

3. B. W. H. A. Rupasinghe and U. D. Annakkage, "Extracting data from the RSCAD electromagnetic simulation platform to perform eigenvalue analysis," *2015 IEEE 10th International Conference on Industrial and Information Systems (ICIIS)*, Peradeniya, 2015, pp. 256-260.

7.3 Proposed Future Work

This thesis presented a time domain simulation based method to determine linear equivalent models of two different power system device models. The proposed procedure can be packaged into a software tool, preferably as a part of an EMT power

system simulation program, so that it can be applied to a wide range of power system devices. Apart from the linear development of the tool, the researcher has identified possible future directions of this research.

- This research neglects the presence of noise in the measurements as the proposed methods are based on simulations. The application of the proposed procedure can be extended to real systems if the system identification procedures could be improved to handle noisy signals.

- Application of the proposed method may be applied to achieve equivalent reduced order linear models of large power systems that will allow for faster and cheaper simulation.

- Application of the proposed procedure in real power system devices will enable determining more accurate transfer functions of components such as multimass turbines and will enable more realistic analysis of power system electromechanical modes.

- The eigenstructure assignment method used in the proposed procedure uses Simulated Annealing as the candidate meta heuristic optimization procedure. The efficiency of using other meta heuristic optimization methods such as genetic algorithm and ant-colony optimization can be explored to improve the efficiency of the complete algorithm.

- The proposed Mason's Gain Rule application may be incorporated with established block oriented system identification techniques [66] to include *a priori* knowledge of subsystem blocks, in order to improve the the model identification.

References

[1] M. J. Gibbard, N. Martins, J. J. Sanchez-Gasca, N. Uchida, V. Vittal, and L. Wang, "Recent applications of linear analysis techniques," *IEEE Transactions on Power Systems*, vol. 16, pp. 154–162, Feb 2001.

[2] J. J. Sanchez-Gasca, "Toward the automated computation of electromechanical modes from transient simulations," *IEEE PES General Meeting, PES 2010*, 2010.

[3] P. Kundur, *Power System Stability and Control*. McGraw-Hill Education, 1994.

[4] S. Mohajeryami, A. R. Neelakantan, I. N. Moghaddam, and Z. Salami, "Modeling of deadband function of governor model and its effect on frequency response characteristics," in *2015 North American Power Symposium (NAPS)*, pp. 1–5, Oct 2015.

[5] "Ieee recommended practice for excitation system models for power system stability studies," *IEEE Std 421.5-2016 (Revision of IEEE Std 421.5-2005)*, pp. 1–207, Aug 2016.

[6] *PSS/E 33.0 Operations Manual*. Power Technologies International, Siemens Energy, Inc., 2012.

[7] *SSAT Operations Manual*. DSA Tools, Powertech Labs Inc., 2012.

[8] *PSCAD Operations Manual*. HVDC Research Centre, Manitoba Hydro International Inc., 2012.

[9] O. Elgerd, *Electric Energy Systems Theory: An Introduction*. Tata McGraw-Hill, 1983.

[10] J. Yan, C. C. Liu, and U. Vaidya, "Pmu-based monitoring of rotor angle dynamics," *IEEE Transactions on Power Systems*, vol. 26, pp. 2125–2133, Nov 2011.

[11] C.-W. Liu, J. S. Thorp, J. Lu, R. J. Thomas, and H.-D. Chiang, "Detection of transiently chaotic swings in power systems using real-time phasor measurements," *IEEE Transactions on Power Systems*, vol. 9, pp. 1285–1292, Aug 1994.

[12] J. Aghaei, M. Zarei, M. Asban, S. Ghavidel, A. Heidari, and V. G. Agelidis, "Determining potential stability enhancements of flexible ac transmission system devices using corrected transient energy function," *IET Generation, Transmission Distribution*, vol. 10, no. 2, pp. 470–476, 2016.

[13] A. A. Fouad, A. Ghafurian, K. Nodehi, and Y. Mansour, "Calculation of generation-shedding requirements of the b. c. hydro system using transient energy functions," *IEEE Transactions on Power Systems*, vol. 1, pp. 17–23, May 1986.

[14] T. Kailath, *Linear Systems*. Information and System Sciences Series, Prentice-Hall, 1980.

[15] J. R. Lucas, U. D. Annakkage, C. Karawita, D. Muthumuni, and R. Jayasinghe, "Inclusion of small signal stability assessment to electromagnetic transient programs," in *Fourth lASTED International Conference*, pp. 1–5, 2008.

[16] S. H. Wright, "Determination of synchronous machine constants by test reactances, resistances, and time constants," *Transactions of the American Institute of Electrical Engineers*, vol. 50, pp. 1331–1350, Dec 1931.

[17] K. N. Stanton, "Measurement of turboalternator transfer functions using normal operating data," *Electrical Engineers, Proceedings of the Institution of*, vol. 110, pp. 2001–2007, November 1963.

[18] G. S. Hope, S. T. Nichols, and J. Carr, "Measurement of transfer functions of power system components under operating conditions," *IEEE Transactions on Power Apparatus and Systems*, vol. 96, pp. 1798–1808, Nov 1977.

[19] J. Sanchez-Gasca and D. J. Trudnowski, "Identification of electromechanical modes in power systems," tech. rep., IEEE Power and Energy Society, 06 2012.

[20] L. Ljung, *System identification : theory for the user / Lennart Ljung. –*. Prentice-Hall information and system sciences series, Englewood Cliffs, NJ: Prentice-Hall, 1987.

[21] J. R. Smith, F. Fatehi, C. S. Woods, J. F. Hauer, and D. J. Trudnowski, "Transfer function identification in power system applications," *IEEE Transactions on Power Systems*, vol. 8, pp. 1282–1290, Aug 1993.

[22] D. J. Trudnowski, M. K. Donnelly, and J. F. Hauer, "Advances in the identification of transfer function models using prony analysis," in *1993 American Control Conference*, pp. 1561–1562, June 1993.

[23] I. Kamwa, R. Grondin, E. J. Dickinson, and S. Fortin, "A minimal realization approach to reduced-order modelling and modal analysis for power system response signals," *IEEE Transactions on Power Systems*, vol. 8, pp. 1020–1029, Aug 1993.

[24] D. J. Trudnowski, J. M. Johnson, and J. F. Hauer, "Making prony analysis more accurate using multiple signals," *IEEE Transactions on Power Systems*, vol. 14, pp. 226–231, Feb 1999.

[25] J. J. Sanchez-Gasca and J. H. Chow, "Computation of power system low-order models from time domain simulations using a hankel matrix," *IEEE Transactions on Power Systems*, vol. 12, pp. 1461–1467, Nov 1997.

[26] H. Okamoto, A. Kurita, J. J. Sanchez-Gasca, K. Clark, N. W. Miller, and J. H. Chow, "Identification of low-order linear power system models from emtp simulations using the steiglitz-mcbride algorithm," *IEEE Transactions on Power Systems*, vol. 13, pp. 422–427, May 1998.

[27] J. J. Sanchez-Gasca and J. H. Chow, "Performance comparison of three identification methods for the analysis of electromechanical oscillations," *IEEE Transactions on Power Systems*, vol. 14, pp. 995–1002, Aug 1999.

[28] D. I. Trudnowski, "Order reduction of large-scale linear oscillatory system models," *IEEE Transactions on Power Systems*, vol. 9, pp. 451–458, Feb 1994.

[29] I. Kamwa and L. Gerin-Lajoie, "State-space system identification-toward mimo models for modal analysis and optimization of bulk power systems," *IEEE Transactions on Power Systems*, vol. 15, pp. 326–335, Feb 2000.

[30] L. Dosiek and J. W. Pierre, "Estimating electromechanical modes and mode shapes using the multichannel armax model," *IEEE Transactions on Power Systems*, vol. 28, pp. 1950–1959, May 2013.

[31] H. Liu, L. Zhu, Z. Pan, J. Guo, J. Chai, W. Yu, and Y. Liu, "Comparison of mimo system identification methods for electromechanical oscillation damping estimation," in *2016 IEEE Power and Energy Society General Meeting (PESGM)*, pp. 1–5, July 2016.

[32] T. Katayama, *Subspace Methods for System Identification by Tohru Katayama.* Communications and Control Engineering, 2005.

[33] N. Zhou, S. Member, J. W. Pierre, S. Member, J. F. Hauer, and L. Fellow, "Initial Results in Power System Identification From Injected Probing Signals Using a Subspace Method," vol. 21, no. 3, pp. 1296–1302, 2006.

[34] S. A. N. Sarmadi and V. Venkatasubramanian, "Inter-area resonance in power systems from forced oscillations," *IEEE Transactions on Power Systems*, vol. 31, pp. 378–386, Jan 2016.

[35] P. Van Overschee, B. De Moor, P. V. Overschee, and B. D. Moor, "Subspace Identification for Linear System: Theory - Implementation - Applications," *Conference Proceedings of the International Conference of IEEE Engineering in Medicine and Biology Society*, vol. 2008, pp. 4427–30, 1996.

[36] J. Quintero, G. Liu, and V. M. Venkatasubramanian, "An oscillation monitoring system for real-time detection of small-signal instability in large electric power systems," in *2007 IEEE Power Engineering Society General Meeting*, pp. 1–8, June 2007.

[37] N. Zhou, J. W. Pierre, and D. Trudnowski, "A stepwise regression method for estimating dominant electromechanical modes," *IEEE Transactions on Power Systems*, vol. 27, pp. 1051–1059, May 2012.

[38] D. P. Wadduwage, U. D. Annakkage, and K. Narendra, "Identification of dominant low-frequency modes in ring-down oscillations using multiple prony models," *IET Generation, Transmission Distribution*, vol. 9, no. 15, pp. 2206–2214, 2015.

[39] J. C. H. Peng and N. K. C. Nair, "Comparative assessment of kalman filter and prony methods for power system oscillation monitoring," in *2009 IEEE Power Energy Society General Meeting*, pp. 1–8, July 2009.

[40] P. Korba, "Real-time monitoring of electromechanical oscillations in power systems: first findings," *IET Generation, Transmission Distribution*, vol. 1, pp. 80–88, January 2007.

[41] J. C. H. Peng and N. K. C. Nair, "Enhancing kalman filter for tracking ringdown electromechanical oscillations," *IEEE Transactions on Power Systems*, vol. 27, pp. 1042–1050, May 2012.

[42] K. K. P. Poon and K. C. Lee, "Analysis of transient stability swings in large interconnected power systems by fourier transformation," *IEEE Transactions on Power Systems*, vol. 3, pp. 1573–1581, Nov 1988.

[43] Z. Tashman, H. Khalilinia, and V. Venkatasubramanian, "Multi-dimensional fourier ringdown analysis for power systems using synchrophasors," *IEEE Transactions on Power Systems*, vol. 29, pp. 731–741, March 2014.

[44] D. R. Ostojic, "Spectral monitoring of power system dynamic performances," *IEEE Transactions on Power Systems*, vol. 8, pp. 445–451, May 1993.

[45] D. Kosterev, C. Taylor, and W. Mittelstadt, "Model validation for the August 10, 1996 WSCC system outage," *IEEE Transactions on Power Systems*, vol. 14, no. 3, pp. 967–979, 1999.

[46] M. Asmine, J. Brochu, J. Fortmann, R. Gagnon, Y. Kazachkov, C. E. Langlois, C. Larose, E. Muljadi, J. MacDowell, P. Pourbeik, S. A. Seman, and K. Wiens, "Model validation for wind turbine generator models," *IEEE Transactions on Power Systems*, vol. 26, pp. 1769–1782, Aug 2011.

[47] X. Wang, J. Xiong, L. Geng, J. Zheng, and S. Zhu, "Parameter identification of doubly-fed induction generator by the levenberg-marquardt-fletcher method," in *2013 IEEE Power Energy Society General Meeting*, pp. 1–5, July 2013.

[48] D. Kosterev, "Hydro turbine-governor model validation in pacific northwest," *IEEE Transactions on Power Systems*, vol. 19, pp. 1144–1149, May 2004.

[49] Z. Huang, M. Kosterev, R. Guttromson, and T. Nguyen, "Model validation with hybrid dynamic simulation," in *2006 IEEE Power Engineering Society General Meeting*, pp. 9 pp.–, 2006.

[50] J. Chen, P. Shrestha, S. H. Huang, N. D. R. Sarma, J. Adams, D. Obadina, and J. Ballance, "Use of synchronized phasor measurements for dynamic stability monitoring and model validation in ercot," in *2012 IEEE Power and Energy Society General Meeting*, pp. 1–7, July 2012.

[51] Z. Huang, P. Du, D. Kosterev, and S. Yang, "Generator dynamic model validation and parameter calibration using phasor measurements at the point of connection," *IEEE Transactions on Power Systems*, vol. 28, pp. 1939–1949, May 2013.

[52] S. L. Marple, *Digital spectral analysis : with applications / S. Lawrence Marple, Jr.* Prentice-Hall signal processing series, Englewood Cliffs, N.J.: Prentice-Hall, 1987.

[53] D. J. Trudnowski, J. R. Smith, T. A. Short, and D. A. Pierre, "An application of prony methods in pss design for multimachine systems," *IEEE Transactions on Power Systems*, vol. 6, pp. 118–126, Feb 1991.

[54] J. F. Hauer, C. J. Demeure, and L. L. Scharf, "Initial results in prony analysis of power system response signals," *IEEE Transactions on Power Systems*, vol. 5, pp. 80–89, Feb 1990.

[55] M. K. Das, A. M. Kulkarni, and P. B. Darji, "Comparison of DQ and Dynamic Phasor based frequency scanning analysis of grid-connected Power Electronic Systems," *19th Power Systems Computation Conference, PSCC 2016*, no. 1, 2016.

[56] M. Fahmy and J. O'Reilly, "Eigenstructure assignment in linear multivariable systems–a parametric solution," *IEEE Transactions on Automatic Control*, vol. 28, pp. 990–994, Oct 1983.

[57] S. Jiang, U. Annakkage, and A. Gole, "A Platform for Validation of FACTS Models," *IEEE Transactions on Power Delivery*, vol. 21, pp. 484–491, Jan. 2006.

[58] B. W. H. A. Rupasinghe and U. D. Annakkage, "A procedure to identify an accurate linear model of a synchronous machine," in *2017 IEEE Power and Energy Conference at Illinois (PECI)*, pp. 1–7, Feb 2017.

[59] B. W. H. A. Rupasinghe and U. D. Annakkage, "Incorporating a black-boxed synchronous machine model into a linear analysis of a power system," in *2017 IEEE Manchester PowerTech*, pp. 1–6, June 2017.

[60] S. J. Mason, "Feedback theory-some properties of signal flow graphs," *Proceedings of the IRE*, vol. 41, pp. 1144–1156, Sept 1953.

[61] S. J. Mason, "Feedback theory-further properties of signal flow graphs," *Proceedings of the IRE*, vol. 44, pp. 920–926, July 1956.

[62] L. Xu, "Enhanced control and operation of dfig-based wind farms during network unbalance," *IEEE Transactions on Energy Conversion*, vol. 23, pp. 1073–1081, Dec 2008.

[63] D. H. R. Suriyaarachchi, U. D. Annakkage, C. Karawita, and D. A. Jacobson, "A procedure to study sub-synchronous interactions in wind integrated power systems," *IEEE Transactions on Power Systems*, vol. 28, pp. 377–384, Feb 2013.

[64] R. Pena, J. C. Clare, and G. M. Asher, "Doubly fed induction generator using back-to-back pwm converters and its application to variable-speed wind-energy generation," *IEE Proceedings - Electric Power Applications*, vol. 143, pp. 231–241, May 1996.

[65] D. H. R. Suriyaarachchi, *Sub-synchronous interactions in a wind integrated power system.* PhD thesis, University of Manitoba, Winnipeg, MB, Canada, 9 2014.

[66] W. Greblicki, *Nonparametric system identification / Włodzimierz Greblicki, Mirosław Pawlak.* New York: Cambridge University Press, 2008.

[67] S. Kirkpatrick, C. D. Gelatt, and M. P. Vecchi, "Optimization by simulated annealing," *Science*, vol. 220, pp. 671–680, may 1983.

[68] S. Kirkpatrick, "Optimization by simulated annealing: Quantitative studies," *Journal of Statistical Physics*, vol. 34, pp. 975–986, mar 1984.

[69] N. Metropolis, A. W. Rosenbluth, M. N. Rosenbluth, A. H. Teller, and E. Teller, "Equation of state calculations by fast computing machines," *The Journal of Chemical Physics*, vol. 21, pp. 1087–1092, jun 1953.

[70] A. C. Aitken, *Determinants and Matrices.* Oliver and Boyd, 9th edition. ed., 1967.

Appendix A

Simulated Annealing

Simulated Annealing

Annealing Process of Metals

Annealing is a heat treatment of metals, usually carried out to soften them. In a metallurgic sense, this softness is achieved by achieving the lowest energy metal structure. In the process, first, the metal is brought to a high temperature. It may even go into the liquid phase. This way, the molecules gain energy and move fast and randomly. Then, the red hot or liquid metal is allowed to cool down, slowly. When cooling down, the molecules lose energy and settles down to a low energy structure. The slower the cooling process, the more probable it is to achieve the minimum energy state. The opposite of this process is quenching, where the heated metal is cooled suddenly, so that a structure close to a crystalline structure is achieved. This is done to harden metals.

In simulated annealing [67, 68], the objective function is analogous to the energy of the metals. The decision variables are analogous to the metal molecules. Decision variables are randomly perturbed iteratively and lower objective function values are accepted as approaching the global minimum value. In addition, during the initial iterations, the probability of accepting a solution, even if its objective function is higher, is more. This is analogous to the high-energy random movement of metal molecules in the annealing process. During the later iterations, this probability is less. This change of probability as iterations advance, is analogous to the temperature of the metal, which goes down (cool down) as time goes by. This heuristic characteristic is introduced to the algorithm by the Metropolis Criterion [69].

Metropolis Criterion

- If, the new state contains lower total energy compared to the previous state, then the new state is accepted.
- Else, the new state is accepted with the probability given by Eq A.1.

$$p(\Delta E) = e^{-\left(\frac{\Delta E}{K_B \times T}\right)} \tag{A.1}$$

Where:

ΔE = is the change occurred in the total energy of the solid due to the perturbation

K_B = is the Boltzmann's constant

T = is the temperature of the substance

The Metropolis criterion explains the possibility of achieving the minimum energy state at a given temperature.

Simulated Annealing Optimization Technique

The Simulated Annealing optimization algorithm as applied in the problem at hand is illustrated in Fig.A.1.

Optimization parameters

There are three types of parameters in this algorithm, namely the initial temperature T_1, cooling rate r_c and the Boltzman Constant K_B. The ideal initial temperature and cooling rate in the physical process of annealing depends on the material considered. Similarly the initial temperature and cooling rate in simulated annealing too depends on the optimization problem. Highly nonlinear problems with a large number of decision variables require higher initial temperatures. Higher initial temperatures and slower cooling rate extends the time for convergence but increase the probability of reaching the global optimum.

Saving the best solution

Due to the heuristic nature of the algorithm, it is possible to achieve a better solution than solution converged to at the end. Therefore, the *best solution so far* should be saved.

Perturbing the Variables

The decision variables of this optimization problem are the free parameters of the eigenstructure assignment procedure. The free parameters are given a maximum of 10% random perturbation according to Eq. A.2.

$$\mathbf{f}_i^k = \mathbf{f}_i^{k-1} + \Delta\mathbf{f}_i \tag{A.2}$$

Where $\Delta\mathbf{f}_i$ is a randomly generated vector with values between $\pm 10\% \times f_i^k$.

Stopping Criteria

Two stopping criteria were chosen for the simulated annealing algorithm.

Stop if:

$$iter \geq iter_{max} \tag{A.3a}$$

$$T_{iter} \leq T_{min} \tag{A.3b}$$

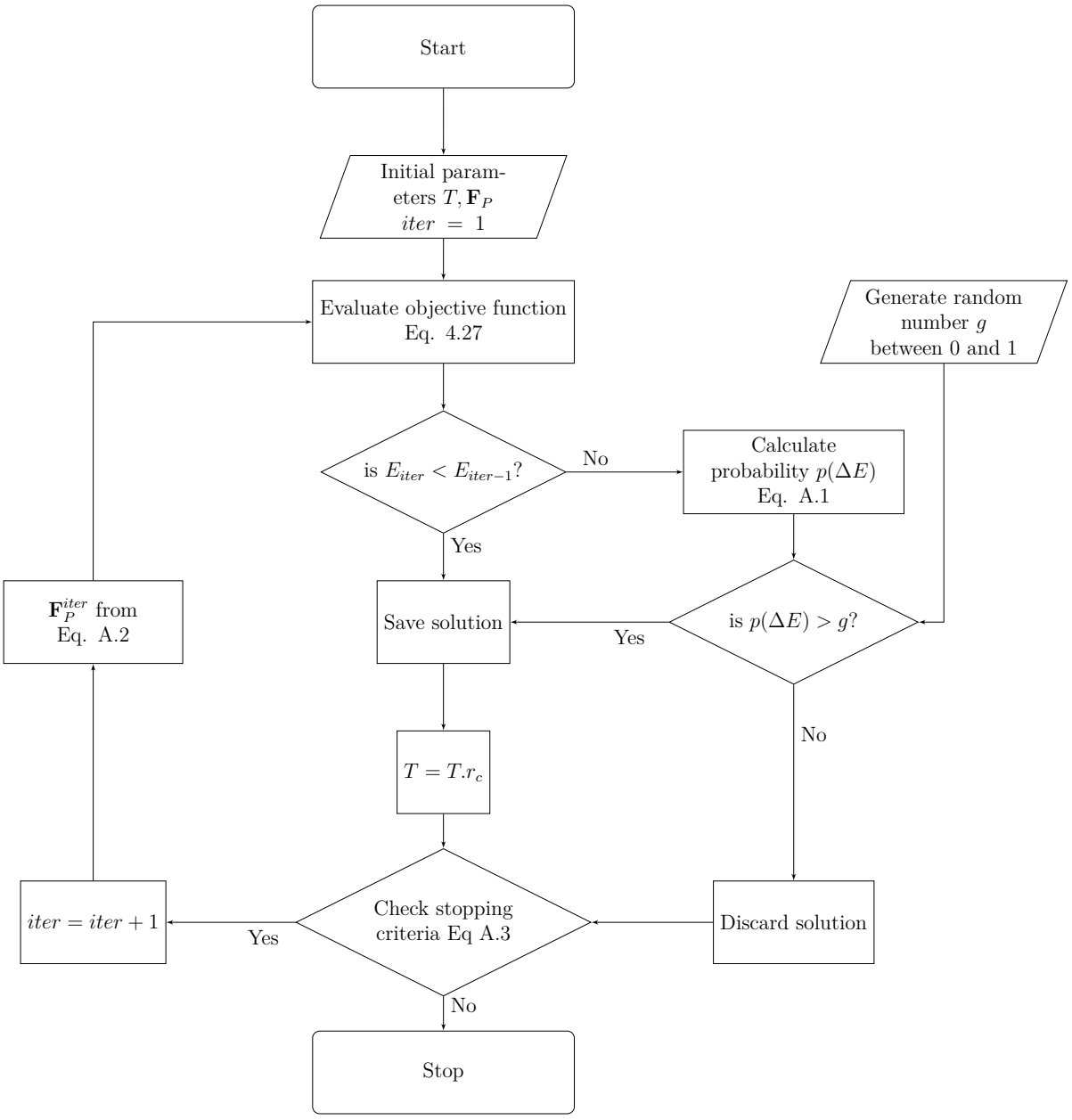

Fig. A.1: Simulated annealing algorithm flow chart

Appendix B

Linear Algebraic Preliminaries for Application of Mason's Gain Rule

Mason's Gain Rule

According to the Mason's Rule [60, 61], the path transmission, or, the effective transfer function, from a source to a sink may be stated as:

$$T = \frac{1}{\Delta}\{\text{the sum of [forward path transmission } (N)\text{] for all possible paths}\} \quad \text{(B.1)}$$

where

$$\begin{aligned} N \;=\; & 1- \;\; \text{Transmission of all loops not intersecting this forward path, } \textit{taken one at a time} \\ & + \;\; \text{Transmission of all loops not intersecting this forward path, multiplied two at a time, taken in non-intersecting pairs} \\ & - \;\; \text{Transmission of all loops not intersecting this forward path, multiplied two at a time, taken in non-intersecting pairs} \\ & + \;\; \text{etc.} \end{aligned}$$

$$\begin{aligned} \Delta \;=\; & 1- \;\; \text{All loop transmissions taken one at a time} \\ & + \;\; \text{All loop transmissions not intersecting each other, taken two at a time} \\ & - \;\; \text{All loop transmissions not intersecting each other, taken three at a time} \\ & + \;\; \text{etc.} \end{aligned}$$

Linear Algebraic Manipulations

Let there be polynomials $a_i(s)$, $x_i(s)$ and $b_i(s)$ of variable s related as:

$$a_i(s)x_i(s) = b_i(s) \tag{B.2}$$

where

$$\begin{aligned} a_i(s) &= \sum_{k=0}^{m} a_{i,k}s^k \\ b_i(s) &= \sum_{k=0}^{n} b_{i,k}s^k \\ x_i(s) &= \sum_{k=0}^{n-m} x_{i,k}s^k \end{aligned}$$

Polynomials $a_i(s)$, $x_i(s)$ and $b_i(s)$ can be represented by their coefficient vectors $\mathbf{a_i}$, $\mathbf{x_i}$ and $\mathbf{b_i}$.

where:

$$\begin{aligned} \mathbf{a_i^T} &= \begin{bmatrix} a_{i,m} & a_{i,(m-1)} & \dots & a_{i,1} & a_{i,0} \end{bmatrix} \\ \mathbf{x_i^T} &= \begin{bmatrix} x_{i,(n-m)} & x_{i,(n-m-1)} & \dots & x_{i,1} & x_{i,1} \end{bmatrix} \\ \mathbf{b_i^T} &= \begin{bmatrix} b_{i,n} & b_{i,(n-1)} & \dots & b_{i,1} & b_{i,0} \end{bmatrix} \end{aligned}$$

Relationship in Eq. B.2 can be represented by convolution of vectors as follows:

$$\mathbf{a_i} * \mathbf{x_i} = \mathbf{b_i} \tag{B.5}$$

Let $\mathbf{A_i} \in \mathbb{R}^{[n+1]\times[n-m+1]}$ be the convolution matrix of $\mathbf{a_i}$, with regard to $\mathbf{x_i}$.

$$\mathbf{A_i x_i} = \mathbf{b_i} \tag{B.6}$$

where:

$$\mathbf{A_i} = \begin{bmatrix} a_{i,m} & & & & \\ a_{i,(m-1)} & a_{i,m} & & & \\ \cdots & a_{i,(m-1)} & a_{i,m} & & \\ a_{i,1} & \cdots & a_{i,(m-1)} & \ddots & \\ a_{i,0} & a_{i,1} & \cdots & \ddots & a_{i,m} \\ & a_{i,0} & a_{i,1} & \ddots & a_{i,(m-1)} \\ & & a_{i,0} & \ddots & \cdots \\ & & & \ddots & a_{i,1} \\ & & & & a_{i,0} \end{bmatrix}$$

Cauchy-Binet Formula

Let

$$\begin{aligned} \mathbf{P} &\in \mathbb{R}^{[r\times n]} \\ \mathbf{Q} &\in \mathbb{R}^{[n\times r]} \\ [n] &= \{1, ..., n\} \\ [r] &= \{1, ..., r\} \\ \binom{[n]}{r} &= \{r \textit{ combinations of } [n]\} \\ S &\in \binom{[n]}{m} \\ \mathbf{P}_{[r],S} &\in \mathbb{R}^{[r\times r]} \\ \mathbf{Q}_{S,[r]} &\in \mathbb{R}^{[r\times r]} \end{aligned}$$

The Cauchy–Binet formula then states.

$$\det(\mathbf{PQ}) = \sum_{S\in\binom{[n]}{m}} \det(\mathbf{P}_{[m],S}) \det(\mathbf{Q}_{S,[m]}) \tag{B.7}$$

Appendix C

Test System Data

Table C.1: Generator and network parameters of the test system shown in Fig. 4.1

Generator rating	500 MVA
System base MVA	500 MVA
Generator base voltage	22 kV
Network base voltage	22 kV
Generator model	GENROU
Transformer leakage reactance	0
Transmission line reactance	0.025 pu
Transmission line resistance	0

Table C.2: Bus voltages of the test system shown in Fig. 4.1

Bus	**Base Voltage (kV)**	**Voltage (pu)**	**Angle (deg)**
1	230	1.0000	0.0000
2	230	1.0536	4.0818
3	22	1.0765	5.5974

Table C.3: Dynamic data of the synchronous machine of the test system shown in Fig. 4.1

T'_{do}	T_{do}"	T'_{qo}	T_{qo}"	H	D
8.69	0.03	0.31	0.04	3	0

X_d	X_q	X'_d	X'_q	X_d" $= X_q$"	X_l
0.73	0.4845	0.304	0.304	0.25	0.12

Table C.4: Synchronous machine controller data of the test system shown in Fig. 4.1

ESAC4A Exciter	**STAB1 Stabilizer**	**TGOV1 Governor**
$T_R = 0.02$ s	$K/T_w = 2\ s^{-1}$	$R = 0.06$
$T_C = 1$	$T_w = 2$ s	$T_1 = 0.5$ s
$T_B = 10$ s	$T_1/T_3 = 0.08$	$T_2 = 1$ s
$K_A = 100$ s	$T_3 = 5$ s	$T_3 = 1$ s
$T_A = 0.01$ s	$T_2/T_4 = 0.08$	
	T_4= 5 s	

Table C.5: Network data for DFIG SMIB System shown in Fig. 6.1

Parameter	Value
Wind farm network voltage	33 kV
Collector transformer MVA	200 MVA
Collector transformer leakage reactance	6%
Network resistance	0.4713 Ω
Network reactance	0.7766 Ω
Network susceptance	5.42 $\times 10^{-4}$S
Transmission line resistance	0.05 Ω/km
Transmission line inductance	0.0089 mH/km
Transmission line capacitance	0.0089 μF/km

Table C.6: DFIG generator data for system shown in Fig. 6.1

Parameter	Value
Rated power	2MW
Radius	37.5m
Performance coefficient	0.28
Air density	1.225 kg/m^3
Gear ratio	10.909
Rated voltage	690 V
Base MVA	2 MVA
Stator resistance	0.0012 Ω
Rotor resistance	0.0013 Ω
Stator leakage inductance	0.0584 mH
Rotor leakage inductance	0.0629 mH
Mutual inductance	2.4961 mH
DC capacitance	25 mF
DC voltage	1000 V
Converter transformer base	0.6 MVA
Transformer leakage reactance	6%
Blade inertia	4 s
Hub inertia	0.3 s
Generator inertia	0.42 s
Shaft stiffness constants	0.3 pu/rad

Table C.7: Definitions of symbols used in Fig. 6.3

Symbol	Definition
ΔQ_{Sref}	Stator reactive power reference
$\Delta\omega_{rref}$	Rotor speed reference
ΔV_{dcref}	DC link voltage reference
ΔQ_{gref}	Grid-side converter reactive power reference
ΔQ_s	Stator reactive power (measured)
$\Delta\omega_r$	Rotor speed (measured)
ΔV_{dc}	DC link voltage (measured)
ΔQ_g	Grid-side converter reactive power (measured)
ΔI^*_{Dr}	D-axis rotor current controller reference
ΔI^*_{Qr}	Q-axis rotor current controller reference
ΔI^*_{dg}	d-axis grid side converter current controller reference
ΔI^*_{qg}	q-axis grid side converter current controller reference
ΔI_{Dr}	D-axis rotor current controller (measured)
ΔI^*_{Qr}	Q-axis rotor current controller (measured)
ΔI_{dg}	d-axis grid side converter current controller (measured)
ΔI_{qg}	q-axis grid side converter current controller (measured)
ΔV^*_{Dr}	D-axis rotor voltage reference
ΔV^*_{Qr}	Q-axis rotor voltage reference
ΔV^*_{dg}	d-axis grid side voltage reference
ΔV^*_{qg}	q-axis grid side voltage reference
ΔV_{Dr}	D-axis actual rotor voltage
ΔV_{Qr}	Q-axis actual rotor voltage
ΔV_{dg}	d-axis actual grid side voltage
ΔV_{qg}	q-axis actual grid side voltage
ΔP_g	Grid-side converter real power injection to the grid
ΔP_r	Rotor-side converter real power injection to the rotor
C	DC capacitance
V_{dc0}	Steady state DC link voltage
H_g	Inertia constant of the induction machine
ΔT_{mg}	Mechanical torque input to the rotor
ΔT_m	Mechanical torque input to the turbine
Δv_w	Wind speed
G_T	Turbine transfer function
G_{Q_s}	Stator reactive power controller transfer function
G_{ω_r}	Rotor speed controller transfer function
$G_{V_{dc}}$	DC link voltage controller transfer function
G_{Q_g}	Grid-side converter reactive power controller transfer function
$G_{I_{Dr}}$	D-axis rotor current controller transfer function
$G_{I_{Qr}}$	Q-axis rotor current controller transfer function
$G_{I_{dg}}$	d-axis grid side converter current controller transfer function
$G_{I_{qg}}$	q-axis grid side converter current controller transfer function
s	Laplacian variable

Appendix D
Proof of Theorem 1

Theorem 1 For a state space described by $\mathbf{A} \in \mathbb{R}^{n\times n}$, $\mathbf{B} \in \mathbb{R}^{n\times r}$ and $\mathbf{C} \in \mathbb{R}^{r\times n}$,

$$\dot{\mathbf{x}} = \mathbf{A}\mathbf{x} + \mathbf{B}\mathbf{u} \tag{D.1}$$
$$\mathbf{y} = \mathbf{C}\mathbf{x} \tag{D.2}$$

the transfer function matrix between the inputs and outputs are given by:

$$\mathbf{W} = \mathbf{C}(\mathbf{I}s - \mathbf{A})^{-1}\mathbf{B} \tag{D.3}$$

$$\det(\mathbf{W}) = \frac{p(s)}{\det(s\mathbf{I} - \mathbf{A})} \tag{D.4}$$

where $p(s)$ is a polynomial in s of order $n - r$.

Proof 1 *Let* $\mathbf{z} = \mathbf{\Psi}\mathbf{x}$, $\mathbf{\Psi} = \mathbf{\Phi}^{-1}$ *and* $\mathbf{x} = \mathbf{\Phi}\mathbf{z}$
Modal decomposition of the state space:

$$\mathbf{\Phi}\dot{\mathbf{z}} = \mathbf{A}\mathbf{\Phi}\mathbf{z} + \mathbf{B}\mathbf{u} \tag{D.5}$$
$$\dot{\mathbf{z}} = \mathbf{\Psi}\mathbf{A}\mathbf{\Phi}\mathbf{x} + \mathbf{\Psi}\mathbf{B}\mathbf{u} \tag{D.6}$$
$$\mathbf{y} = \mathbf{C}\mathbf{\Phi}\mathbf{z} \tag{D.7}$$

Let

$$\begin{aligned}
\mathbf{C}' &= \mathbf{C}\boldsymbol{\Phi} \\
\mathbf{B}' &= \boldsymbol{\Psi}\mathbf{B} \\
\boldsymbol{\Lambda} &= \boldsymbol{\Psi}\mathbf{A}\boldsymbol{\Phi} \\
\boldsymbol{\Phi} &= \textit{Normalized right eigenvector matrix} \\
\boldsymbol{\Psi} &= \textit{Normalized left eigenvector matrix}
\end{aligned}$$

$\boldsymbol{\Lambda}$ *is the diagonal matrix of eigenvalues of* $\boldsymbol{A}$.

$$\boldsymbol{\Lambda} = \begin{bmatrix} \lambda_1 & & & \\ & \lambda_2 & & \\ & & \ldots & \\ & & & \lambda_n \end{bmatrix} \tag{D.8}$$

Now, Eq. D.3 can be rewritten as follows:

$$\mathbf{W} = \mathbf{C}'(\mathbf{I}s - \boldsymbol{\Lambda})^{-1}\mathbf{B}' \tag{D.9}$$

For any matrix $\mathbf{M}$*, the symbol* $adj(\mathbf{M})$ *denotes the well known cnocept of adjoint matrix of* $\mathbf{M}$.

$$\mathbf{W} = \frac{\mathbf{C}'adj(\mathbf{I}s - \boldsymbol{\Lambda})\mathbf{B}'}{\det(\mathbf{I}s - \boldsymbol{\Lambda})} \tag{D.10}$$

$$adj(\mathbf{I}s - \boldsymbol{\Lambda}) = \begin{bmatrix} a_1 & & & \\ & a_2 & & \\ & & \ldots & \\ & & & a_n \end{bmatrix} \tag{D.11}$$

where

$$a_k = \prod_{\substack{i=1 \\ i \neq k}}^{n} (s - \lambda_i) \tag{D.12}$$

$$\mathbf{H} = \mathbf{C}'adj(\mathbf{I}s - \boldsymbol{\Lambda})\mathbf{B}' \tag{D.13}$$

Let:

$$
\begin{aligned}
[r] &= \textit{all indices}[1, 2, ...r] \\
\binom{[n]}{r} &= \textit{all combinations of } n \textit{ choose } r \\
S &= \textit{set of indices in a chosen combination of } n \textit{ choose } r
\end{aligned}
$$

Applying Cauchy-Binet Formula [70]:

$$
\det(\mathbf{H}) = \sum_{S \in \binom{[n]}{r}} \left(\prod_{S \in \binom{[n]}{r}} a_k \right) \det(\boldsymbol{C'}_{[r],S}) \det(\boldsymbol{B'}_{S,[r]}) \tag{D.14}
$$

$$
\prod_{S \in \binom{[n]}{r}} a_k = \prod_{S \in \binom{[n]}{r}} \prod_{\substack{i=1 \\ i \neq k}}^{n} (s - \lambda_i) \tag{D.15}
$$

Right hands side of Eq D.15 can be factored as:

$$
\prod_{S \in \binom{[n]}{r}} a_k = \left(\prod_{i=1}^{n} (s - \lambda_i) \right)^{r-1} \prod_{S'} (s - \lambda_j) \tag{D.16}
$$

where $S' = \{\textit{Compliment of } S\}$

But

$$
\prod_{i=1}^{n} (s - \lambda_i) = \det(s\mathbf{I} - \mathbf{\Lambda}) \tag{D.17}
$$

Also

$$
\begin{aligned}
\det(\boldsymbol{C'}_{[r],S}) \det(\boldsymbol{B'}_{S,[r]}) &= \det(\boldsymbol{C}_{[r],S} \Phi_{[r],S} \Psi_{S,[r]} \boldsymbol{B}_{S,[r]}) && \text{(D.18)} \\
&= \det(\boldsymbol{C}_{[r],S}\ \mathbf{I}\ \boldsymbol{B}_{S,[r]}) && \text{(D.19)} \\
&= \det(\boldsymbol{C}_{[r],S} \boldsymbol{B}_{S,[r]}) && \text{(D.20)}
\end{aligned}
$$

From Eq. D.14, D.16, D.17 and D.20

$$
\begin{aligned}
\det(\mathbf{H}) = \det(s\mathbf{I} - \mathbf{\Lambda})^{r-1} & \sum_{S \in \binom{[n]}{r}} \left(\prod_{S'} (s - \lambda_j) \right) \\
& \times \det(\boldsymbol{C'}_{[r],S}) \det(\boldsymbol{B'}_{S,[r]})
\end{aligned} \tag{D.21}
$$

From Eq. D.10

$$\mathbf{W} = \frac{\mathbf{H}}{\det(\mathbf{I}s - \mathbf{\Lambda})} \tag{D.22}$$

$$\det(\mathbf{W}) = \frac{\det(\mathbf{H})}{\det(\mathbf{I}s - \mathbf{\Lambda})^r} \tag{D.23}$$

$$\det(\mathbf{W}) = \frac{\det(s\mathbf{I} - \mathbf{\Lambda})^{r-1}}{\det(\mathbf{I}s - \mathbf{\Lambda})^r} \sum_{S \in \binom{[n]}{r}} \left(\prod_{S'} (s - \lambda_j) \right) \times \det(\boldsymbol{C}_{[r],S} \boldsymbol{B}_{S,[r]}) \tag{D.24}$$

$$\det(\mathbf{W}) = \frac{1}{\det(\mathbf{I}s - \mathbf{\Lambda})} \sum_{S \in \binom{[n]}{r}} \left(\prod_{S'} (s - \lambda_j) \right) \times \det(\boldsymbol{C}_{[r],S} \boldsymbol{B}_{S,[r]}) \tag{D.25}$$

Therefore

$$\det(\mathbf{W}) = \frac{p(s)}{\det(s\mathbf{I} - \mathbf{A})} \tag{D.26}$$

and

$$p(s) = \sum_{S \in \binom{[n]}{r}} \left(\prod_{S'} (s - \lambda_j) \right) \det(\boldsymbol{C}_{[r],S} \boldsymbol{B}_{S,[r]}) \tag{D.27}$$

Order of $p(s)$ *is* $n - r$.